GEOLOGY OF TASIK PERGAU JELI, KELANTAN AND ROCK SLOPE MASS RATING ALONG GERIK-JELI HIGHWAY

By

LOW KEAN HONG

A thesis submitted in fulfilment of the requirements for the degree of Bachelor of Applied Science (Geosciences) with Honours

FACULTY OF EARTH SCIENCE

UNIVERSITI MALAYSIA KELANTAN

2019

DECLARATION

I declared that this thesis entitled "GEOLOGY OF TASIK PERGAU JELI, KELANTAN AND ROCK SLOPE MASS RATING ALONG GERIK-JELI HIGHWAY" is the result of my own research except as cited in the references. The thesis has not been accepted for any degree and is not concurrently submitted in candidature of any other degree.

Signature : _____

Name : _____

Date : _____

APPROVAL

I hereby declare that I have read this thesis and in my opinion this thesis is sufficient in terms of scope and quality for the award of the degree of Bachelor of Applied Science (Geoscience) with Honors"

Signature : _____

Name of Supervisor : _____

Date : _____

ACKNOWLEDMENT

First of all, I would like to take this chance to thank to Faculty of Earth Science University Malaysia Kelantan (UMK) for giving me this chance to work with Final Year Project (FYP). It allows me to apply the knowledge that had been learnt in the lecture class in conducting the research project. Besides that, this research project also help to develop my critical thinking, and practical skill in the field. It also improves my discipline on the management of time so that I could be able to complete my research on time.

Next, I would like to address my special thanks of gratitude to my supervisor, Mr. Shukri Bin Mail who had given me a lot of ideas and advices in completing the research. Under his guidance, I could be able to conquer the difficulties and obstacles in completing FYP. Besides that, I would like to thank to my academic advisor, Mr Arham Muchtar Achmad Bahar who had guided me in completing my geological map.

Furthermore, I would like to express my gratitude of thanks to both of my parents who providing continuous financial support in renting the car to study area and the expenses of doing thin section. They also be my listener who always listen to my difficulties and the problems that I faced during my research.

Finally yet importantly, I would like also to extend my gratitude to my coarse mates who had accompanied me to explore and carried out research in my study area.

Geology of Tasik Pergau Jeli, Kelantan and Rock Slope Mass Rating along Gerik-Jeli Highway

ABSTRACT

Rock slope failure is a geological hazard that can endanger the human safety as well as causes the destruction of the bridge, highway, or urban houses. The excavation of rocks to build Gerik-Jeli highway had caused the instability of slopes. Therefore, Slope Mass Rating (SMR) of slope along the Gerik-Jeli highway at north Kelantan was conducted. The objectives of this research is to produce geological map of Tasik Pergau Jeli, Kelantan with the scale of 1:25000 and determine the value of Slope Mass Rating of slopes that are prone to fail through the kinematic analysis and Rock Mass Rating (RMR). Geological mapping at Tasik Pergau Jeli, Kelantan identified lithology of the study area was made up entirely of feldspathic granite. Discontinuity survey and Schmidt hammer rebound test were conducted in five respective slopes along Gerik-Jeli highway. The data collected from the discontinuities survey and Schmidt hammer rebound test were used in kinematic analysis and to determine the value Rock Mass Rating of the slopes. RMR classified four out of five slopes into Class II (good rock) whereas another slope into Class III (fair rock). Kinematic analysis showed that only one slope was unstable whereas other slopes were stable. SMR value was then determined in each discontinuities set of unstable slope. Joint set 1, joint set 2 and joint set 3 in unstable slope had SMR value of 17 (completely unstable), 43 (partially unstable), and 58 (partially unstable) respectively. The result from this research was significant in informing the citizens and engineer about the stability of rock slope at the highway so that the precaution and mitigation measures can be taken before the failure of slope.

Geologi Tasik Pergau Jeli, Kelantan dan Pengelasan Jasad Cerun sepanjang lebuh raya Gerik-Jeli

ABSTRAK

Kegagalan cerun batuan merupakan bencana geologi yang mengancam keselamatan manusia dan menyebabkan kerosakan jambatan, lebuh raya, atau rumah. Penggalian batuan untuk pembinaan lebuh-raya Gerik-Jeli mengakibatkan ketidakstabilan cerun. Oleh sebab itu, pengelasan jasad cerun (SMR) dilaksanakan di sepanjang lebuh raya Gerik-Jeli yang terletak di bahagian utara Kelantan. Objectif kajian ini dilakukan ialah untuk menghasilkan peta geologi dengan skala 1:25000 di Tasik Pergau Jeli, Kelantan dan menentukan nilai pengelasan jasad cerun pada cerun yang berpotensi gagal melalui pengelasan jasad batuan (RMR) dan analisis kinematic kestabilan cerun. Pemetaan geologi di Tasik Pergau Jeli, Kelantan mengenal pasti lithologi keseluruhan di kawasan kajian terdiri daripada feldspathic granite. Survei ketakselanjaran dan ujian pantulan tukul Schmidt dilaksanakan di lima cerun sepanjang lebuh raya Gerik-Jeli. Data-data yang diperoleh daripada survei ketakselanjaran dan ujian pantulan tukul Schmidt akan digunakan untuk analisis kinematik kestabilan cerun dan mengira nilai pengelasan jasad batuan cerun. Pengelasan jasad batuan klasifikasikan empat cerun ke Kelas II, iaitu batuan kualiti baik manakala satu cerun diklasifikasikan ke Kelas III iaitu batuan kualiti sederhana. Analisis kinematik menunjukkan hanya satu cerun yang tidak stabil manakala cerun yang lain adalah stabil. Oleh itu, nilai pengelasan jasad cerun ditentukan pada setiap ketakselanjaran set di cerun yang tidak stabil. Daripada kiraan pengelasan jasad cerun, ketakselanjaran set 1, ketakselanjaran set 2 dan ketakselanjaran set 3 didapati mempunyai nilai SMR 17 (ketidakstabilan sepenuh), 43 (ketidakstabilan sebahagian), dan 58(ketidakstabilan sebahagian) masing-masing. Hasil daripada kajian ini adalah penting untuk memaklumkan kestabilan cerun di lebuh raya Gerik-Jeli kepada orang awam dan jurutera supaya tindakan amaran dan kerja mitigasi dapat dilakukan sebelum kegagalan cerun

TABLE OF CONTENT

LIST OF TABLES

LIST OF FIGURES

LIST OF ABBREVIATIONS

UCS	Uniaxial Compressive Strength
MPa	Mega Pascal
SMR	Slope Mass Rating
RMR	Rock Mass Rating
PPL	Plane polarized light
RQD	Rock Quality Designation
R_N	Rebound number of Type-N Schmidt hammer
R_L	Rebound number of Type-L Schmidt hammer
J	Joint set
N_J	Pole of joint set
Ort	Orthoclase
Bt	Biotite
Pl	Plagioclase
Qtz	Quartz
Sp	Sphene
F_1 F_2 F_3 F_4	Adjusting factor of joints (refer Table 2.6)
ISRM	International Society of Rock Mechanic

LIST OF SYMBOL

σ	Principal stress
ϕ	Friction angle
β_j , ψ	Dip angle of discontinuities
β_f , ψ	Dip angle of slope face
α_j	Dip direction of discontinuities
α_f	Dip direction of slope face
%	Percentage

LIST OF EQUATION

CHAPTER 1

INTRODUCTION

1.1 Background of Study

In this modern era, infrastructures are the element that can lead to modernisation and civilisation in a nation. Malaysia's persistent drive to develop and upgrade its infrastructure has resulted in one of the most well developed infrastructure among the newly industrializing countries of Asia. The nation's persistent drive to develop and upgrade the infrastructure has become the greatest benefit to business in Malaysia. The construction sector in Malaysia, therefore, plays an important role in supporting the economy of the country. The civil engineering projects such as construction of dam for power station, railway, highway, urban houses and factory require the excavation of rock cuts. These construction activities may cause the instability of rock, which results in slope failure if the rock slope is not properly excavated.

Slope failure is one of the destructive geological hazards beside flood. Failure of slope can be man-made or occurs naturally which can cause hazards towards human and environment. Rock slides or falls from the slope can cause flooding due to the blockage of river and destruction of landscape. Besides that, the slope failure can result in damage to urban houses, traffic delay, loss of agricultural land and business disruptions. Therefore, this study aims to study the rock slope failure by collecting and gathering the discontinuities data from the field. The Slope Mass Rating (SMR) will be employed to carry out the rock slope assessment.

1.2 Problem Statement

The excavation of rocks to build Gerik-Jeli highway had caused the instability of rock slope along Gerik-Jeli highway. The slope failure along the highway had became the problem in this research. The rock mass sliding or toppling down from the slope causes the blockage of the highway. Rafek & Komoo (1989) had added that the Gerik-Jeli Highway is one of the eight locations identified and declared by the Malaysian Public Works Department as a high-risk, landslide-prone area.

Many rock slope failure analysis have been done at Gerik-Jeli highway previously. Many researchers such as Shuib, Hj Taib, & Abdullah (2006) use the kinematic analysis method to study the stability of rock slope at the study area. The kinematic analysis used by them may be less accurate because the analysis depends on the amount of discontinuities data taken from the site. The stereonet-based kinematic analysis assumes that the tightly cluster orientation of discontinuities exists. However, the discontinuities data obtained at the field are widely scattered which creates uncertainties. Therefore, Gerik-Jeli highway will be considered for further research in order to present the stability of rock slope accurately.

1.3 Expected Outcome

This study will be conducted to find the potential of rock slope failure at Gerik-Jeli highway. By determining the location of the potential of rock slope failure at Gerik-Jeli highway, the study would address the warning at the location of potential rock slope failure to the road users who pass through the Gerik-Jeli highway. Jabatan Kerja Raya (JKR) would benefit from this study by acquiring the information of potential of rock slope failure. From the obtained information, they would be able to do the mitigation of rock slope failure at the highway. Therefore, the unnecessary and costly repairing and rebuilding work of the road would be avoided if the rock slopes have potential to fail. The company of construction would get the information of rock slope stability from this study before the infrastructures such as building; houses and bridge are built at around Gerik-Jeli highway. This would help to reduce the risk of the building or bridges to collapse.

1.4 Justification

The early research done by Shuib, Hj Taib, & Abdullah (2006) and Rafek & Komoo (1989) at Gerik-Jeli highway do not adequately explain the stability of the rock slope. The previous methodology employed in the study area only provide identification of the mode of rock slope failure. The detail of the potential of rock slope failure is not provided. The more detail survey on the stability of rock slope is required.

1.5 Objective

1. To produce geological map of study area with the scale of 1:25000 at Tasik Pergau, Jeli. The information of lithology, geomorphology, stratigraphy and structural geology obtained from 25 km^2 study area are used to produce geological map.

2. To determine the value of Slope Mass Rating of rock slopes that have potential to fail. The value of Slope Mass Rating is determined through the kinematic analysis and Rock Mass Rating of rock slope. The value of Slope Mass Rating is calculated by adding together the rating value of the parameters of Rock Mass Rating; rating value of the relationship between dip and dip direction of discontinuities and slope face; and rating value of the excavation method of slope.

1.6 Scope of study

The study will involve the geological mapping at the study area. The lithology, structure, dimension and weathering grade of the outcrops at the study area will be recorded as well as the geomorphology, elevation and location of the outcrop. The rock samples collected from field will be thin-sectioned for the use of petrographic analysis.

This study will use the stereonet-based kinematic analysis to identify the mode of rock slope failure at the study area. The kinematic analysis is based on the stereographic projection analysis. It will analyse the potential for the various modes of rock slope failures such as plane, wedge, and toppling failures that occur due to the presence of unfavourably oriented discontinuities. The study will also calculate the Slope Mass Rating (SMR) value when the mode of slope failure is identified. SMR

value will be calculated by adding the rating values for the parameters of Rock Mass Rating (RMR) with the rating value for the relationship between joints and slope faces, known as adjusting value of joint. The study will acquire the parameters of Uniaxial Compressive Strength (UCS) of rock mass, Rock Quality Designation (RQD), spacing of discontinuities, groundwater condition, condition of discontinuities, dip and dip direction of slope face and discontinuities to find the value of SMR.

1.7 Significance of study

The stability of natural or man-made rock slopes is a significant subject that will be assessed by civil and mining engineer because the rock slope failure will result in a significant cost and serious personnel safety problem to the operators. In these situations, the slope stability assessment becomes crucial for the engineering work and for the economy. Many areas such as road construction, dam installation and mine excavation require the stability analysis of rock slope. The finding from this study will provide the detailed information to allow the engineer to select the proper and safe area for the road construction, mine excavation and dam installation purposes. The study will give the exposure of the engineering geology of the study area for future research.

1.8 Study Area

The study area of this research is located in Tasik Pergau, Jeli Kelantan. Kelantan is positioned in the northeast of Peninsular Malaysia. The border of Kelantan are Terengganu that is due to the southeast; Perak is due to the west; Narathiwat Province of Thailand is due to north and Pahang is due to south. Pergau is situated at the Jeli district of Kelantan. Tasik Pergau is one of the attractive places for tourist in Pergau. The lakes are man-made lakes, due to the construction of the respective hydroelectric dams at Temenggor and Pergau. The square size of the study area at Pergau is 25km^2 with the coordinate boundary located at 5°38'59.61"N, 101°40'15.09"E; 5°38'59.61"N, 101°42'58.14"E; 5°36'17.65"N, 101°42'58.14"E and 5°36'17.65"N, 101°40'15.09"E. The highest elevation of the study area is around 860m whereas the lowest elevation is around 280m.

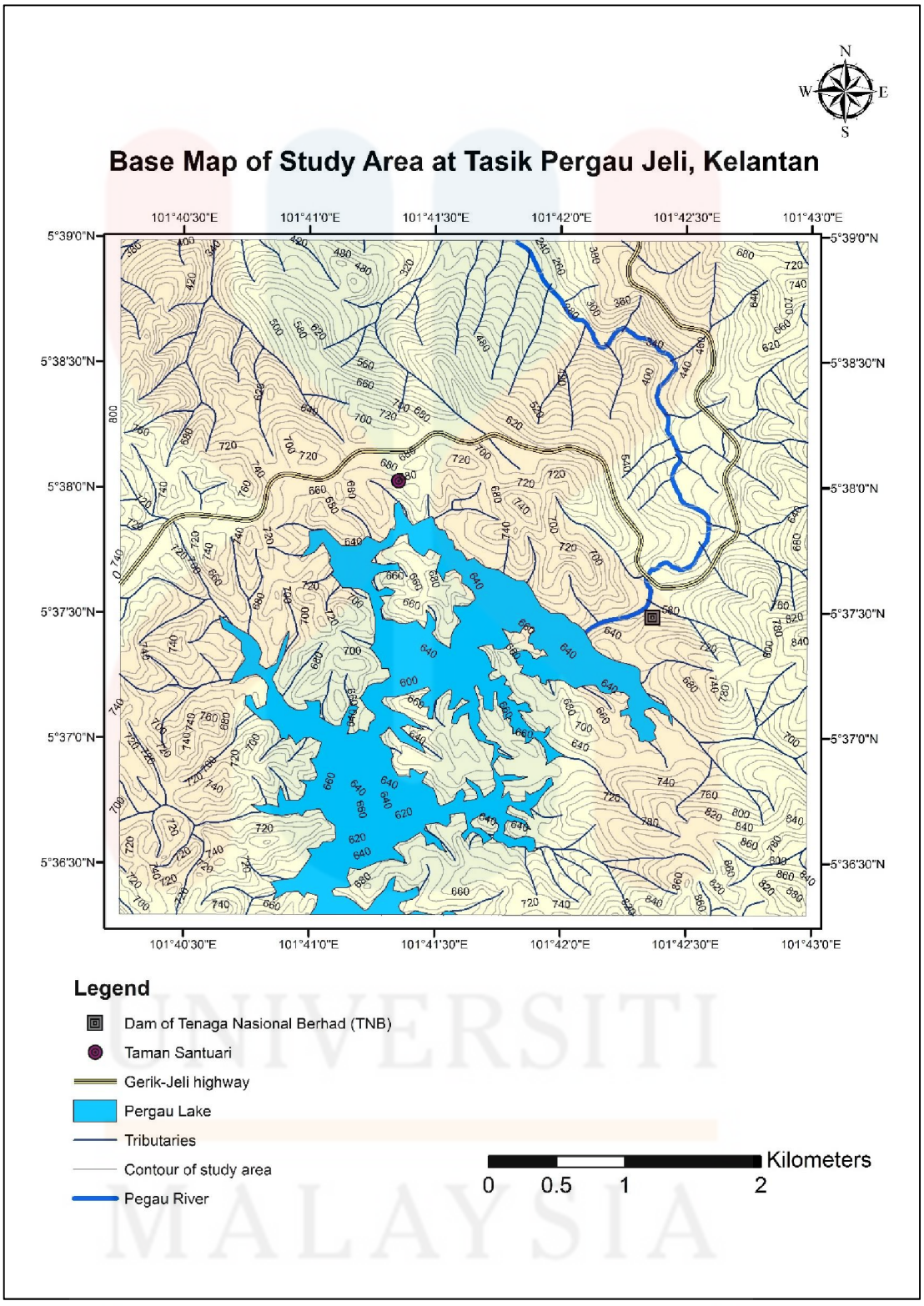

Figure 1.1: Base map of study area at Tasik Pergau, Jeli Kelantan

CHAPTER 2

LITERATURE REVIEW

2.1 Introduction

This chapter will discuss the geology of study area at Kelantan, including the regional geology, geological setting, stratigraphy and structural geology. This chapter will also discuss the kinematic analysis of rock slope, discontinuity survey, rock mass rating and slope mass rating.

2.2 Regional Geology

The study conducted by Hutchinson (1977) in Peninsular Malaysia resulted in the deduction, which divided the granitoid rocks in Peninsular Malaysia into three belts based on the lithology and petrochemistry of granite that are the Main Range granite, Central Belt and Eastern Belt granite. The Main Range granite composes of S-type, ilmenite series granitoid, which intruded into the Paleozoic host rocks during the Permo-Triassic Period. The Central Belt granite composes of S-type, ilmenite series granitoid of Triassic age with minor intrusion of Cretaceous I-type, magnetite series granitoid. The Eastern Belt granite composes of I-type, magnetite series granitoid and intrudes into the Paleozoic host rocks during Permo-Triassic Period.

Cobbing *et al*. (1986) had divided the granitic rocks into two provinces which are the Main Range granite and Eastern granite, with the assumption that the Central Belt granite and Eastern Belt granite are similar. The Main Range granite has been

regarded to be constituted exclusively of S-type granite of mainly Triassic age. In contrast, the Eastern province granite is dominated by I-type with subordinate compositional overlap S-type granites of Permo-Triassic age. Small I-type plutons of Cretaceous age are present in the central part of Peninsular Malaysia.

The recent detailed geology of Kelantan was compiled by (Hutchison, C.S. & Tan, D.K. (Department of Geology, 2009) in Geology of Peninsular Malaysia 2009. The stratigraphy of Kelantan can be chronologically divided into era of Paleozoic, Mesozoic, and Cenozoic by sedimentary rocks, metasediments, metamorphic rocks and granitic rocks. Kelantan granitic rocks can be divided into two. First main granite body is located in the west side and stretch along western Kelantan until the boundary of Perak and Pahang. The second granite is located on the northeastern border of Terengganu. It is located within the boundary range. Both Main Range granite and Boundary Range granite are generally of Middle age. The study area is located at the northwestern part of Kelantan that belongs to the geological setting of Stong Complex as shown as in Figure 2.1.

2.3 Geological Setting

The Stong Complex consists of varieties of plutonic and metamorphic rocks that underlie Gunung Stong and its environs in the northwestern part of Kelantan (D. Santokh, et al, 1984).

Santokh (1984) had mapped the geology of the eastern part of the Stong Complex and concluded the essential part of the complex where it is a granitic core that was part of magmatic association with large inclusion of metasediments.

MacDonald (1967) had made the summary in his memoir of North Kelantan that the element on which the Stong Complex formed was described as an "Injection Complex" which have a great complexity and was the protrusion from the Main Range granite batholith. He, however, stated that there is a difference in term of granitic element of the Stong Complex from the Main Range granite batholith.

Gobbett & Tjia (1973) reported that the eastern part of the complex consists of acid gneiss and other high grade of metamorphic rock. They later stated that the eastern margin of the complex was faulted by Gua Musang Formation greenschist facies.

Summary account for the geology of the Stong Complex (Santokh, 1984) conclude that the Stong complex is made up of three elements that are named as Berangkat Tonalite, Kenerong Granite and Noring Granite in order to the youngest. Noring Granite as shown in Figure 2.1 extends continuously from Gunung Berangkat until the border of Thailand of the East-West highway. Kenerong Granite is present in narrow strip of eastern margin but along Sungai Balah and most of the west side of Stong Complex has the characteristics of megacrystic pink alkali feldspar.

Ghani (2006) stated that the location of Stong Complex is at the north and importantly it composed of three plutonic components, which is Berangkat Tonalite, Kenerong Microgranite and Noring Granite. The Noring Granite is undeformed granite different from the older granite of Berangkat and Kenerong. It is also the largest component of the Stong Complex. Distinct feature of Noring would be megacryst pinkish colour of alkali feldspar. The granite mineral composition would be alkali feldspar, plagioclase, biotite, hornblende, sphene, apatite, allanite, epidote, zircon, magnetite, pyrite and ilmenite.

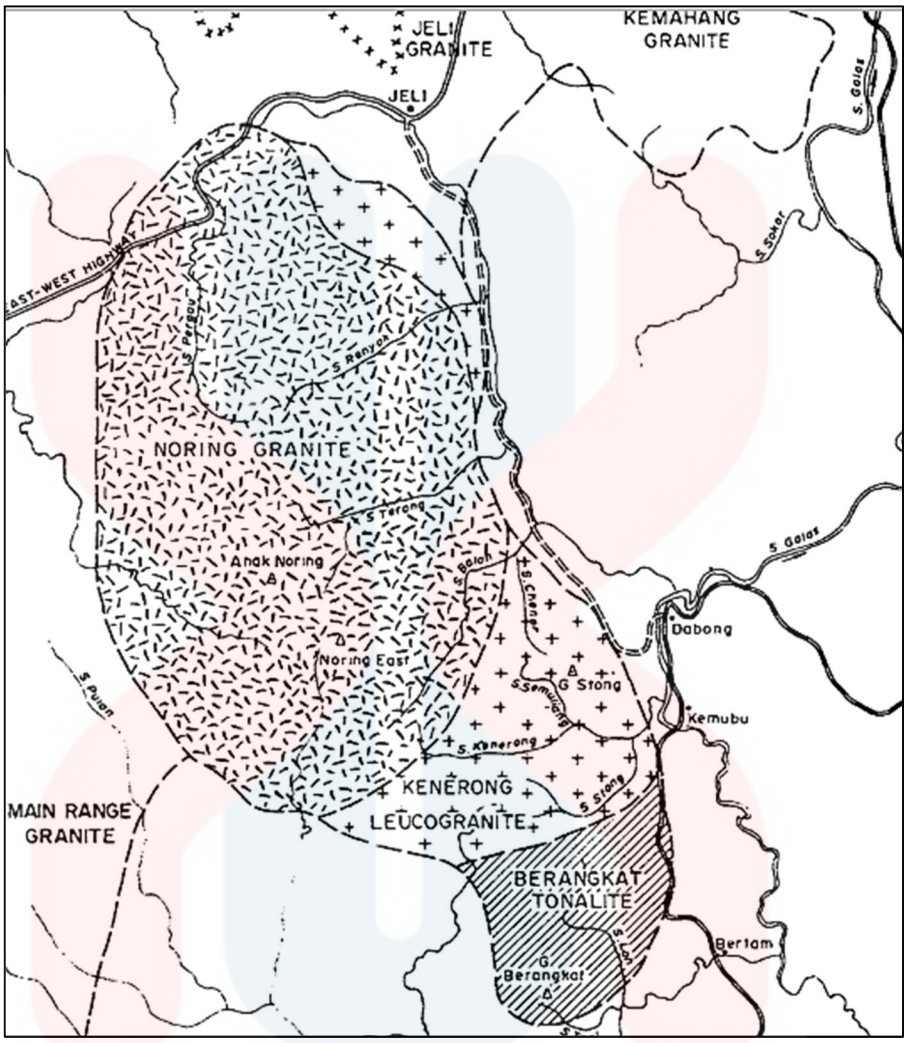

Figure 2.1: Distribution of various granite units based upon aeromagnetic and spectrometric data (Santokh, 1984).

2.4 Stratigraphy

Stratigraphy that exposed the study area, Tasik Pergau, Jeli Kelantan is Noring Granite.

Noring Granite detailed textural and petrographical study was presented by Azman (2000). Based on his study, the granite major mineral phases are alkali feldspar, plagioclase, quartz, biotite and hornblende. Accessory mineral phase present are such ilmenite, pyrite, magnetite, zircon, epidote, allanite, apatite and sphene.

Plagioclase crystal size in Noring Granite is euhedral to subhedral in shape. Other features such as inclusion and regular zoning are present with with simple and polysynthetic twinning. Plagioclase in in some place has been replaced by microcline which indicates plagioclase crystal has been crystallised earlier than microcline. Vance (1969) concluded that this type of feature could only be produced in magmatic environment.

Noring Granite distinct large alkali feldspars, give the granitic rock distinct porphyritic feature in hand specimen. Main types of alkali feldspar found are from perthitic orthoclase, which shows euhedral in shape in hand specimen but in thin section appear to be very irregular in shape. Twinning of alkali feldspar is simple and small oriented euhedral inclusions, oriented subparallel to the crystal faces of granite host alkali feldspar draws conclusion that it is a magmatic minerals.

Mantling of plagioclase over orthoclase is present formed by mantled feldspar (Azman, 2000). Mymerkite and granophyric intergrowths are present in plagioclase and orthoclase but are not common. Quartz mineral shows mostly anhedral in shape and occurs as sub-grains.

Accessory mineral of Noring Granite is dominantly composed of sphene. There are two types of sphene in the rock. First is euhedral to subhedral in shape in shape where found scattered or associated with hornblende-biotite clots. Shown faint pleochroism from brown to pale brown and this type can be seen in hand specimen. Second type of sphene is anhedral in shape and occurs in biotite. Opaque mineral found in this Noring Granite rock is magnetite.

Bedrock found in the area of the dam site consists predominantly of coarse grained biotite granite with some porphyry dikes. The bedrock is obscured by residual soil and alluvium on the dam abutments and by localized alluvium upstream of the dam site.

Petrographic descriptions of granite from exploration drill holes at the dam site are granite that is generally coarse grained and porphyritic consisting of pink orthoclase feldspar laths, pale grey to white plagioclase feldspar laths, clear quartz and dark green to brown biotite and amphibole. The general appearance is grey white with pink molting. In some drill holes this granite has undergone chemical alteration associated with hydrothermal activity.

2.5 Structural Geology

Peninsular Malaysia was formed when the Sinoburmalaya block to the west collides with the Eastmal-Indosinia block to the east. The Bentong-Raub Suture that can be traced northward into Thailand and southward into the Banka and Billiton Islands represents the zone of collision. This collision accompanied by the major tectonic event during Late Triassic has resulted in rock deformation in the Malay-Thai Peninsula.

The folding of pre-orogeny sedimentary successions in the study area forms a series of synclines and anticlines. The folding is characterised by asymmetric, tight and open folds that cause the repeated and overturn sequence in the older sedimentary rock. The NW-SE and N-S trending fold axes are sub-parallel to the long axis of the Malay Peninsula and most of the bedding planes dip towards the east with various dip angles.

The faulting structures are also widespread throughout the study area. Due to the thick cover and deep tropical weathering, fault zones are seldom exposed at more than a few places along their traces. Fault are generally varies in width characterised by fractured, sheared, or mylonitised rocks. There are several faults which are mainly of strike-slip and normal faults, trending N-S, NW-SE and NE-SW. The major faults are Long-Kolok fault (NE-SW), Pergau fault (NE-SW), Kalai-To Mo fault (N-S) and Ka To-Bu fault (MacDonald, 1955).

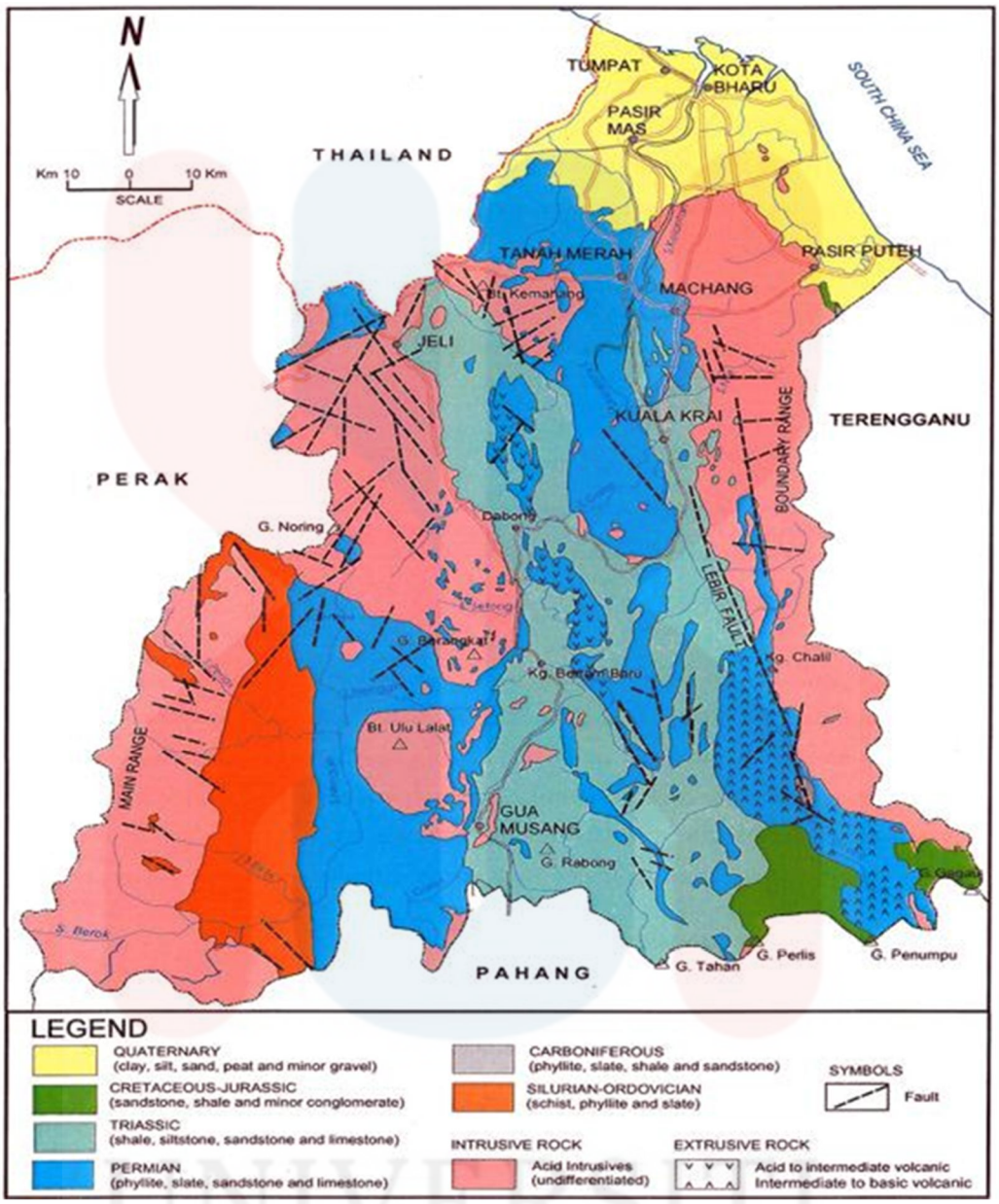

Figure 2.2: Geological map of Kelantan by (Hutchison, C.S. & Tan, D.K. (Department of Geology, 2009)

2.6 Rock Slope Stability Assessment

The rocks can be classified into three types, which are igneous rock, sedimentary rock, and metamorphic rock. These three types of rocks are differentiated by their composition, texture and their formation. The weathering and tectonic processes can change the physical and chemical composition of the rock. Due to this processes, the discontinuities set including joints, faults, cracks, lineation and cleavage developed in the rock. The presence of discontinuities in the rock will affect the strength of the rock to a great extent. The deformation of rock joints have a significant effect on the total deformation of rock mass encountered in rock engineering practice. Joints and joint fillings contribute to cause of instability in man-made rock slope or natural rock slope. The characteristic of discontinuities that are related to the instability of the rock slope include orientation, persistence, roughness, and infilling (Wyllie & Mah, 2004).

Rafek & Komoo (1989) had conducted detailed discontinuities survey along the Gerik-Jeli highway and deduced that the rock slope failure is affected by the structure and geometry of the slope. The instability of rock slope along the Gerik-Jeli highway is highly controlled by the unfavourable orientation of discontinuities with respect to the slope face. Shuib, Hj Taib, & Abdullah (2006) added that the metamorphic rock and metasediment along the highway are highly subjected to mechanical weathering and chemical decomposition which resulting in unstable condition of the rock slope. The unstable condition of the rock slope is aggravated by the presence of numerous discontinuities. Discontinuities that dip about the same angle as the dip of the slope constituting the rock slope failure prone condition. Thus, structural control process is the dominant factors that give rise to the plane, wedge and toppling rock slope failure.

2.7 Effect of Discontinuity on Slope Stability

The persistence, spacing, infilling and roughness are significant factors influencing the stability of the slope. The orientation is the prime geological factor that controls the stability of the slope. The Figure 2.3 represents three slopes excavated in a rock mass containing joint set J1 and joint set J2. J1 dips about 45^{o} out the face whereas J2 dips into the face at about 60^{o}. In Figure 2.3(a), the plane failure is probably to occur due to the greater persistence of J1 than the slope height and widely spaced of J1. Both J1 and J2 of slope at Figure 2.3(b) are closely spaced and have low persistent. Therefore, the slope is considered stable. In Figure 2.3(c), toppling failure may exist because J2 is persistent and closely spaced, forming series thin slabs dip ping into the face (Wyllie & Mah, 2004).

2.8 Identification of modes of slope instability

Based on Wyllie & Mah (2004), slope failure can be classified into major 4 types as shown in Figure 2.4. The different type of slope failures are associated with different geological structures. The modes of slope instability can be distinguished by stereo plot. When accessing the mode of instability, the slope face must be included in the stereo plot since sliding can only occur as the result of movement towards the free face created by the cut. In identifying the modes, the structural data from the field will be plotted on the stereonet, number of significant pole concentrations may be present. It is important to identify those pole concentrations that represent potential failure plane and eliminate those structures that are not involved in slope failures. Markland (1972) had developed those tests for identifying the important pole concentration.

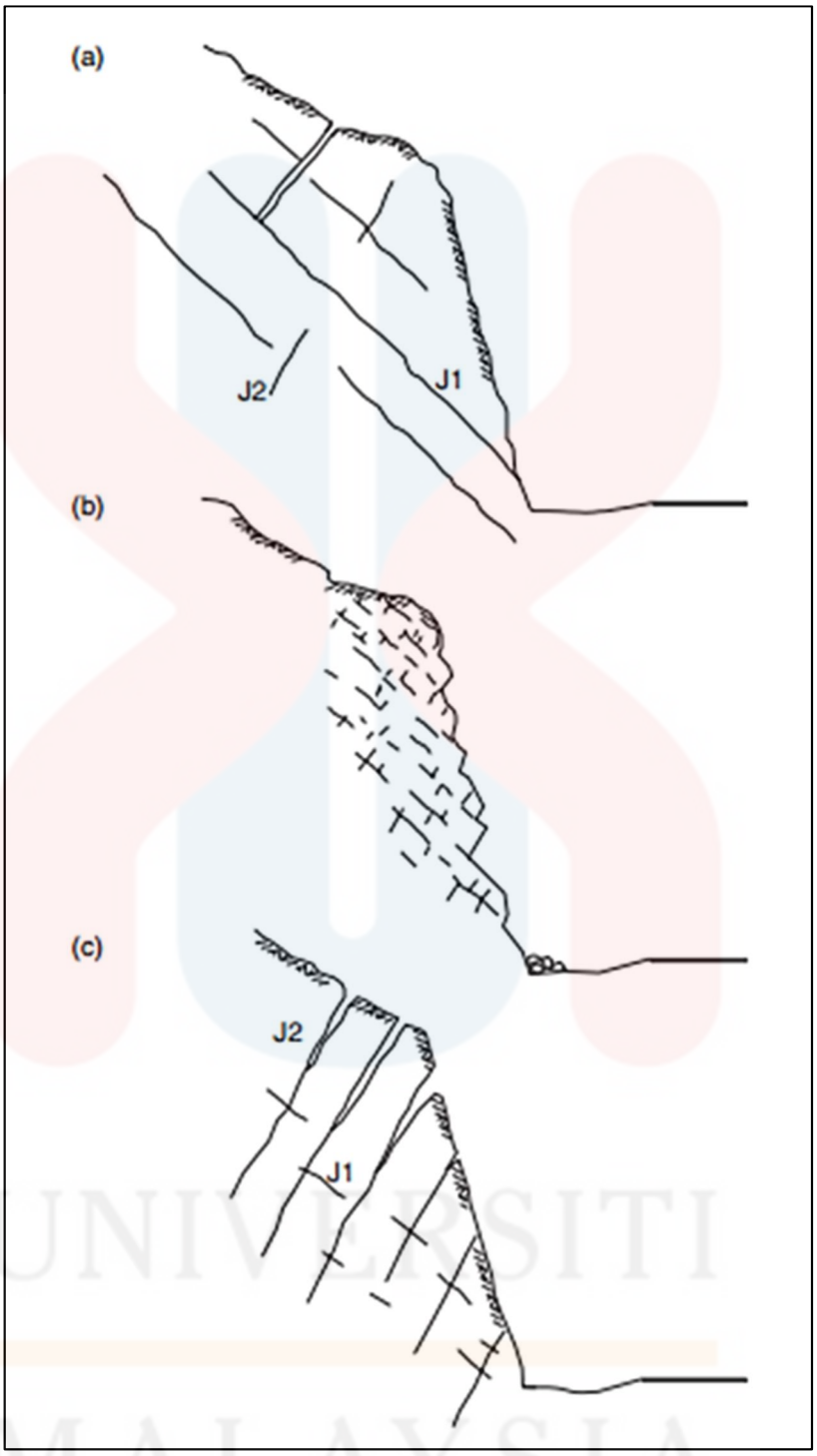

Figure 2.3: Effect of joint on the stability of slope (Wyllie & Mah, 2004).

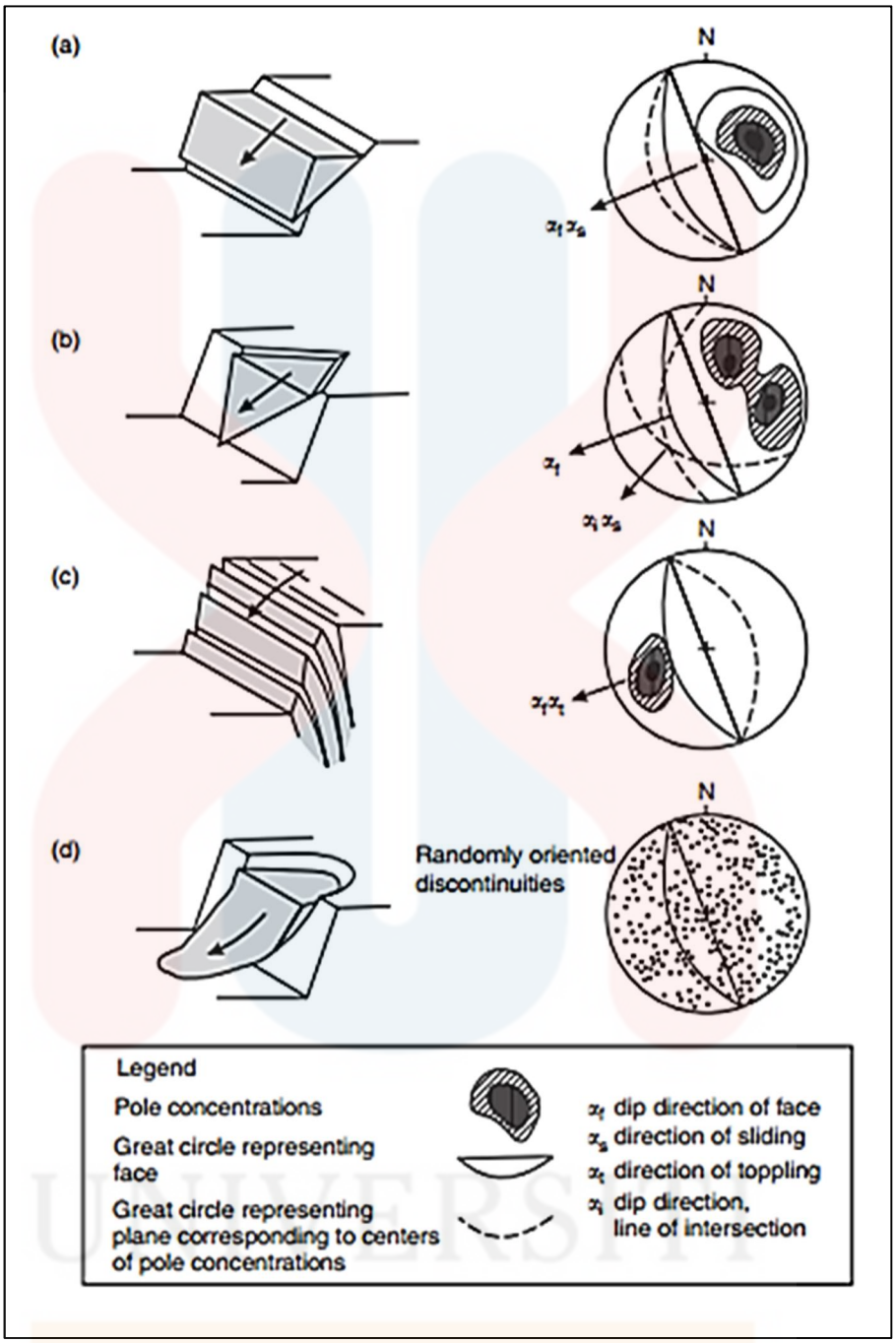

Figure 2.4: Main types of block failures (a) Plane; (b) Wedge; (c) Toppling; (d) circular (Wyllie & Mah, 2004).

In Figure 2.5(a), the plane and wedge failure may occur when the dip of sliding plane for the case of plane failure or the plunge of intersection of plane for the case of wedge failure, be less than the dip of the slope face. ($\psi_i < \psi_f$). That is, the sliding surface "daylight" in the slope face. The test can also differentiate between sliding of wedge on two planes along the line of intersection, or along only one of the planes

such that a plane failure occur. In Figure 2.5(b), the wedge will slide on both planes if the dip directions of the two planes lie outside the included angle between α_i (trend of intersection line) and α_f (dip direction of face). If the dip direction of one plane A as shown in Figure 2.5(c) lies within the included angle between α_i and α_f, the wedge will slide on only that plane.

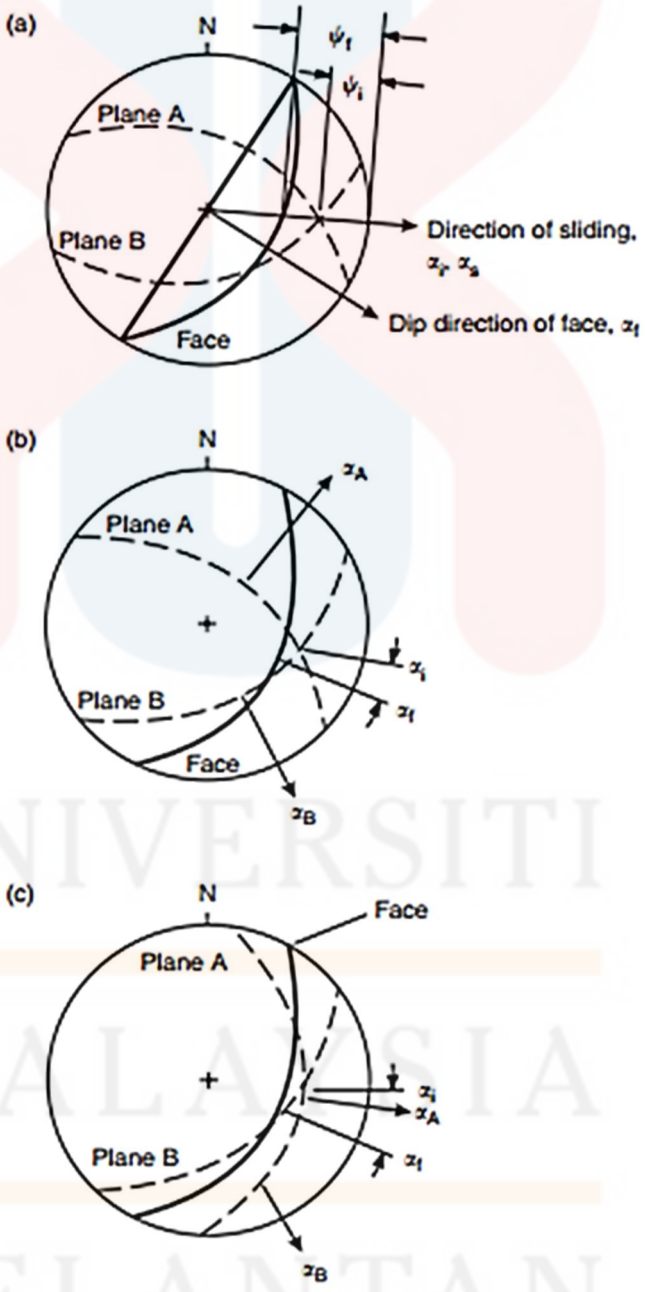

Figure 2.5: Identification of plane and wedge failure on stereonet (Wyllie & Mah, 2004).

2.9 Kinematic analysis

Kinematic analysis is employed to examine the direction in which a block will slide and give an indication of stability conditions when the type of block failure has been identified on the stereonet. Kinematic analysis is carried out under stereographic projection. The analysis on the stereonet gives a good indication of stability conditions but it does not account for external forces such as water pressures or reinforcement comprising tensioned rock bolts, which can have a significant effect on stability. In Figure 2.6, an example of kinematic analysis is shown which contains three sets of discontinuities AA, BB, and CC. The potential for these discontinuities to result in slope instability depends on the dip and dip direction relative to the slope face (Wyllie & Mah, 2004).

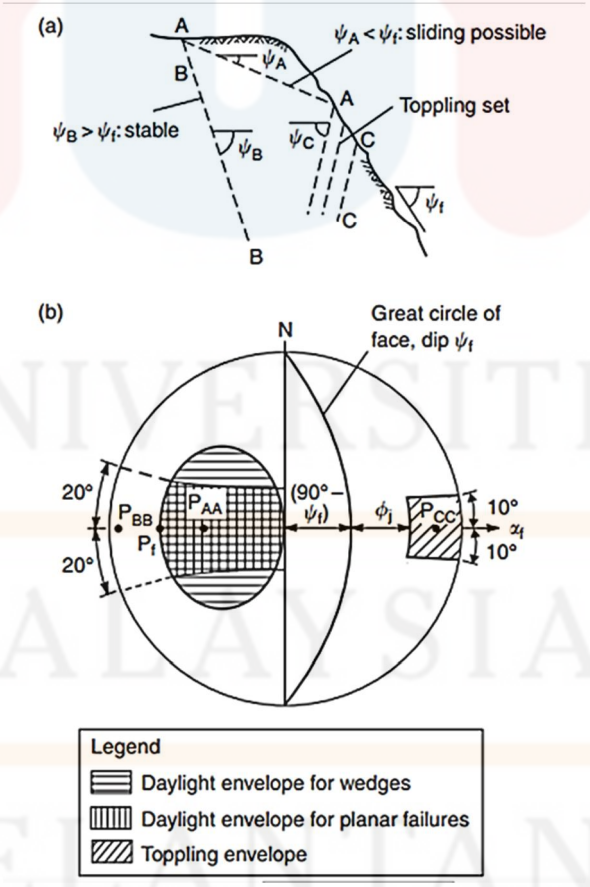

Figure 2.6: Kinematic analysis of blocks of rock in slope: (a) Discontinuity set in slope; (b) daylight envelope on equal area stereonet (Wyllie & Mah, 2004).

2.9.1 Kinematic analysis of plane failure

In Figure 2.6, the planar block is potentially unstable because plane AA dips gentler angle than the slope face ($\psi_A < \psi_f$) which means plane AA daylights on the face. Plane BB dips steeper than the dip of slope face and does not daylight ($\psi_B > \psi_f$). Thus, sliding is not possible on plane BB. Plane CC dips into the face and sliding is impossible to occur on these plane, even though toppling failure is possible. The poles of discontinuities sets and the pole of slope face are plotted on the stereonet. The slope is potentially unstable when the poles of the plane lie inside the pole of slope face or termed daylight envelope. The stability of the slope is also influenced by the dip direction of the discontinuity set. If the dip direction of the discontinuity differs from the dip direction of face by more than about 20^o, the plane sliding is not possible. The block will be stable if $|\alpha_A - \alpha_f| > 20^o$ because under these condition, thickness of intact rock will increase at one end of the block which will have sufficient strength to resist failure. On stereonet, this restriction on the dip direction of the planes is shown by two lines defining dip direction of ($\alpha_f + 20^o$) and ($\alpha_f - 20^o$). These two lines designate the lateral limits of the daylight envelope on Figure 2.5(b).

2.9.2 Kinematic analysis of wedge failure

In the kinematic analysis of wedge failure, the pole of the line of intersection of the two discontinuities is plotted on the stereonet. The wedge sliding is possible if the pole daylights on the face which is ($\psi_i < \psi_f$). The direction of wedge sliding is less restrictive than the direction of plane sliding because there are two planes to form release surfaces. The daylight envelope for the pole of line of intersection is bigger than those in plane failures.

2.9.3 Kinematic analysis for toppling failure

Toppling failure occurs when the dip direction of the discontinuities dipping into the face within about 10^o of the dip direction of the face so that a series of slabs are formed parallel to the face. Besides that, the dip of discontinuities must be steep enough for interlayer slip to occur. The slip of toppling will only occur if the direction of applied compressive stress is at angle greater than friction angle of the face, φ_j. The direction of the major principal stress in the cut is parallel to the dip angle of face, ψ_f, so interlayer slip and toppling failure will occur on plane with dip ψ_p when the following condition are met,

$$(90^o - \psi_f) + \varphi_j < \psi \tag{2.1}$$

The envelope defining the orientation of these planes lies at the opposite side of the stereonet from the sliding envelopes (Goodman & Bray, 1976).

2.9.4 Friction cone

Kinematic analysis using friction core is carried out by assuming the shear strength of the sliding surface comprises only friction without cohesion. In Figure 2.7(a), the block at rest on an inclined plane with friction angle of φ between the block and plane. The vector of force normal to the plane must lie within the friction cone at condition of resting. The pole to the plane is in the same direction as the normal force when the only force of gravity acting on the block. Therefore, the block will be stable when the pole lie within the friction angle.

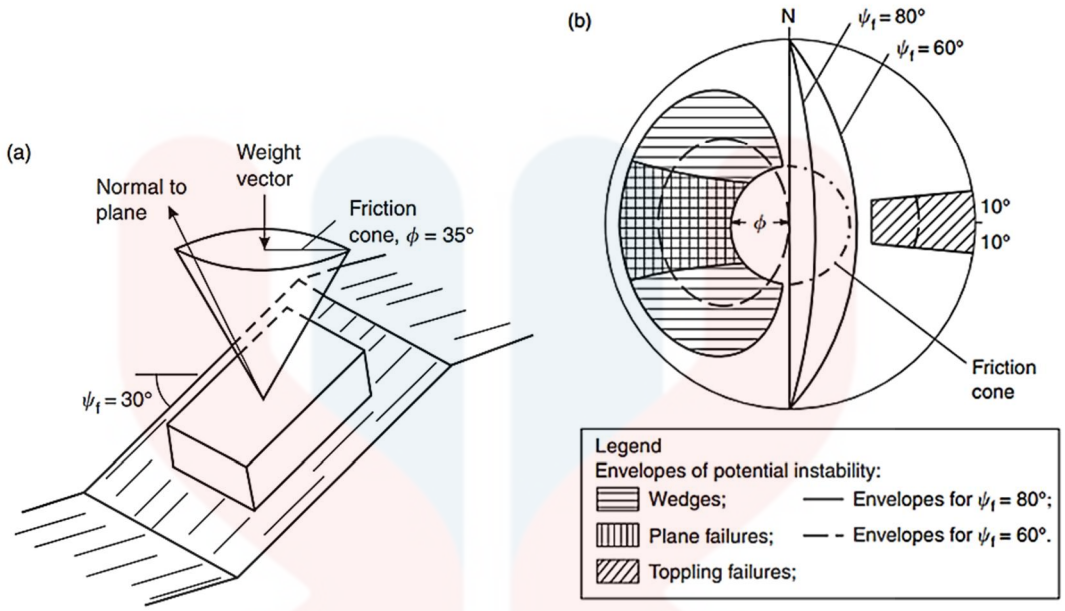

Figure 2.7: Combined kinematic and simple stability analysis using friction cone concept: (a) friction cone in relation to block at rest on an inclined plane; (b) stereographic projection of friction cone superimposed on "daylighting" envelopes (Wyllie & Mah, 2004).

2.10 Rock Mass Rating (RMR)

Based on the study of engineering rock mass classification, Bienaswki (1989) had developed RMR system, which is applied to the case study of tunnel, chamber, slope, foundation and mine. RMR system had been modified several times but the principal despite of the changes remains the same. The rock mass rating system (RMR) or Geomechanics Classifications was developed by Bienaswki since 1972 and was modified over the years as more case histories become available. There are parameters that are used to classify rock mass using RMR which are uniaxial compressive strength of rock (UCS), RQD, spacing of discontinuities, condition of discontinuities, groundwater condition and orientation of discontinuities. The rock mass ratio RMR is determined with the help of fifth parameters available included UCS (score 0-15), RQD (score 3-20), condition of discontinuities (0-30), groundwater condition (0-15),

and spacing of discontinuities (5-20). By totalling up the scores of the rock variables, the RMR value can be calculated and the rock quality is determined. Table 2.1 shows the RMR system giving the rating for each of the parameter listed above. These rating are summed to give a value of RMR.

2.10.1 Rock Quality Designation (RQD)

The rock quality index RQD is defined as the percentage of scanline or borehole core that consists of intact lengths over 0.1 m (Deere & Deere, 1988). The correct procedure for measuring RQD is illustrated in Figure 2.8. Palmstrom (1982) has suggested that when the core is unavailable, the RQD may be estimated from the number of joints per unit volume, in which the number of joints per meter for each joint set is added. The conversion for clay-free rock masses is,

$$RQD = 115 - 3.3J_v \tag{2.2}$$

where, J_v represents the total number of joints per cubic meter.

Table 2.1: RMR classification parameters and their rating (Bienaswki, 1989).

Parameters			Range of Values						
1	Strength of Intact Rock Material	Point-load Strength index	>10 Mpa	4 - 10 MPa	2 - 4 Mpa	1 - 2 Mpa	For this low range Uniaxial compressive test is preferred		
		Uniaxial compressive strength	>250 Mpa	100 - 250 MPa	50 - 100 MPa	25 - 50 MPa	5 - 25 Mpa	1 - 5 MPa	<1 MPa
	Rating		15	12	7	4	2	1	0
2	Drill core Quality RQD		90% - 100%	75% - 90%	50% - 75%	25% - 50%	<25%		
	Rating		20	17	13	8	3		
3	Spacing of discontinuities		>2 m	0.6 - 2.0 m	200 - 600 mm	60 - 200 mm	<60 mm		
	Rating		20	15	10	8	5		
4	Condition of discontinuities	Discontinuity length (persistence)	<1 m	1 - 3 m	3 - 10 m	10 - 20 m	>20 m		
		Rating	6	4	2	1	0		
		Separation (aperture)	None	<0.1 mm	0.1 - 1.0 mm	1 - 5 mm	>5 mm		
		Rating	6	5	4	1	0		
		Roughness	Very rough	Rough	Slightly rough	Smooth	Slickensided		
		Rating	6	5	3	1	0		
		Infilling (gouge)	None	Hard filling <5 mm	Hard filling >5 mm	Soft filling <5 mm	Soft filling >5 mm		
		Rating	6	4	2	2	0		
		Weathering	Unweathered	Slightly weathered	Moderately weathered	Highly weathered	Decomposed		
		Ratings	6	5	3	1	0		
5	Ground water	Inflow per 10 m tunnel length (l/m)	None	<10	10 - 25	25 - 125	>125		
		(Joint water press)/ (Major Principal σ)	0	<0.1	0.1 - 0.2	0.2 - 0.5	>0.5		
		General conditions	Completely dry	Damp	Wet	Dripping	Flowing		
	Rating		15	10	7	4	0		

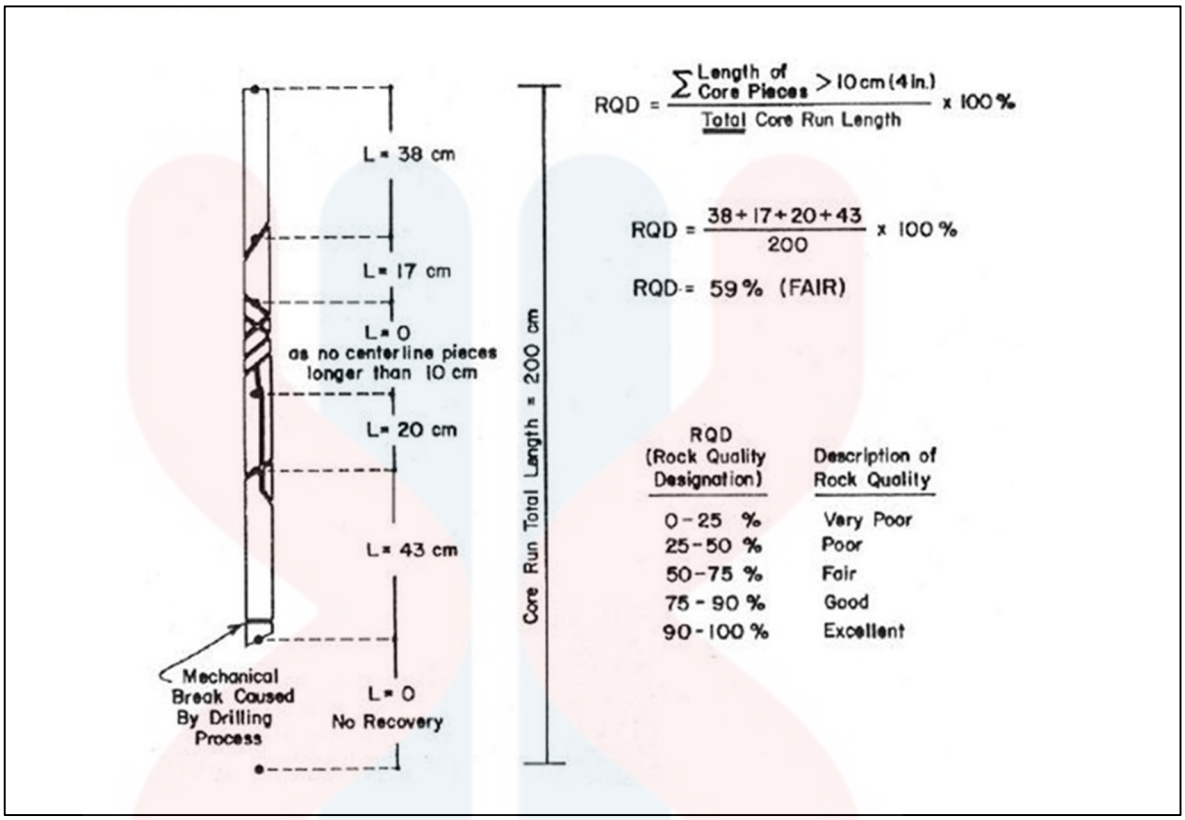

Figure 2.8: Procedure for measurement and calculation of rock quality designation (Deere & Deere, 1988)

2.10.2 Uniaxial Compressive Strength (σ_c)

Highest strength limit of the rock mass termed uniaxial compressive strength. ISRM (1978) states that the compressive strength of rock mass is the significant component of shear strength and deformability. Uniaxial compressive strength is given as the mean strength rock materials in which the rock samples are taken away from the fault, joint, discontinuities or weathered rocks. The classification of uniaxial compressive strength of rock suggested by ISRM (1978) is shown in Table 2.2.

Table 2.2: Classification of uniaxial compressive strength (ISRM, 1978)

Soil	$\sigma_c < 0.25$ MPa
Extremely low strength	$\sigma_c = 0.25$ - 1 MPa
Very low strength	$\sigma_c = 1$ - 5 MPa
Low strength	$\sigma_c = 5$ - 25 MPa
Medium strength	$\sigma_c = 25$ - 50 MPa
High strength	$\sigma_c = 50$ - 100 MPa
Very high strength	$\sigma_c = 100$ - 250 MPa
Extremely high strength	$\sigma_c > 250$ MPa

The uniaxial compressive strength can be tested in the field or laboratory. Schmidt hammer rebound test is one of the field test that can be used to determine the uniaxial compressive strength. The test can be performed on the surface of rock materials obtained from freshly broken rock. In practice, the rebound number from Schmidt hammer test ranged from 10 to 60. The lowest number of rebound means the rock is the weakest and has lowest compressive strength where $\sigma_c \leq 20$MPa. The highest rebound number indicates that the rock is strong and has highest uniaxial compressive strength where $\sigma_c \geq 150$MPa. When the rebound number and rock density are obtained, the correlation can be made with correlation chart suggested by ISRM (1978) in Figure 2.9. The rebound number depends on the direction of Schmidt hammer applied on wall of rock mass. The rebound number is minimum when the hammer applied vertically downwards to the surface of rock. The rebound number is maximum when it is vertically upwards. Therefore, the correction is made based on the table shown in Table 2.3 (ISRM, 1978).

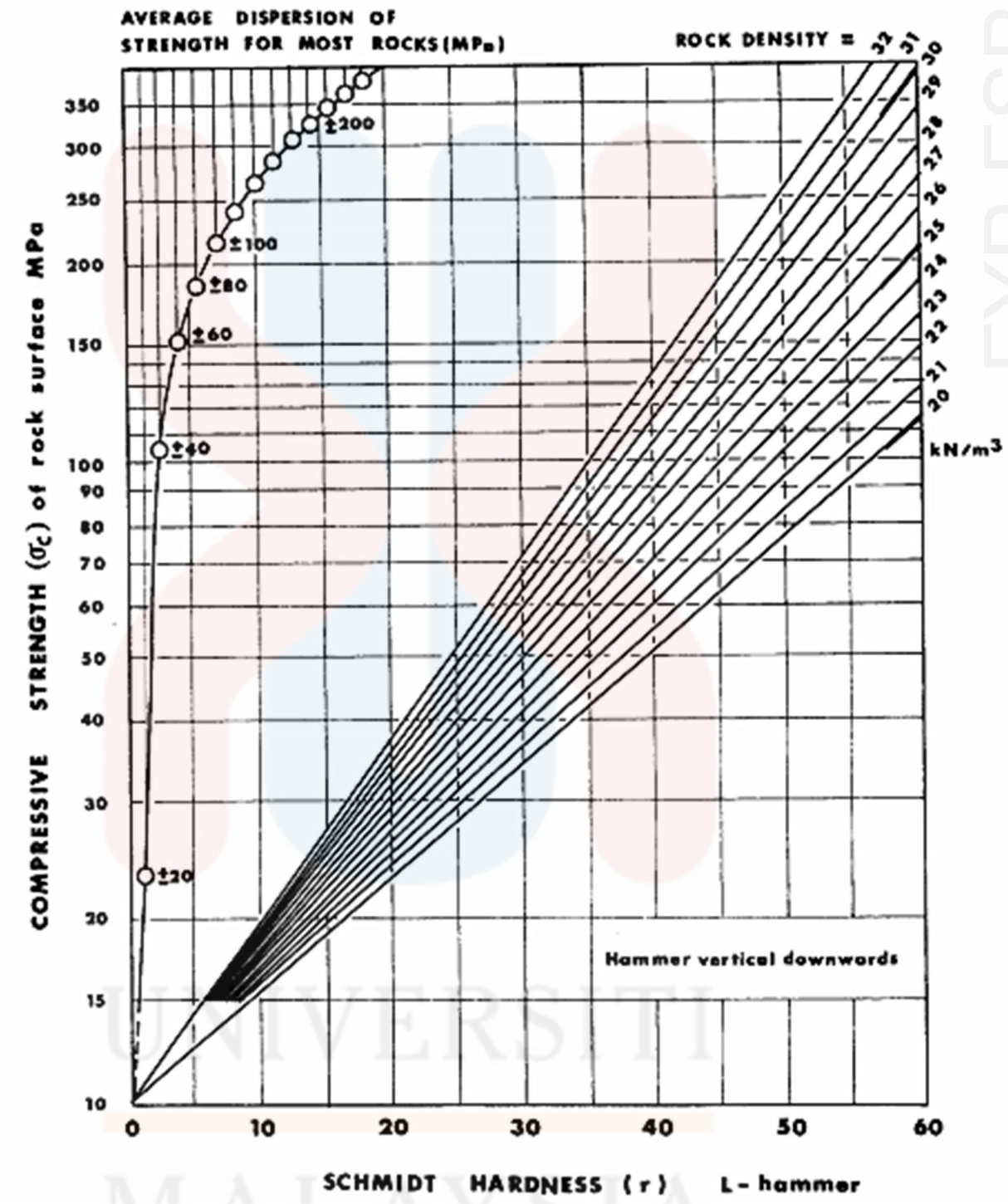

Figure 2.9: Correlation chart for Schmidt hammer, relating rock density, compressive strength and rebound number (ISRM, 1978)

Table 2.3: Correction for reducing measured Schmidt hammer rebound when the hammer is not used vertically downwards (ISRM, 1978)

Rebound r	Downwards $\alpha = -90^\circ$	Downwards $\alpha = -45^\circ$	Upwards $\alpha = +90^\circ$	Upwards $\alpha = +45^\circ$	Horizontal $\alpha = 0^\circ$
10	0	−0.8	---	---	−3.2
20	0	−0.9	−8.8	−6.9	−3.4
30	0	−0.8	−7.8	−6.2	−3.1
40	0	−0.7	−6.6	−5.3	−2.7
50	0	−0.6	−5.3	−4.3	−2.2
60	0	−0.4	−4.0	−3.3	−1.7

2.10.3 Condition of Discontinuities

The condition of discontinuities include roughness, aperture, persistence and infilling material of discontinuity. All these parameters can contribute to the determination of the value of RMR and SMR.

(a) Roughness is an important parameter in controlling the shear strength of rock discontinuities. Surface roughness of discontinuity can be characterized by waviness and unevenness Waviness is a large scale of undulations, which tends to cause dilation during shear displacement whereas unevenness is a small scale of roughness that tends to be damaged during displacement unless the discontinuity wall is high in strength. A simple and time-saving method to evaluate the roughness of the surface is by evaluating through the roughness profile provided by ISRM (1978) as shown in Figure 2.10

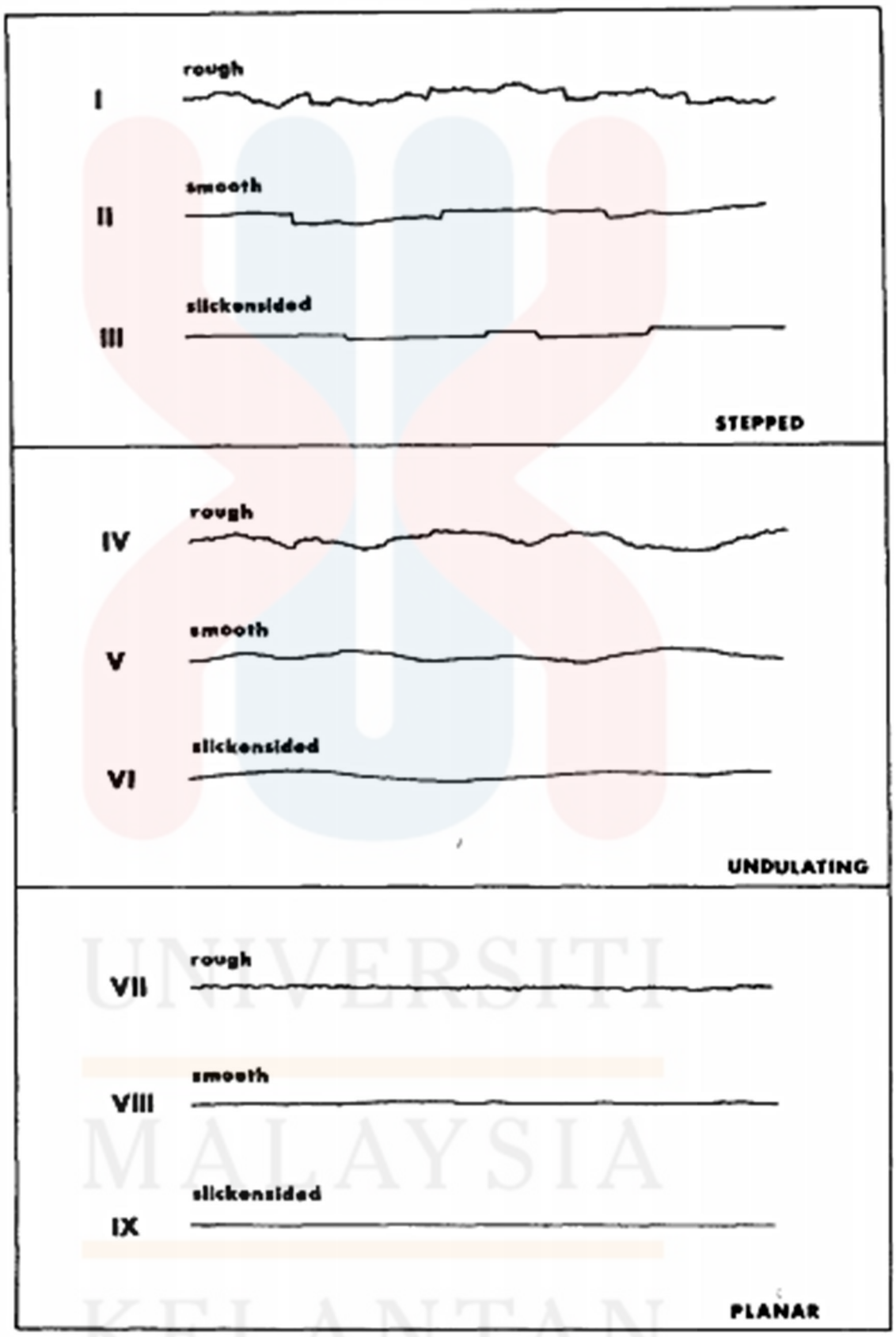

Figure 2.10: Roughness profile and suggested nomenclature (ISRM, 1978)

(b) Aperture is the perpendicular distance that separate the adjacent rock walls of an open discontinuity in which the spacing is filled with water or air. The shear movement of discontinuities, tensile opening or solution by water can cause the aperture. The sizes of the apertures are categorized by ISRM (1978) in the Table 2.4.

Table 2.4: Description of aperture (ISRM, 1978)

Aperture	Description	
<0.1 mm	Very tight	"Closed" features
0.1–0.25 mm	Tight	
0.25–0.5 mm	Partly open	
0.5–2.5 mm	Open	"Gapped" features
2.5–10 mm	Moderately wide	
>10 mm	Wide	
1–10 cm	Very wide	"Open" features
10–100 cm	Extremely wide	
>1 m	Cavernous	

(c) The persistence is the areal extent or the size of discontinuity within the plane (ISRM, 1978). It is the measurement of trace length or continuity of discontinuity on the surface of exposures as shown in Figure 2.11. The low persistence of discontinuity tends to terminate at short trace length along the surface. The high persistence of discontinuity tends to form a long trace length. The modal trace length can be described in the scheme as shown in Table 2.5.

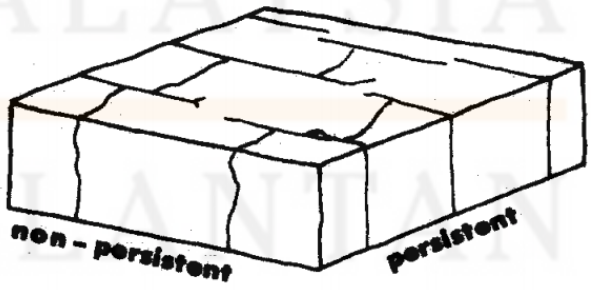

Figure 2.11: Sketches of persistence in rock block

Table 2.5: Model trace length of aperture (ISRM, 1978)

Very low persistence	.< 1 m
Low persistence	1–3 m
Medium persistence	3–10 m
High persistence	10–20 m
Very high persistence	> 20 m

2.10.4 Spacing and orientation of discontinuities

The stability of rock structure is governed by the average distance between adjacent pairs of joints that control the size of individual block masses. The number of discontinuities count in which an intersection line of known length is measured and expressed as a mean of joint spacing.

2.10.5 Groundwater condition

The general condition of groundwater can be described as either completely dry, damp, wet, dripping, or flowing. The rate of inflow of groundwater in litres per minute per 10 meters of the excavation should be determined in case of tunnels or mine drifts. If the water pressure data are available, these should be stated and expressed in term of the ratio of the water pressure to the major principal stress.

2.11 Slope Mass Rating (SMR)

The slope mass rating (SMR) introduced by Romana (1985) is obtained from RMR by adding a factorial adjustment factor depending on the relative orientation of joints and slope and another adjustment factor depending on the method of excavation. Formula for calculating SMR is,

$$SMR = RMR_B + (F_1 \times F_2 \times F_3) + F_4 \quad (2.3)$$

where

RMR_B = Rock Mass Rating of rock according to Bieniawski

F_1 = value between dip direction of discontinuity set, α_j and dip direction of slope face, α_s. It ranged from 1.00 to 0.15

F_2 = Discontinuities dip angle, β_j in the planar mode of failure. Its value varies from 1.00 to 0.15.

F_3 = Relationship between the dip of discontinuities, β_j and the dip of slope face, β_s. All the F_3 values are negative

F_4 = Adjustment factor that considers the method of excavation

The Table 2.6 shows the adjusting factors for joint.

The calculated value of SMR can be used to describe the stability of slope as shown in Table 2.7. The higher the value of SMR, the more stable the slope is.

Table 2.6: Adjusting factor for joints (Romana, 1985)

ADJUSTING FACTORS FOR JOINTS (F_1, F_2, F_3)	αj = DIP DIRECTION OF JOINT; βj = DIP OF JOINT; αs = DIP DIRECTION OF SLOPE; βs = DIP OF SLOPE				
	VERY FAVOURABLE	FAVOURABLE	FAIR	UNFAVOURABLE	VERY UNFAVOURABLE
PLANE FAILURE $\lvert \alpha j - \alpha s \rvert$ =	> 30°	30° - 20°	20° - 10°	10° - 5°	< 5°
TOPPLING $\lvert \alpha j - \alpha s - 180° \rvert$ =					
F_1 VALUE	0.15	0.40	0.70	0.85	1.00
RELATIONSHIP	$F_1 = (1 - \sin \lvert \alpha_j - \alpha_s \rvert)^2$				
$\lvert \beta j \rvert$ =	< 20°	20°-30°	30°-35°	35°-45°	>45°
F_2 VALUE — PLANE FAILURE	0.15	0.40	0.70	0.85	1.00
F_2 VALUE — TOPPLING	1.00				
RELATIONSHIP	$F_2 = tg^2 \beta j$				
PLANE FAILURE $\beta j - \beta s$ =	>10°	10°-0°	0°	0°-(-10°)	<(-10°)
TOPPLING $\beta j + \beta s$ =	< 110°	110°-120°	>120°	-	-
F_3 VALUE	0	-6	-25	-50	-60
RELATIONSHIP	F_3 (BIENIAWSKI ADJUSTMENT RATINGS FOR JOINTS ORIENTATION, 1976)				
F_4 ADJUSTING FACTOR FOR EXCAVATION METHOD	F_4 = EMPIRICAL VALUES FOR METHOD OF EXCAVATION				
	NATURAL SLOPE	PRESPLITTING	SMOOTH BLASTING	BLASTING or MECHANICAL	DEFICIENT BLASTING
F_4 VALUE	+15	+10	+8	0	-8

Table 2.7: Description of SMR classes

Class No	V	IV	III	II	I
SMR	**0-20**	**21-40**	**41-60**	**61-80**	**81-100**
Description	Very Bad	Bad	Normal	Good	Very Good
Stability	Completely Unstable	Unstable	Partially Stable	Stable	Completely Stable
Probable Type of Failure	Big Planar or Rotational	Planar or Big Wedge	Planar or many Wedges	Blocks	None
Support	Re-excavation	Important corrective measures	Systematic supports	Occasional supports	None

CHAPTER 3

MATERIAL AND METHODOLOGY

Methodology is an important part of this study. It describes the method in setting up the study, data acquisition, data analysis and data interpretation in the study.

3.1 Material

a) Geological hammer

It is used to break and split the rock fragment from the outcrop of the rocks. It is also used to obtain a fresh surface of a rock to determine its composition, bedding orientation, nature, mineralogy, history, and field estimate of rock strength

Figure 3.1: Geological hammer

b) Global positioning system (GPS)

GPS is used to locate the coordinate of the current position in the field. It is used to mark and record the position of the outcrop and the tracks in the field. Besides that, the GPS can be used to observe the contour map of the study area. The data from the GPS can then be transferred to the desktop in the form of shape file.

Figure 3.2: Global Positioning System (GPS)

c) Compass

Compass is used to determine the direction in the field. It is used to measure the orientation of geological structures such as bedding plane, fault plane and joint. It can also be used to measure the angle of inclination of the geological structures.

Figure 3.3: Compass

d) Tape

Tape is used to measure the dimension of the outcrop as well as the thickness of the bedding. It is also used as a scanline to measure the spacing and aperture of the joints.

Figure 3.4: Measuring Tape

e) Hydrochloric acid

Hydrochloric acid is used in the field as an indicator of the presence of carbonate. The carbonate rocks will react with hydrochloric acid to release the bubbles of carbon dioxide.

Figure 3.5: Hydrochloric acid

f) Plastic sample

It is used to collect the rocks samples

Figure 3.6: Plastic samples

g) Schmidt Hammer

Schmidt hammer is used to determine the compressive strength and hardness of the rock. The reading of the measurement is recorded on the hammer itself.

Figure 3.7: Schmidt hammer

3.2 Software used for analysis

a) DIPS 5.0

The software that used to analyse and visualise the structural data using equal-angle or equal area projection. It used to present the discontinuities data collected in the form scatter plot, rosette diagram and contour plot. From the contour plot of discontinuity data, the mean orientation and angle of mean great circle can be determined. Mean orientations are calculated and set statistics such as confidence and variability cones can be displayed using the software.

b) ArcGIS 2.0

ArcGIS 2.0 is used to input the dataset of the study area and digitize it together with the satellite image. It is used to draw the geological map as well as to construct the cross-section of the geological map.

c) Microsoft Excel

Microsoft Excel is the program that used to input the discontinuities data from the field. The data input will be exported as TEXT file to be used in the STEREONET and DIPS 5.0 software.

d) STEREONET

This software is used to plot the slope and discontinuity data such as slope face, friction cone, envelop of slope face as well as to carry out the kinematic analysis to estimate the plane wedge or toppling slope failure.

3.3 Preliminary study

Preliminary study is done to get the information and knowledge about the study area. The method used in the previous research for the analysis of rock slope will be reviewed. Reading materials such as published journals, articles, book and other resources are collected and referred so that they will be used in the study. These materials are collected from Library of University Malaysia Kelantan, and Geology of Mineral and Geosciences department of Malaysia and internet.

3.4 Preparation of topography map

When the location of the study area is confirmed, the data of the study area will be given by the supervisor and input into the ArcGIS software. The topography map of Tasik Banting, Gerik with the perimeters of 5 km x 5 km will be produced by digitizing it with the Google Earth image. The area of the study area is 25km^2 with the boundary located at 5°38'59.61"N, 101°40'15.09"E; 5°38'59.61"N, 101°42'58.14"E; 5°36'17.65"N, 101°42'58.14"E and 5°36'17.65"N, 101°40'15.09"E. Before conducting the fieldwork, the linear structures that is known as lineament are identified first in the topography map so that to ease the field work.

3.5 Field Assessment

The study will involve field assessment work at the study area. The estimated duration of the fieldwork at the study area is around 2 months and half. Field assessment involved geological mapping and rock slope assessment. In rock slope assessment, total five rock slopes will be analysed.

3.5.1 Geological mapping and outcrop sampling

The study will start with the geological mapping of the study area. Before going to the field, the traverse will be planned on the topography map. By using topography map and GPS, the study area will be assessed and explored by walking. The outcrops found will be recorded in the GPS and plotted on the topography map. The features of the outcrops will be described and recorded in the notebook. The lithology, structure, dimension and weathering grade of the outcrops will be recorded as well as the geomorphology, elevation and location of the outcrop. The strike and dip of the bedding of the outcrops will be measured by compass and recorded. The fresh samples of outcrops will be collected by plastic samples for the petrographic analyses purposes.

3.5.2 Schmidt hammer rebound test

Schmidt hammer is used to determine the compressive strength and hardness of the rock. The SH consists of a spring-loaded piston which is released when the plunger is pressed against a surface as shown as in Figure 3.8. The impact of the piston onto the plunger transfers the energy to the material. The extent to which this energy is recovered depends on the hardness of the material, which is expressed as a percentage of the maximum stretched length of the key spring before the release of the piston to its length after the rebound. Type-N Schmidt hammer with the impact energy of 2.207 Nm will be used in this study, as it is more ideally suited for field-testing and less sensitive to surface irregularities when compared with Type-L Schmidt hammer (Aydin, 2008) The rebound number of Type-N Schmidt hammer, R_N obtained from the field will be converted into rebound number of Type-L Schmidt hammer, R_L using the equation 3.1 suggested by Look (2007). The correlation of R_N and R_L is only

available when $R_L > 30$ and $R_N > 40$. The rebound number, R_L obtained will be corrected based on the Table 2.3.

$$R_N = 1.0646R_L + 6.3673 \quad (3.1)$$

The R_{true} value can be correlated with the chart introduced by ISRM (1978) as shown in Figure 2.9 to get the UCS value.

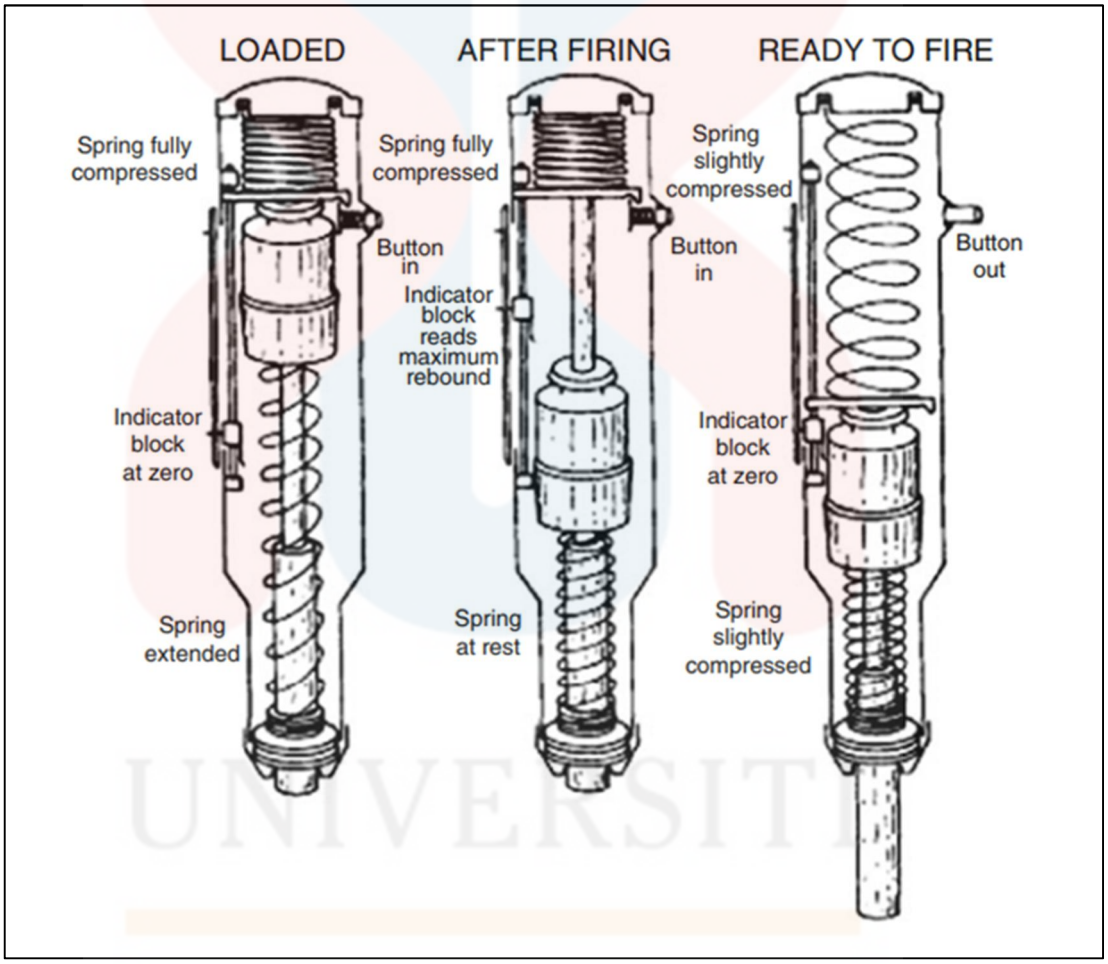

Figure 3.8: Operational principal of Schmidt hammer (Aydin, 2015)

3.5.3 Discontinuities survey

Discontinuities survey will be conducted on three respective rock slopes in the study area. Discontinuities survey comprises of the measurement of orientation, persistence, aperture, frequency, spacing of the joints. The examining of the roughness of discontinuity surface and calculation of RQD will also be included in the survey. In the field, the scanline or measuring tape of 20m long is set up on the exposed face. Equal length of scanlines are established in orthogonal direction in order to obtain the true three-dimensional characterisation of rock mass

(a) Measurement of orientation of joints: All joints orientation within 20m scanline will be taken in each slope. The dip and dip direction of the joints in the exposed surface will be measured by using compass that has clinometer.

(b) Measurement of persistence of joints: The trace length of all joints intersecting the 20m scanline will be measured and recorded in survey sheets.

(c) Measurement of spacing of joints: The spacing of joints will be measured at the distance between the points where the discontinuities intersect the scanline through the rock mass as shown in Figure. The RQD (%) of the rock mass can be calculated by using the formula introduced by Palmstrom (1982) which is shown in Eq 2.2.

(d) Examining roughness and water condition of discontinuity: The roughness of joints along the scanline are described based on the scheme of roughness profile provided by ISRM (1978). The water condition will be evaluated as dry, damp, wet, dripping or flowing in the joints.

The clusters poles of discontinuity data acquired from the respective three rock slopes will be plotted on stereonet of DIP 5.0 computer software. DIP 5.0 will contour the poles of discontinuity and great circles for the

representative set of discontinuity can be found. The representative great circle of discontinuity set will be used in the kinematic analysis.

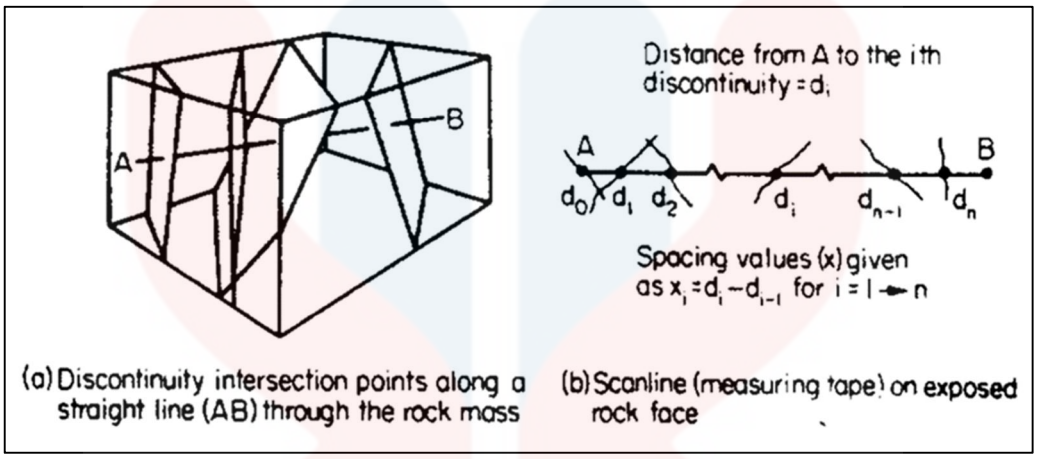

Figure 3.9: Measurement of spacing discontinuities (Priest & Hudson, 1976)

3.6 Kinematic Analysis by stereographic projection

The discontinuities data, friction angle, dip and dip direction of slope faces obtained from three rock slopes will be projected on the stereonet by using STEREONET computer software. The software will carry out the kinematic analysis on the input data to identify the mode of slope failure and the direction of the possible sliding of the blocks. The condition for the occurrence of slope failure on stereographic projection is explain in Chapter 2 section 2.8

3.7 Slope mass rating (SMR)

When the mode of slope failure is identified by kinematic analysis, the rating values for parameters of RMR that include UCS, RQD, spacing of discontinuities, groundwater condition and condition of discontinuities will be added with rating value of the relationship between orientation of joints and slope as well as rating value for method of excavation. Then the rating of SMR can be calculated as,

$$SMR = RMR_B + (F_1 \times F_2 \times F_3) + F_4$$

Hence, the stability of rock slope will be examined through the rating of SMR

The SMR value obtained is different from the factor of safety. Factor of safety takes account of the shear strength of the rock mass whereas Slope Mass Rating does not. The slope is considered stable when the factor of safety is more than 1 whereas it is unstable if the factor of safety is less than 1. SMR is the index rating of the rock mass ranged from 0 to 100. The higher value of SMR, the more stable the slope is. SMR takes account of the characteristic of discontinuities, relationship between the slope face and the discontinuities dip, parallelism between discontinuities and slope face strike instead of the shear strength of the rock mass.

CHAPTER 4

GEOLOGY

4.1 Introduction

This chapter will discuss about the geology of the study area of size 25km^2 at Pergau Lake Jeli, Kelantan. Geological mapping was conducted to determine the geology of the study area in terms of lithology, geomorphology, and structural geology. The data of lithology, landscape, structures that formed on the outcrop, and the weathering grade of the outcrop were recorded and finally used to produce different types of geological maps. The data on the certain area of the study area cannot be obtained because number of exposed outcrops were limited and the accessibility to the area was dangerous.

4.1.1 Brief Content

The first part of this chapter will discuss about the desk study of geological mapping before conducting the fieldwork. The early interpretation is made based on the topographic map of the study area such as linear structures formed on the topographic map were interpreted as structures or lineament and the types of rock was predicted based on the pattern of contour. Then, the accessibility of the study were found using the satellite image. Next, this chapter will also discuss the observation and traverses as well as the geomorphological information of the study area. Geomorphology is the concerned aspect in geological mapping as the earth surfaces are evolved in time and space due to biological and physiochemical factors acting on them (Perillo, 1995).

Besides that, the type of lithology found will be discussed. This section will described the mineral content within the rocks and petro-genesis of the rock. Structural geology comprising of the cleavage, vein, joint, fault and mechanism of structures also will be discussed. Lastly, the overall data gathered from the fieldworks were used to discuss the historical geology, which is the sequence formation of the study area.

4.1.2 Accessibility

The accessibility of the study area was considered difficult due to the unexplored tropical forest. The canopy of the tropical forest comprised of the giant trees that grow up to 50m and prevent much of the light from reaching the ground. Besides that, the chance of facing wild animals such as boars, snakes, bears, wild cats, and elephants are high. Thus, geological mapping works at the study area became more risky and dangerous.

However, there were still some area that had been explored such as dams of Tenaga Nasional Berhad (TNB), Taman Santuari, and Pergau lake as shown in Figure 4.1.1. The permission letter from the University Malaysia Kelantan was given to TNB and Taman Santuari in order to access those areas. Walking was more preferable choice than driving through those areas due to the muddy and rocky properties of the road.

Another accessibility through the study area is Gerik-Jeli highway that run from the east to the west of the study area. The outcrops were observed and studied along the highway by driving and stopping at the exposed rocks. Next, the study area was accessed by walking through the Pergau River. Most of the rock samples and the data of outcrops were taken from the exposed rock along the Pergau River.

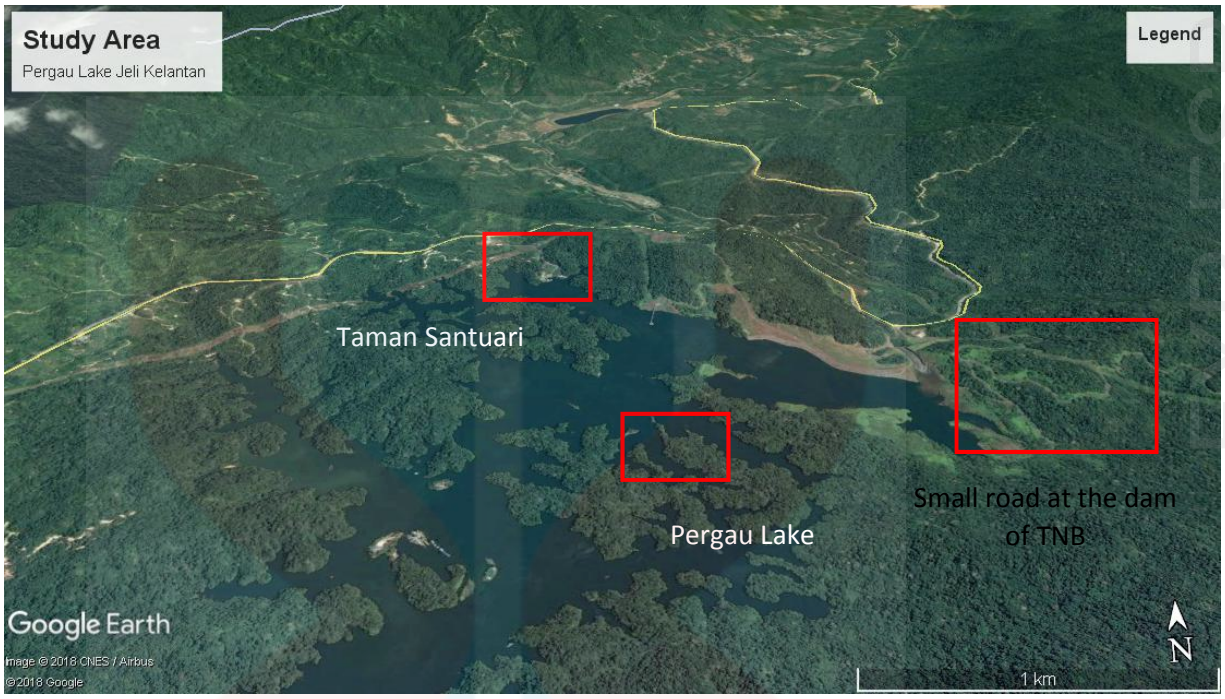

Figure 4.1.1: Accessibility of study area through satellite image

4.1.3 Settlement

Obviously, no suitable places can be settled in the study area based on the Figure 4.1. This is because 60% of the study area is made up of tropical rainforest; 35% made up of lake and 5% are Taman Santuari and TNB dam. There are also no villages that can be stayed overnight and no restaurants can be found in the study area. Thus, it is inconvenient to settle at the study area.

4.1.4 Forestry

Large portion of the study are comprised of tropical rainforest. Some small portion of land was used to build Taman Santuari that was the tourism area of Pergau Lake. The tourists can access to the small islands on Pergau Lake by taking the boat from Taman Santuari. Tenaga Nasional Berhad (TNB) had used some lands on study area to build dams and power station as shown in Figure 4.1.2.

4.1.5 Traverses and Observation

Total five traverses were included in the fieldwork. The traverses in the study area were set up at the Gerik-Jeli highway, Sungai Pergau, small tar roads at the dam of TNB, and small road at Taman Santuari. All of the five traverses in the fieldwork were corresponding in collecting the geomorphological, lithological and structural data of the study area. The traverses map and waypoint map were shown in Figure 4.1.3 and Figure 4.1.4 respectively.

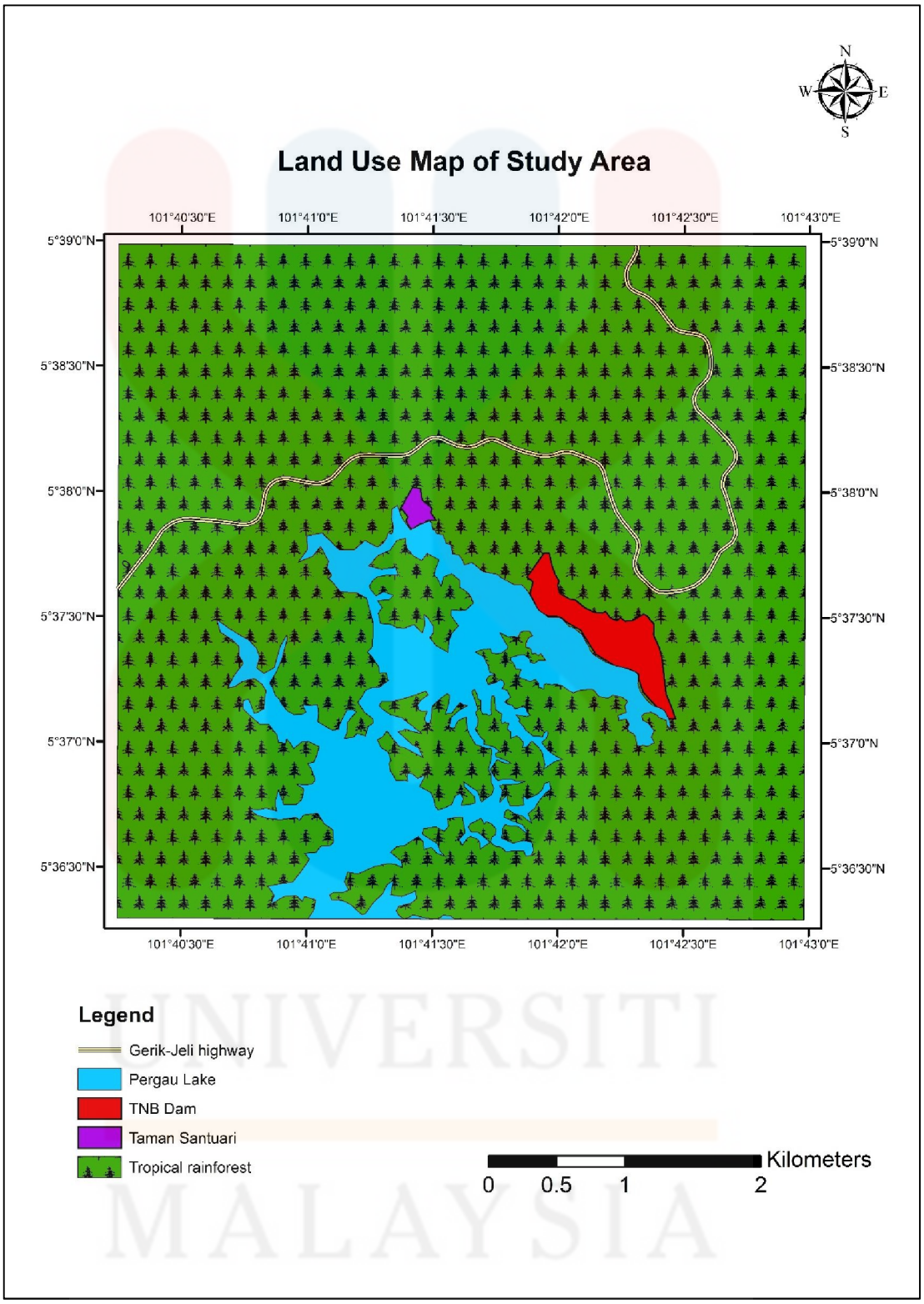

Figure 4.1.2: Land use map of the study area at Tasik Pergau Jeli, Kelantan

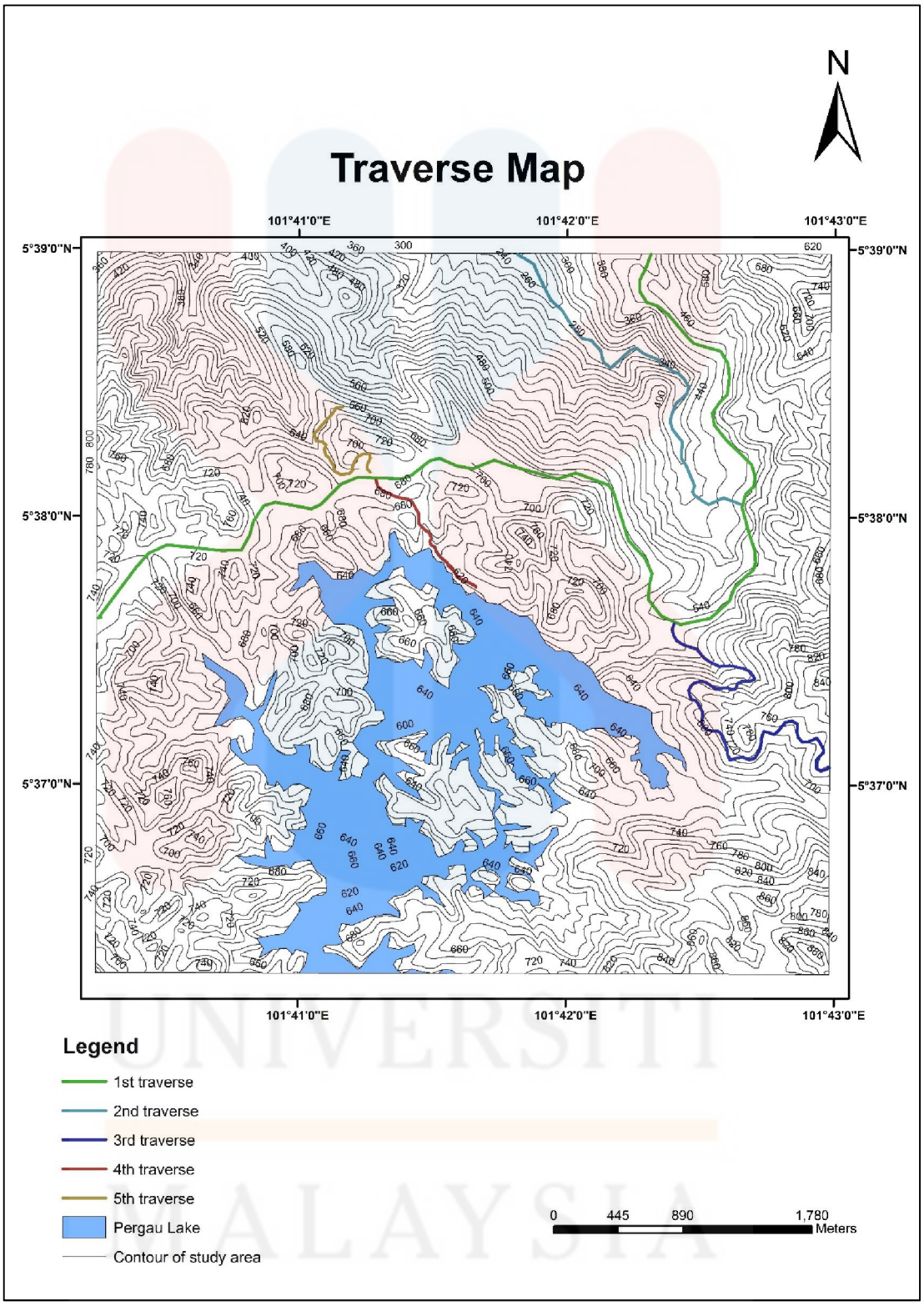

Figure 4.1.3: Traverse map of study area

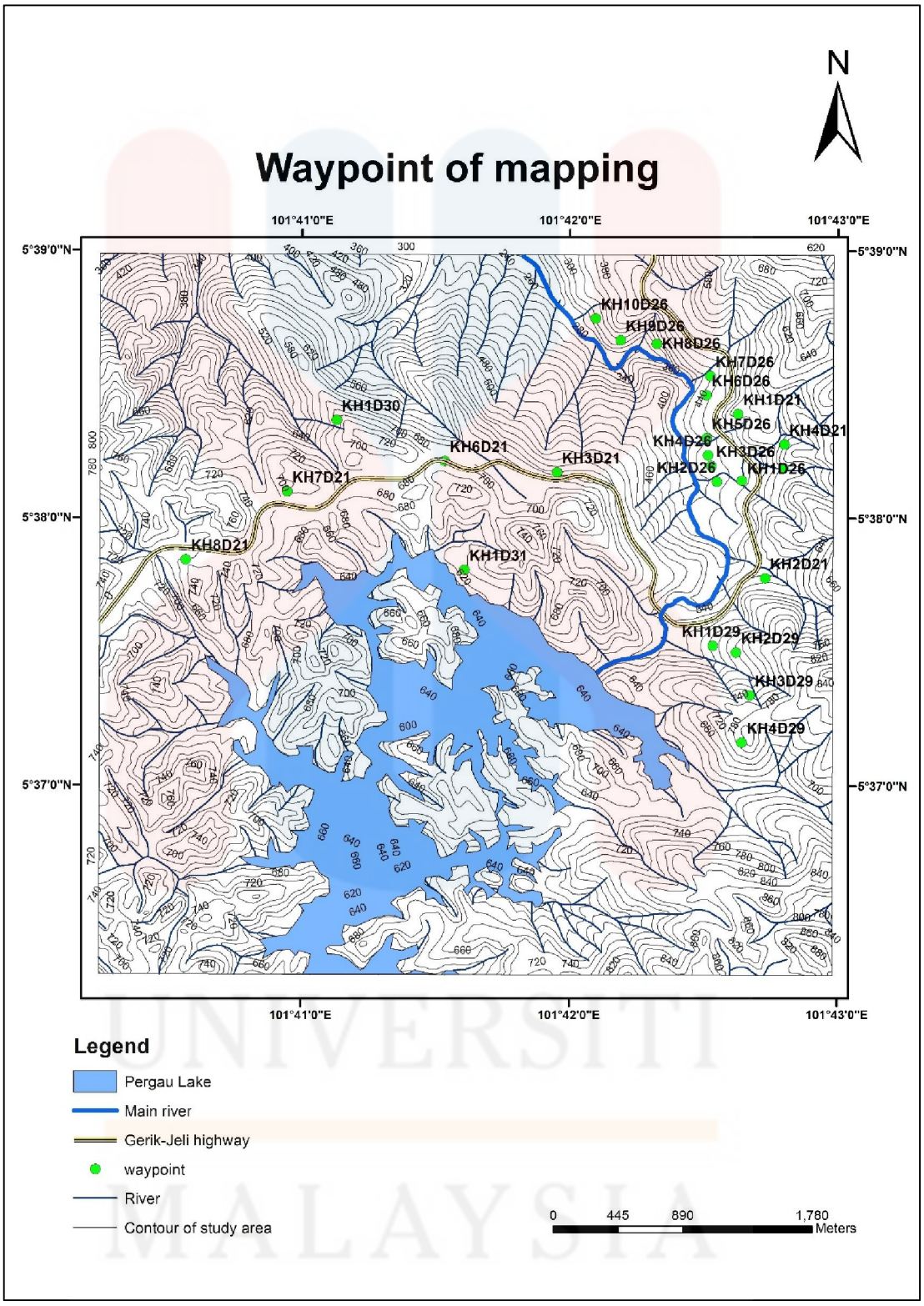

Figure 4.1.4: Waypoint of the geological mapping in study area

1st traverse of fieldwork was located along the Gerik-Jeli highway. The traverse mainly focused on finding the other accessibility, identifying possible rock type, finding the rock slopes along the highway and identifying the topography of the study area. Five exposed outcrops were found at the waypoint of KH1D21, KH2D21, KH3D21, KH4D21, and KH5D21, as shown in waypoint map in Figure 4.1.4. Outcrop at waypoint KH1D21 was exposed at the roadside of Gerik-Jeli highway (5° 38' 23.4"N, 101° 42'37.6"E). The outcrop was highly weathered to spheroidal boulder as shown in Figure 4.1.5. The confirmation was made that the rocks were igneous rock due to the absence of bedding, stratum or foliation on the outcrop. The colour of the rock was between light brown to black. Hence, it became difficulties in differentiating type of igneous rock.

Figure 4.1.5: Outcrop at waypoint KH1D21 (5° 38' 23.4"N, 101° 42'37.6"E)

Second and third outcrop were also found along the roadside of Gerik-Jeli highway at waypoint KH2D21 (5º 37’ 46.6”N, 101º 42’43.7”E) with elevation of 516m and waypoint KH3D21 (5º 38’ 10.3”N, 101º 41’57.1”E) with elevation 615 m respectively. These outcrops were same as the previous outcrop found which was highly weathered and coloured brown to black. The surface of the outcrops were coated with the green algae and surrounded by weeds as shown in Figure 4.1.6.

Figure 4.1.6: Outcrop at waypoint KH2D21 (5º 37’ 46.6”N, 101º 42’43.7”E)

Figure 4.1.7: Outcrop at KH3D21 (5° 38’ 10.3”N, 101° 41’57.1”E)

Forth outcrop at waypoint KH4D21 (5° 38’ 16.6”N, 101° 42’47.9”E) was exposed at small river nearby the roadside of Gerik-Jeli highway. This outcrop was fresh compared to previous outcrops. The rock was light to grey in coloured with coarse-grains of mineral that can be seen with naked eyes. The biotite flakes and pink potash alkali feldspar can be identified easily on the rock. Thus, the assumption was made that the rock was acid intrusive igneous rock due to the coarse-grained and light-coloured properties of the igneous rock. Fifth outcrop was exposed nearby the roadside of highway at waypoint KH5D21 (5° 38’ 11.3”N, 101° 42’47.8”E). It was moderately weathered with some minerals grains visible with naked eye such as alkali feldspar and quartz. The geological structures such as fractures and joints were spotted at this outcrop. The justification was made that the outcrops exposed at 1st traverse were relatively same.

Figure 4.1.8: Outcrop at waypoint KH4D21 (5º 38’ 16.6”N, 101º 42’47.9”E)

Figure 4.1.9: Outcrop at KH5D21 (5º 38’ 11.3”N, 101º 42’47.8”E)

2nd traverse was situated along Sungai Pergau at the northwest side of the study area. Total ten outcrops were discovered at waypoint KH1D26, KH2D26, KH3D26, KH4D26, KH5D26, KH6D26, KH7D26, KH8D26, KH9D26 and KH10D26. First outcrop at waypoint KH1D26 (5º 38' 8.5"N, 101º 42'38.5"E) was found at the river of Pergau. The outcrop was partially weathered by chemical and biological agents of water in the river. The rock identified was an acidic intrusive igneous rock with light to grey colour. The fissures forming around the outcrops indicated that the outcrop had been subjected to differential tectonic forces. The outcrops at waypoints KH2D26 (5º 38' 8.2"N, 101º 42'32.9"E), KH3D26 (5º 38' 11.8"N, 101º 42'31.6"E), KH4D26 (5º 38' 14.2"N, 101º 42'30.9"E) were same with the previous lithology which were acid intrusive igneous rock. The crystals boundaries of the rocks were distinguishable with naked eye and were porphyritic and phaneritic in textures. The euhedral potash pink feldspar can be seen readily in the rock with plagioclase, quartz, flaky biotite and hornblendes. At waypoint KH2D26, the outcrops were structurally deformed with abundant joints and fissures that oriented almost in the same direction. The extensional joints filled with the aplite were observed at this outcrop as shown in Figure 4.1.11. However, outcrops at waypoint KH3D26, did not have many structures observed. The outcrops at KH4D26 comprised of the metasediment enclave. The enclave was believed to originate from the country rock of sedimentary rock that fall into the pluton of the acid igneous rock.

Figure 4.1.10: Outcrop at waypoint KH2D26 (5° 38’ 8.2”N, 101° 42’32.9”E)

Figure 4.1.11: Aplite veins at outcrop KH2D26

Figure 4.1.12: Outcrop at waypoint KH3D26 (5° 38’ 11.8”N, 101° 42’31.6”E)

Figure 4.1.13: Outcrop at waypoint KH4D26 (5° 38’ 14.2”N, 101° 42’30.9”E)

Figure 4.1.14: Metasediment enclave in outcrop KH4D26

The rocks of outcrops at waypoint KH5D26 (5° 38’ 18.0”N, 101° 42’30.6”E), KH6D26 (5° 38’ 27.6”N, 101° 42’30.5”E) and KH7D26 (5° 38’ 31.9”N, 101° 42’31.4”E) were same with the rocks of previous outcrops. They were porphyritic and phaneritic in textures and comprise of pink colour of alkali feldspar phenocrysts bounded only some of its characteristic faces. The crystals size were enlarged when compared with the crystals of previous rocks. The pink potash alkali feldspar, plagioclase, hornblende, quartz and other minerals become coarser. Besides that, metasediment enclaves can also be found at outcrop KH5D26 as well as the aplite vein in outcrop KH7D26.

Figure 4.1.15: Outcrop at KH5D26 (5º 38’ 18.0”N, 101º 42’30.6”E)

Figure 4.1.16: Metasediment enclave at outcrop KH5D26

Figure 4.1.17: Outcrop at waypoint KH6D26 (5º 38’ 27.6”N, 101º 42’30.5”E)

Figure 4.1.18: Aplite vein at outcrop KH7D26

At waypoint KH8D26 (5º 38’ 39.1”N, 101º 42’19.4”E), KH9D26 (5º 38’ 39.9”N, 101º 42’11.3”E) and KH10D26 (5º 38’ 44.8”N, 101º 42’5.7”E), the types of rocks were also same which were acid intrusive igneous rocks. They possess felsic mineral crystals that were visible with the naked eye such as plagioclase, quartz, hornblende, and phenocrysts alkali feldspar. The crystals in the rocks were having the holocrystalline habits. The minerals in the rocks were subhedral to euhedral in shape. At outcrop KH10D26, the acid intrusive igneous rocks were observed in contact with the black colour of fine-grained rocks as shown in Figure 4.1.22. The fine-grained black coloured rocks were believed to be the country rocks that were intruded by the acidic plutons.

Figure 4.1.19: Outcrop at waypoint KH8D26 (5º 38’ 39.1”N, 101º 42’19.4”E)

Figure 4.1.20: Outcrop at waypoint KH9D26 (5° 38’ 39.9”N, 101° 42’11.3”E)

Figure 4.1.21: Contact between acid intrusive igneous rocks (light colour) with the country rock (black colour)

All the exposed outcrops at 3rd, 4th, and 5th traverses were same as the outcrops at 1st and 2nd traverses. However, the outcrops were not as fresh as outcrops found in the 2nd traverse. They were mostly highly weathered by the surrounding environment and some of the outcrops were weathered to form soil. The southeast of the study area cannot be accessed easily. Thus, deduction of the lithology on that area was made based on the contour pattern of topography map. The contour pattern in which 3rd traverse passes through was same as the contour pattern at the southeast of study area. Therefore, the type of rocks in southeast of study area were deduced as acid intrusive igneous rock. Based on the contour pattern and exposed outcrops along the traverses, the entire study area was deduced to have only one type of lithology that was acid intrusive igneous rock.

4.2 Geomorphology

Geomorphology is the study on the landforms that formed on the surface of the earth and the processes that create them. Exergonic processes such as erosion, weathering, transportation, deposition and endogenic processes such as epeirogenic, orogenic, volcanism, magmatism play an important role in forming different types of landforms on the earth surface (Huggett, 2007).

4.2.1 Geomorphologic classification

Geomorphological study of the study area is conducted by in-situ field observation. Before conducting geomorphology observation in the field, types of landforms are predicted on the contour map of the study area. Geomorphology observation attempts to identify the landforms elements in the study area as well as to

determine the processes that form the landforms. Field sketching and photographing were used to record the data of the landforms. From the geomorphologic elevation map as shown in Figure 4.2.3, the highest peak of the study area was 880 m located at the southeast of the study area whereas the lowest peak was 340 m situated at the north of the area. Most of the study area at south were dominated by the zone of elevation 587 m to 660 m from the sea level. The landforms that formed in this zone were mostly hills with gentle slopes. The changes in the elevation of the hills are uniform. The hills in this zone are excavated to produce man-made Pergau Lake. Thus, the outcrop that were found in this zone are severely weathered. The water in the lake weathered and eroded the excavated hills to produce gentle slope of hills.

Figure 4.2.1: Conical hill landform near Pergau Lake (5° 37' 50.5"N, 101° 41'31.5"E)

The landforms that formed at the north region of the study area were mostly mountains ridges. The mountain ridges trending northwest and southeast of the study

area formed a long sharp peak. This indicated that the rocks in this region were strong and resistant to weathering. From the slope map as shown in Figure 4.2.4, the slope gradient of the mountain was extremely high. Therefore, the valleys of the mountains trending due north are very steep. Below the mountains ridges are the U-shaped and V-shaped valleys in which river of Pergau flow. The mountain ridges at the north region of the study area were believed to form due to orogenic processes where force of compression causes the uplift of plutonic rock, forming the ridge of the mountains.

Figure 4.2.2: Mountain ridges at the study area (5° 38' 9.65"N, 101° 42'0.03"E)

The highest peak landform was located at the southeast of the study area. They were mountains with uniform peak and gentle to steep slope gradients. Since all the rocks in the study area were plutonic rocks, the intrusion of the acid rocks batholith causes doming of the landforms in study area to produce mountains and hills. The orogenic processes together with the erosional processes produced mountain ridges and drainage valley landforms in the study area.

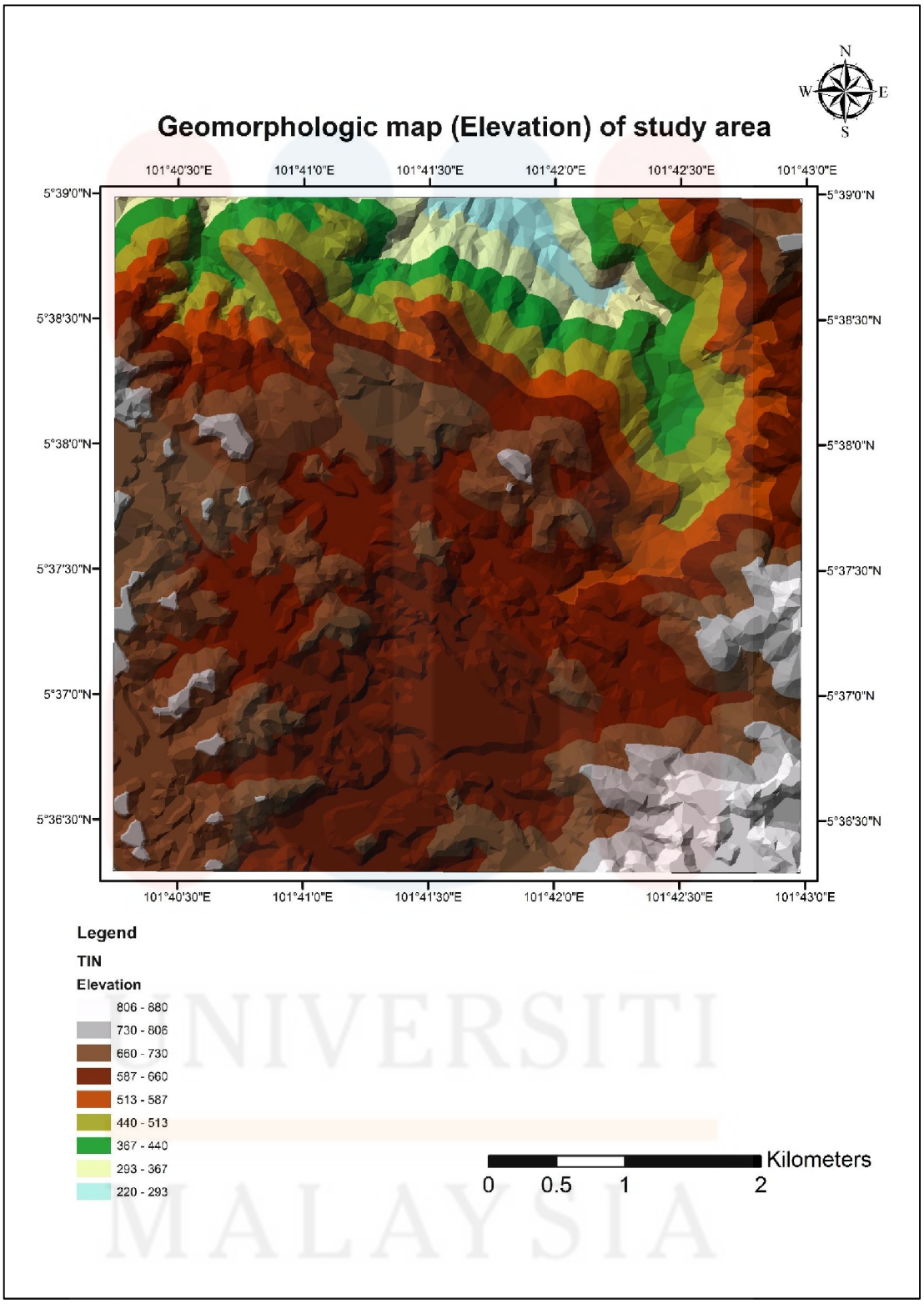

Figure 4.2.3: Geomorphologic map (elevation) of study area at Tasik Pergau Jeli, Kelantan

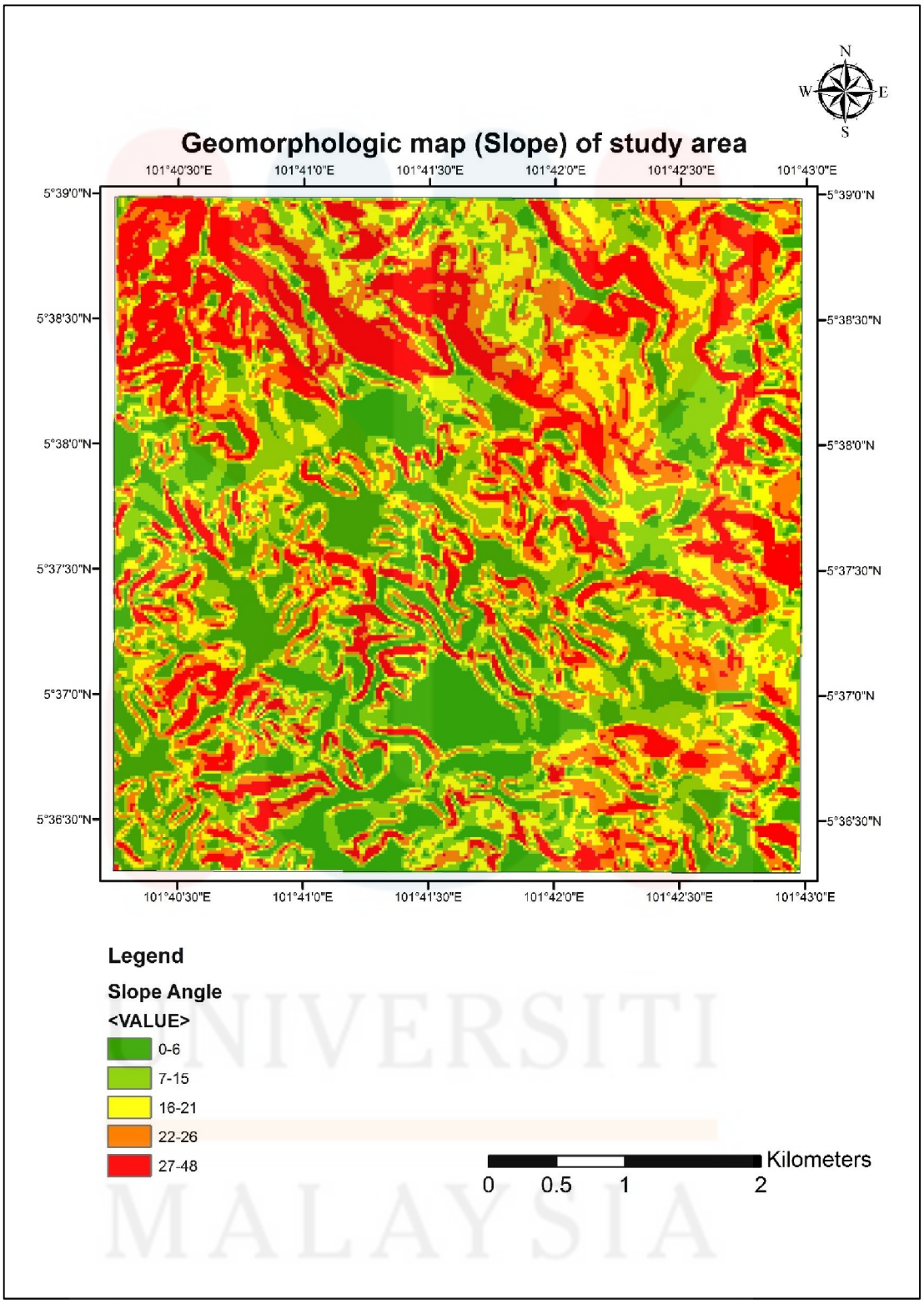

Figure 4.2.4: Geomorphologic map (slope) of study area at Tasik Pergau Jeli, Kelantan

4.2.2 Weathering

Weathering process in Malaysia is rapid due to tropical climate where the country often experiencing hot and wet seasons. These two seasons may sufficiently enough to accelerate the weathering process of the rock in Malaysia.

The rocks in the study area were subjected to both chemical and physical weathering. Generally, the weathering agents in the study area were water, heat, and wind. These agents causes the mechanical disintegration and chemical decomposition of rocks into smaller pieces and particles.

Most of the outcrops along Pergau River were fresh. The minerals in the rocks can be seen clearly with naked eye. There were no internal discoloration or disintegration within the rocks. The outcrops near the river were hard and very difficult to break. However, there were many cracks formed in the outcrops due to mechanical weathering. The change in temperature at night and day caused the rocks to expand and contract. That movement caused the rocks to crack and break apart. Therefore, the weathering grade of outcrop at Pergau Lake was around Grade 1 to Grade 2.

The outcrops that exposed along the Gerik-Jeli highways were moderately weathered and had weathering Grade 2 to Grade 3. Some discoloration on and adjacent to discontinuity surface of outcrops were observed. The discontinuities such as fractures, joints, fissures formed on the outcrops due to mechanical weathering. The outcrops also undergone chemical weathering where the acid intrusive igneous rocks were hydrolysed by the rainwater to produce secondary minerals such as kaolinite, montmorillonite and illite. Some of the outcrops were red in colour because of the presence of iron oxide that produced from the oxidation of the rocks.

4.2.3 Drainage Pattern

Drainage system is the pattern formed by streams, rivers and lakes in a drainage basin. They tend to develop along zones where rock type and structure are most easily eroded. Most of the drainage patterns reflect the original structure and slope or successive events of the surface which had uplifted, depressed, tilted, folded, faulted and so on (Zhang & Guilbert, 2012).

From the Figure 4.2.5, the drainage patterns of the study area were dominated by the dendritic pattern. Long parallel pattern of drainage can also be observed near the northeast of the study area. Based on the drainage pattern map in Figure 4.2.5, the dendritic drainage pattern of streams were branched irregularly in all directions with tributaries joining main river at different angles.

Dendritic drainage patterns in the study area were characterised by the uniform resistant bedrock at the subsurface such as granite, gneiss or diorite. In other words, dendritic drainages will develop in an area where bedrock had equal resistance to erosion and absence of other structural controls such as folds and faults. Therefore, with the presence of dendritic drainage in the study area, it can be deduced that the bedrocks at the subsurface are hard rocks. This provide another evidence that the rock at the study area were made up of acid intrusive igneous rock.

The parallel drainage patterns at the northeast of the study area may indicate that there had the structures in the subsurface such as fault or other linear structures. These structures were predicted to induce the formation of the mountain ridge at the north side of the study area. Besides that, the watershed in the study area were determined as shown on Figure 4.2.6. Watershed is an area where the land collects precipitation. The watershed can be found in the middle and north of the study area.

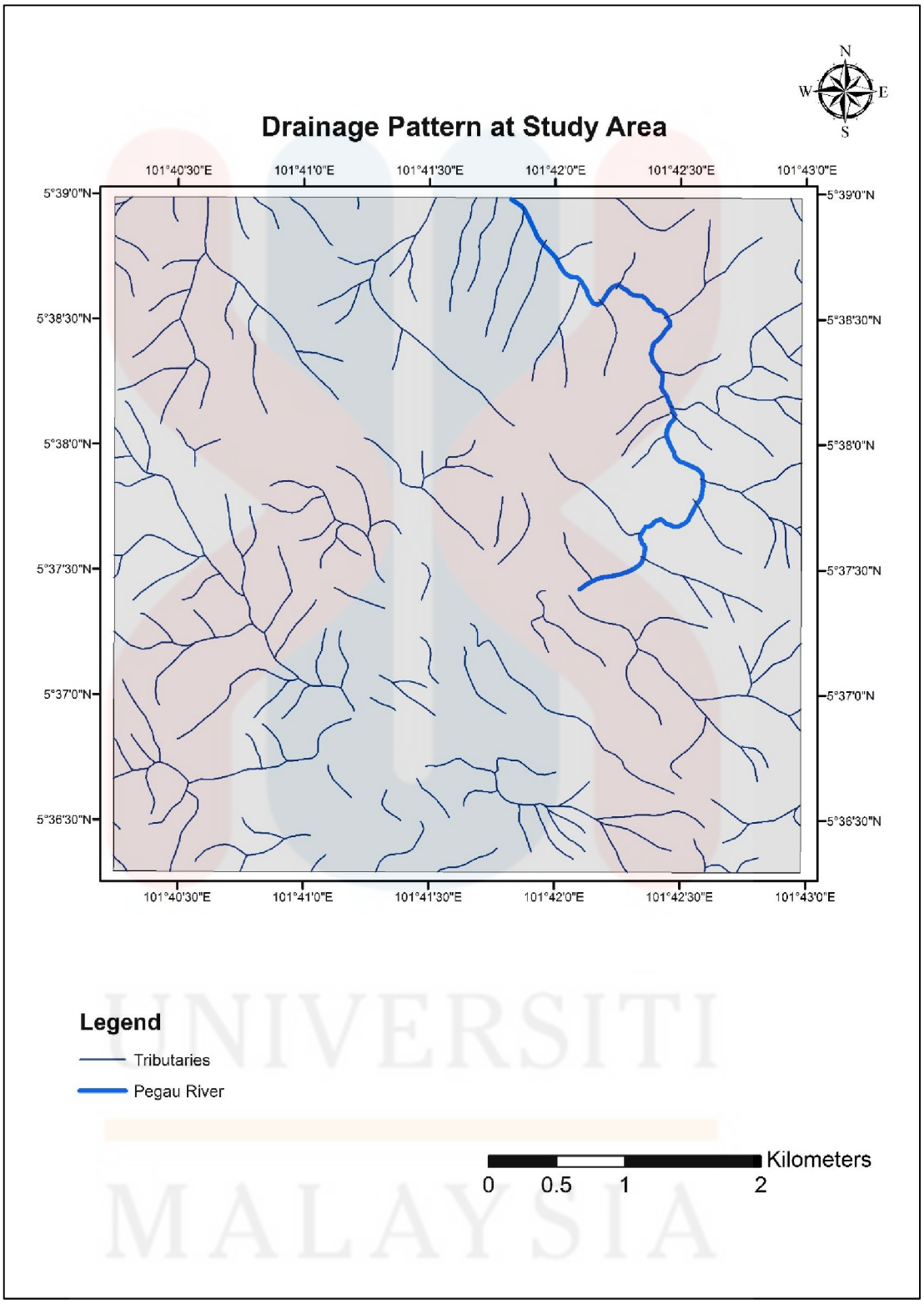

Figure 4.2.5: Map of drainage pattern of the study area at Tasik Pergau Jeli, Kelantan

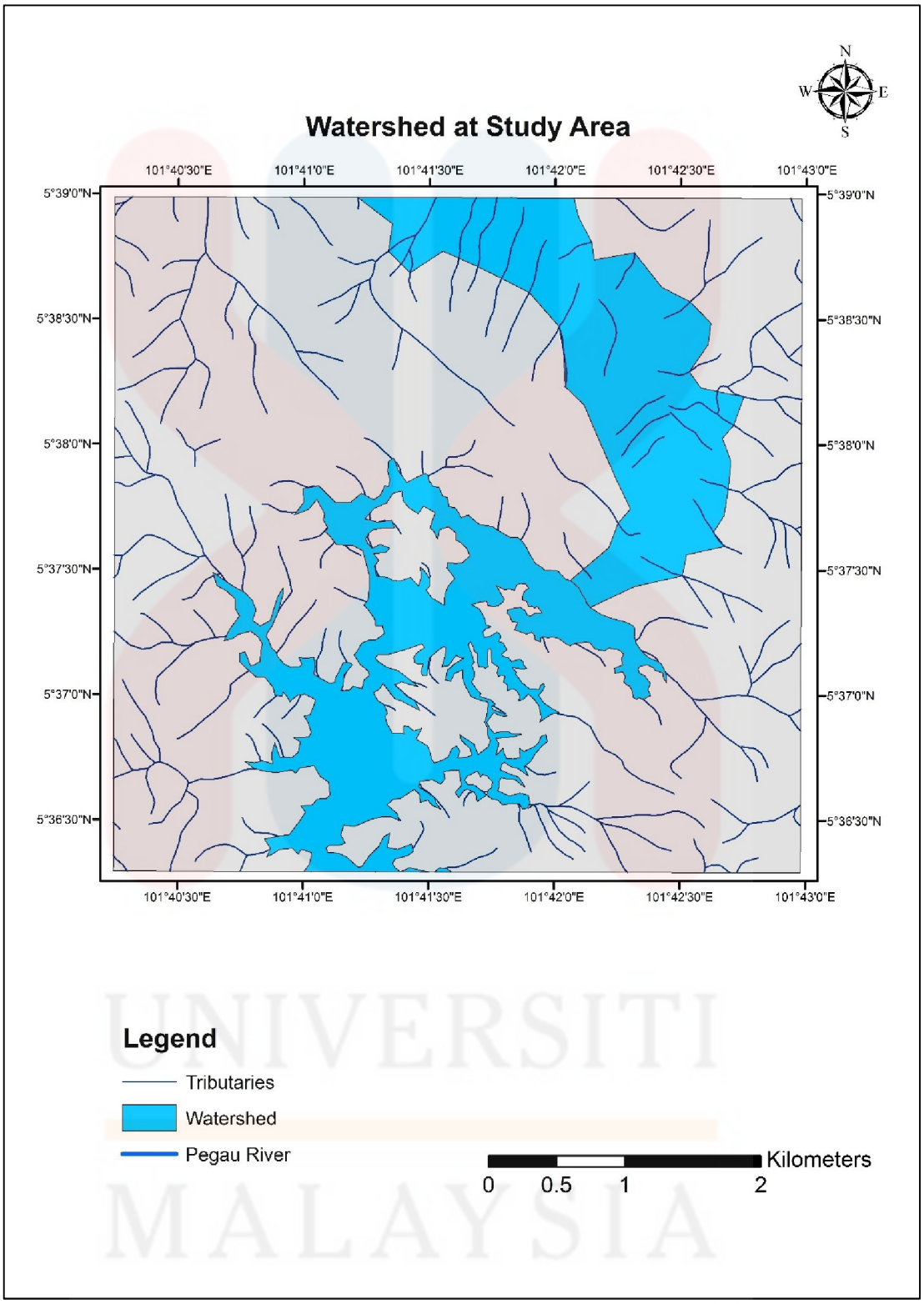

Figure 4.2.6: Map of watershed of study area at Tasik Pergau Jeli, Kelantan

4.3 Lithostratigraphy

Based on the geological map as shown in Figure 4.5.1, the entire lithology of the study area was composed of acid intrusive granite. This granite was one of the granite in Stong Igneous Complex that was Noring Granite. Noring Granite had a distinct feature of porphyritic alkali feldspar and phaneritic in textures.

Samples of rocks collected from the rock sampling in the field were described by macroscopic and microscopic study. The study will describe the characteristics of granitic rock in the study area as well as highlight the mineral composition, texture and its mode of occurrence.

Table 4.1: Lithostratigraphy column of the study area.

Lithology	Description	Units	Period	Era
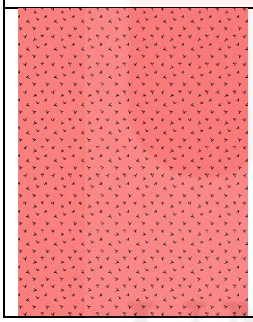	Acid intrusive rock was light in colour. It was characterised by porphyritic and phaneritic textures Felsic minerals dominated in the rocks were quartz, plagioclase, biotite and K-feldspar.	Noring Granite	Cretaceous	Mesozoic

4.3.1 Macroscopic description of lithology

Hand specimen from the study area showed that the colour of granite rock was light in colour and the index colour of the rock was leucocratic. In term of structure, it composed of pegmatitic structures where the rocks was very coarse grained. Texture of the rock was explained in term of crystallinity, granularity and fabric of the rock. The crystallinity of the granitic rock in the study area was holocrystalline since the rock composed wholly of crystals. Granularity of the rock was coarse grain because of

the average crystal diameter was more than 5 mm. Large crystals of alkali feldspar embedded with smaller groundmass can be seen clearly in the hand specimen of granite. Thus, the granite can be considered to have porphyritic in fabric texture. The observation of hand specimen by naked eye as shown in Figure 4.3.1, the granite also constituented of other felsic minerals such as plagioclase with chalky white colour, quartz with light greyish colour and biotite that displays black colour with vitreous lustre.

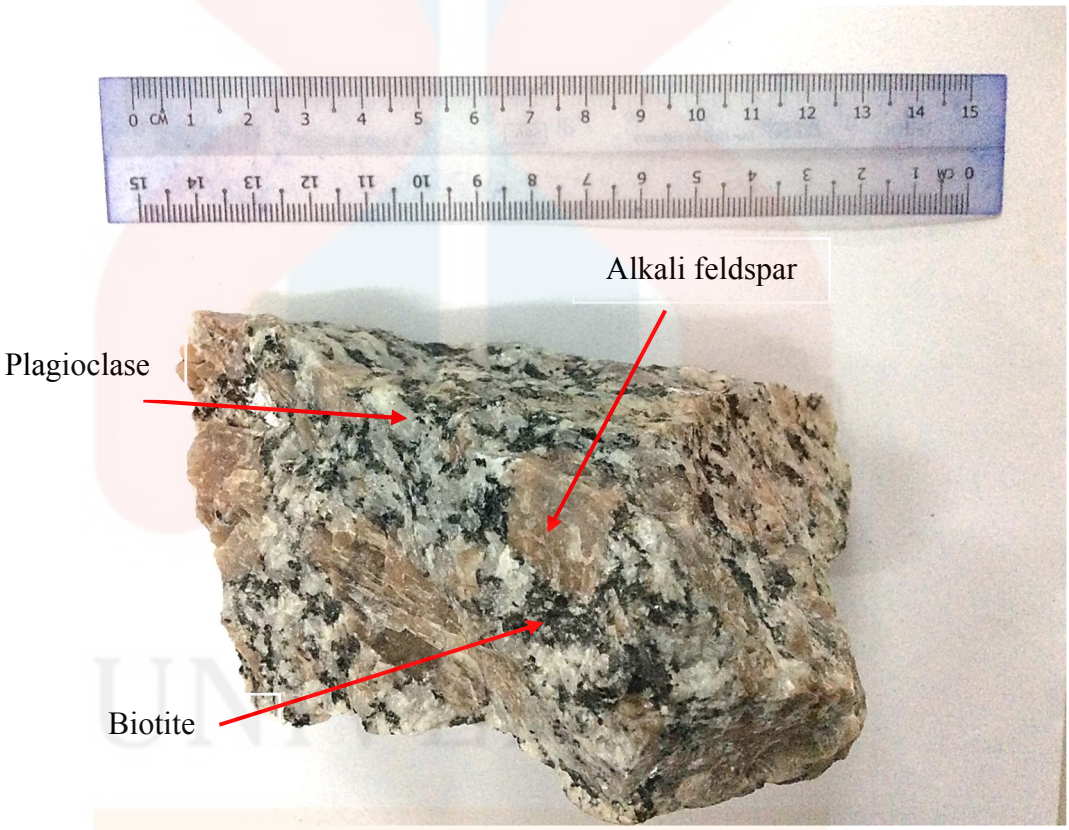

Figure 4.3.1: Hand specimen of granite at waypoint KH8D26

4.3.2 Microscopic description of lithology

Hand specimens collected from the field were thin-sectioning for the purpose of microscopic study of the rock under polarised microscope. Total five thin sections of the granites were studied and the optical properties of the minerals in the granites under microscope were described. Major minerals that were identified under polarized microscope are quartz, alkaline feldspar, plagioclase and biotite. Other accessory mineral identified was sphene. They were identified by their own optical characteristics respectively.

Plagioclase was white to greyish colour in hand specimen. Plagioclase was identified by its optical properties under polarized microscope. It was colourless under plane polarized light microscope (PPL). It did not change the colour during rotation of stage under plane polarized light. This indicated that the plagioclase was non-pleochroic. It was anhedral to subhedral in shape and its size was about 1 to 7 mm. It was grey first order birefringence. Plagioclase was differentiated from alkaline feldspar by the twinning habits of crystal. Plagioclase had both albite and Carlsbad twinning but alkaline feldspar can only have Carlsbad twinning. Inclusion of small biotite and sphene can be observed in the thin section of granite.

Alkali feldspar was anhedral in shape and its size is up to 3 cm. It had grey low first order birefringence under cross-polarized light. Alkali feldspar was colourless in under plane polarized light, which means that it is non-pleochroic. Alkali feldspars showed simple and Carlsbad twinning and perthite intergrowth in the thin section. The main types of alkali feldspar were perthitic orthoclase and often showed euhedral outline in hand specimen but sometimes appears to be irregular in thin section. Simple twinning of the alkali feldspar and the presence of small oriented euhedral inclusions usually plagioclase, oriented subparallel to the crystal faces of the host K-feldspar

suggested that the minerals were magmatic. Mantling of plagioclase over alkali feldspar are common.

Quartz can also be observed under the microscope. It was anhedral in shape and occurred as sub-grains in the thin section. It was colourless to greyish black under plane polarized light. The quartz occurred as individual mineral and some of them were filling up the space between others minerals especially alkali feldspar and plagioclase.

Biotite was the only mafic mineral that was found in the thin section of granite. It had pleochroism colour of brown to dark brown. Most of the biotite had lath shaped with rugged end. Cleavage of biotite was clearly shown and the presence of haloes can be seen under nicol. It normally enclosed many small crystals such as zircon, apatite, and magmatite.

Sphene can also be found in the thin section. It was an accessory mineral, which had pleochroic characteristic. It was brown to dark brown in colour. Sphene was euhedral to subhedral grains and formed a wedge or diamond shaped crystals.

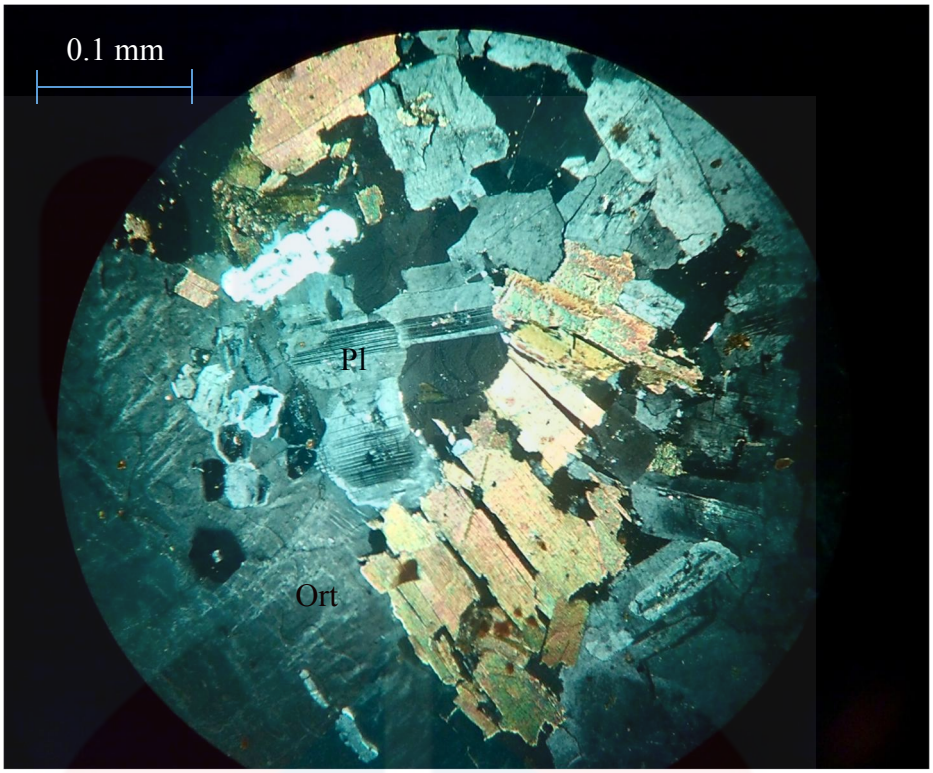

Figure 4.3.2: Thin section of granite showing the mantling of plagioclases (Pl) over alkali feldspar (Ort).

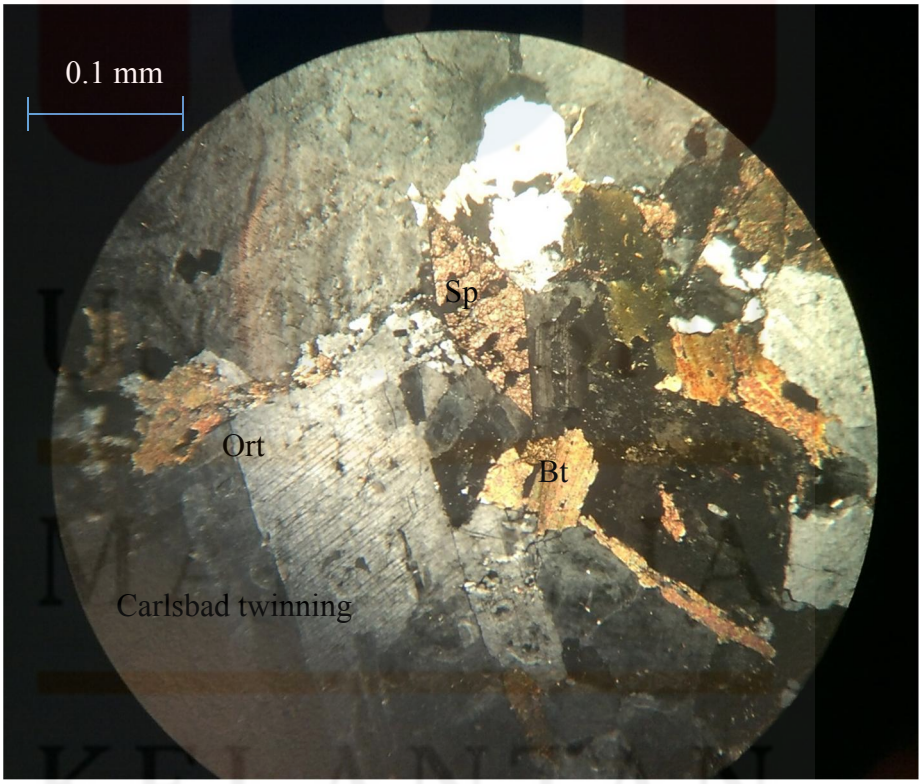

Figure 4.3.3: Thin section of granite showing the inclusion of wedge shape of sphene (Sp) and biotite (Bt) in the orthoclase (Ort) that has Carlsbad twinning.

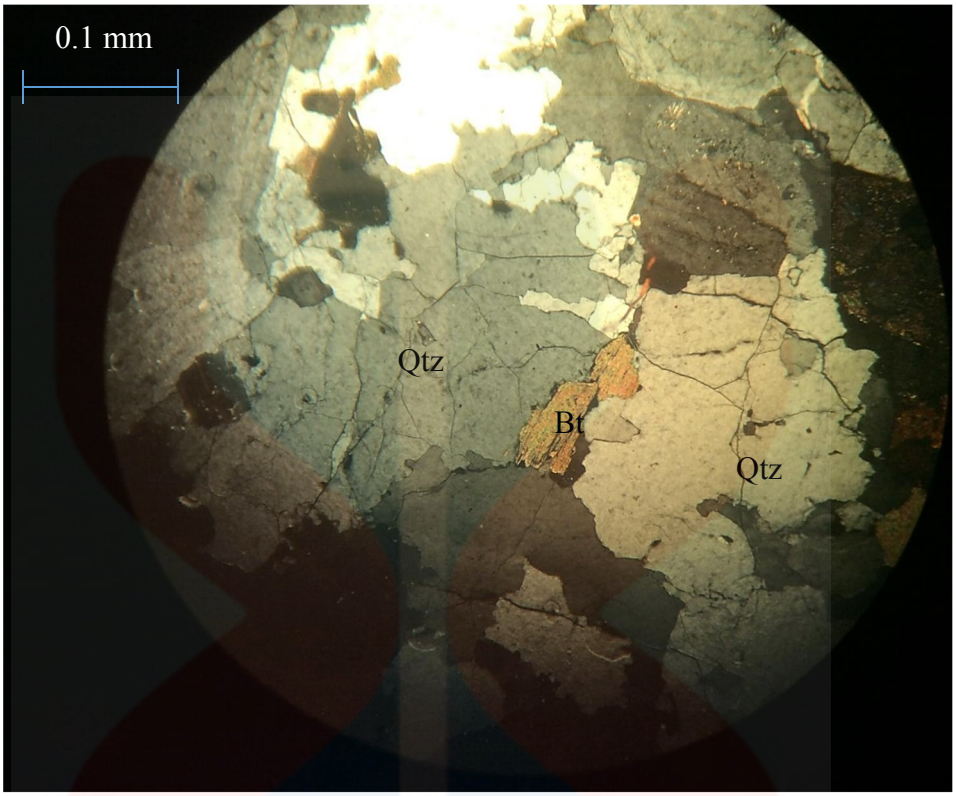

Figure 4.3.4: Thin section of granite showing inclusion of biotite (Bt) in the anhedral shape of quartz (Qtz)

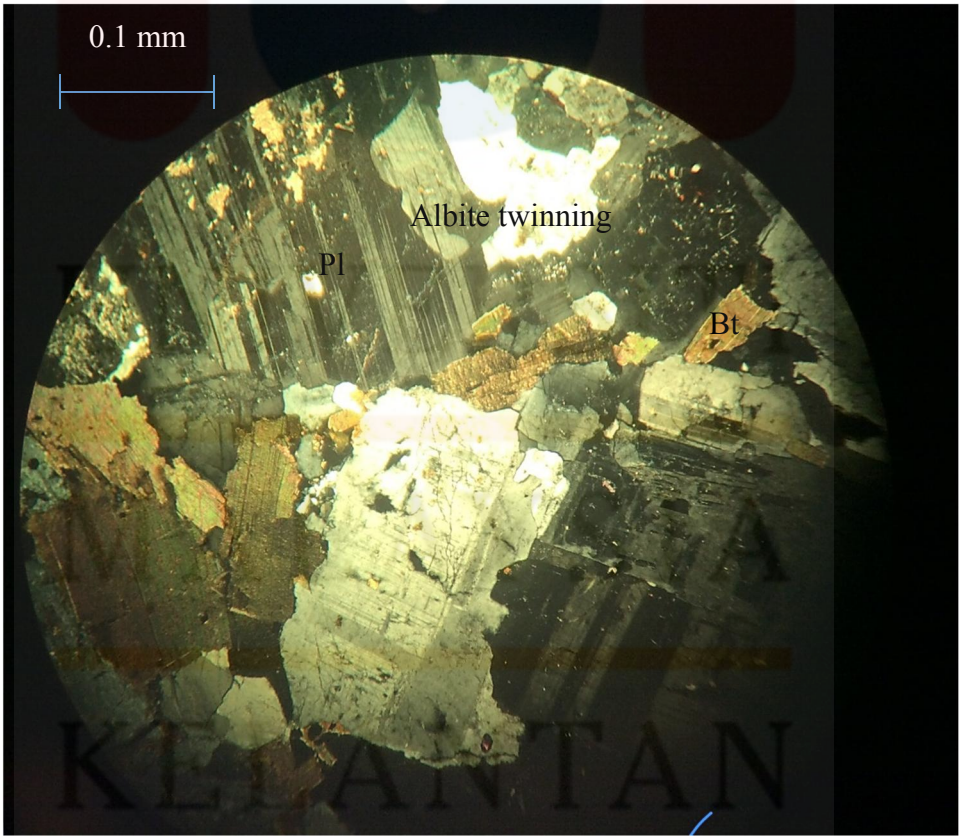

Figure 4.3.5: Thin section of granite showing the albite twinning of plagioclase crystals.

4.4 Structural geology

The study of the geological structures was started with the identification of the linear structures in the topography map. The linear structures were termed lineament which was an expression of the underlying geological structure such as fault. The structural map as shown in Figure 4.4.6 had two lineament that were trending northwest and southeast. Two lineaments were determined based on the elongated forms of contour and straight continuous pattern of small river in the map. The lineaments were interpreted as fracture zone where the granitic rocks in the study area were fractured open by the uplifting of magmatic intrusion. Therefore, the landscape of mountainous ridges with steep valley was formed at the study area.

The geological structures that can only be observed at the study were joints, fractures and veins only. The faults were not visible because there no bedding structures that showed the movement of the rock since all the rocks in the study area were made up of igneous rocks. At the field, the orientation of the fractures were taken in order to determine the direction of the principal stress σ_1 that causes the brittle deformation of granites in the study area.

4.4.1 Joints

Joints developed during the exhumation of rocks following erosion of the overburden. Joints resulted from contraction and expansion due to cooling and decompression respectively. The persistence of the joints were long and their average aperture size were less than 5millimeters.

4.4.2 Fractures

The fractures that were observed in the study area were majority types of extensional fractures and conjugate shear fractures. Regional tectonics, folding, faulting, and internal stress released during cooling might caused the formation of fractures. From the Figure 4.4.1, the adjacent blocks of the rocks moved away from each other in a direction sub perpendicular to the fracture plane.

Figure 4.4.1: Fractures that form on the outcrop of granite

Besides that, many conjugate shear fractures can also be observed in the study area as shown in Figure 4.4.2 and Figure 4.4.3.

Figure 4.4.2: Conjugate shear fractures on the outcrop

Figure 4.4.3: Conjugate shear fractures that formed from brittle deformation

4.4.3 Veins

The observation from the fieldworks found that the aplite veins were present in the outcrop of granite as shown in Figure 4.4.4. Aplite is the fine-grained intrusive igneous rock with granitic minerals composition. Quartz and feldspar often crystallize together in aplite to form a graphic texture but the grains are not visible with naked eye (Wells & Bishop, 1954). The aplite veins seen in the outcrops were pinkish in colour due to higher composition of feldspar. The width of the veins were about 30 mm to 50 mm whereas the lengths were about 1 m to 1.5 m long. Aplite veins were believed to form when there had a secondary intrusion of magma into the fracture of the granitic country rock. The relative rapid cooling of the magma crystallizing the fine-grained aplite veins due to the rapid heat loss of magma to the surrounding granitic country rocks.

Figure 4.4.4: Pinkish aplite vein about 1.0 m long seen on the outcrop

4.4.4 Mechanism of structures

The orientation of discontinuities such as joints and fractures were taken from the fieldwork and plotted in the Rose diagram as shown in Figure 4.4.5. From the Rose diagram, most the discontinuities were trending in the direction from 035° to 075°. This indicated that the principal stress, σ_1 is originating approximately from the direction of NE-SW. The compressive stresses from this direction pushed the rocks and caused them to produce discontinuities as a result of brittle deformation.

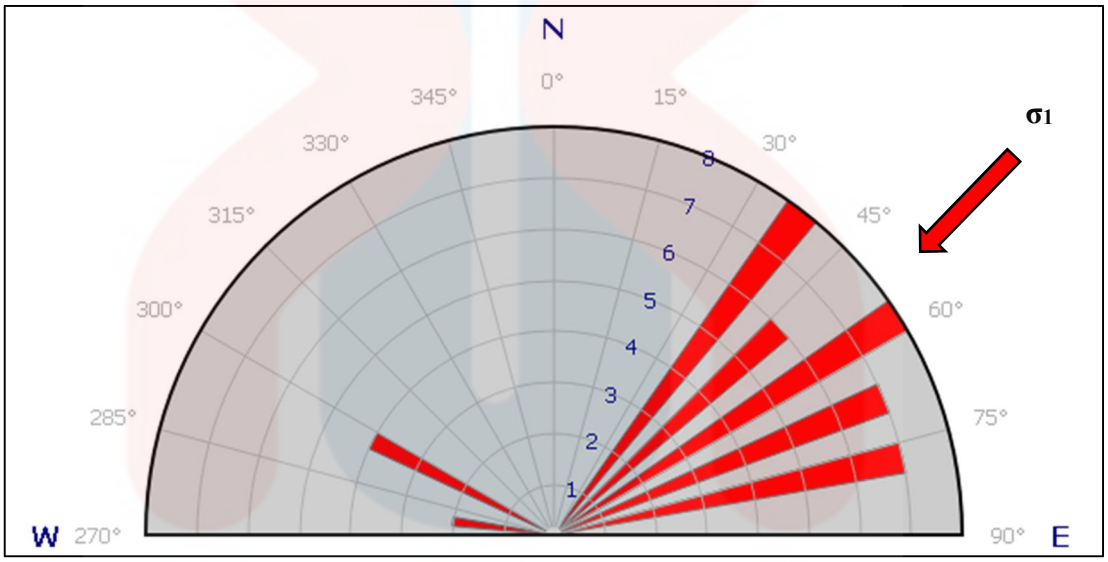

Figure 4.4.5: Rose diagram for the orientation of discontinuities collected from the study area

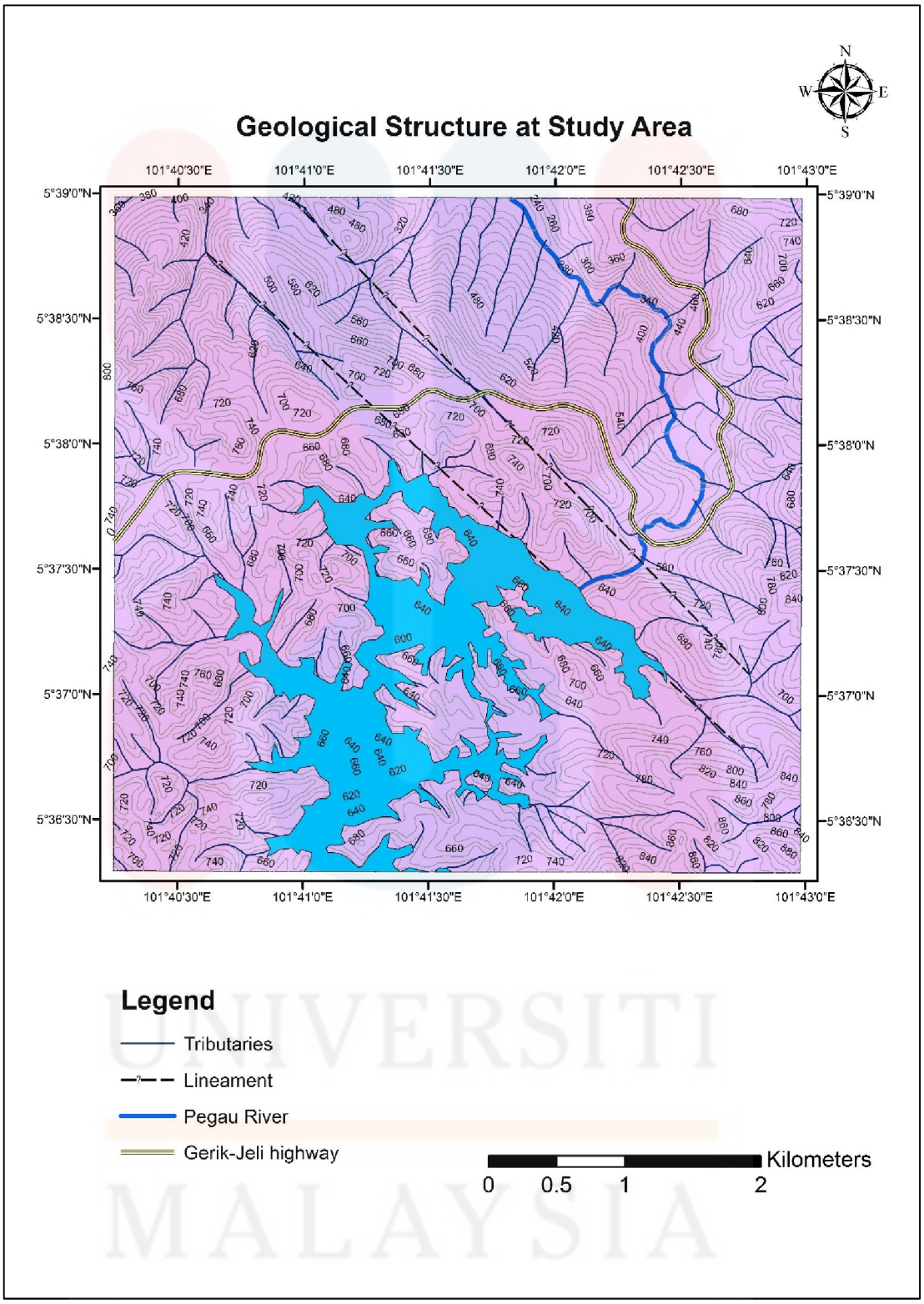

Figure 4.4.6: Structure map of the study area at Tasik Pergau Jeli, Kelantan

4.5 Historical Geology

The granitic rocks in the study area belong to Noring Granite unit. Noring granite was the largest plutonic rock located at the north of Stong Complex (Ghani, 2009). The pluton of Stong Complex was believed to be originated from the protrusion of Main Range granite batholith (MacDonald, 1967). Decompression melting and melting due to heat transfer resulting in the formation of magma. The flowing of less dense magma raised up the overlying rock Cretaceous period. The weight of the overlying rock created pressure at depth that squeezed the magma upward to form various intrusive igneous settings such as dikes, sills and plutons. The magma started to cool gradually at depth and the minerals started to crystallize according to Bowen's reaction series. Early-formed crystals tended to be relatively mafic and this removed the magnesium and iron from the magma. The remaining magma became more felsic and crystallize to form intrusive felsic rocks.

After the first intrusion of magma, there were second intrusion of magma where it mixed with the primary magma. This can be proved by the mantled texture of alkali feldspar as shown in Figure 4.3.2. The formation of mantled texture was due to magma mixing. The plagioclase rim probably precipitated from a different magma type to the Noring magma probably of andesitic composition. The alkaline feldspar that had crystallised in the Noring magma acted as substrates for the growth of plagioclase, producing the mantled texture. The aggregates of individual crystals that had floated together in the magma attached to the alkaline feldspar. Besides that, secondary magma intrusion can also proved by the presence of aplite veins where the secondary magma intruded to the fracture of the country rock and cooled rapidly to form fine-grained crystal aplite.

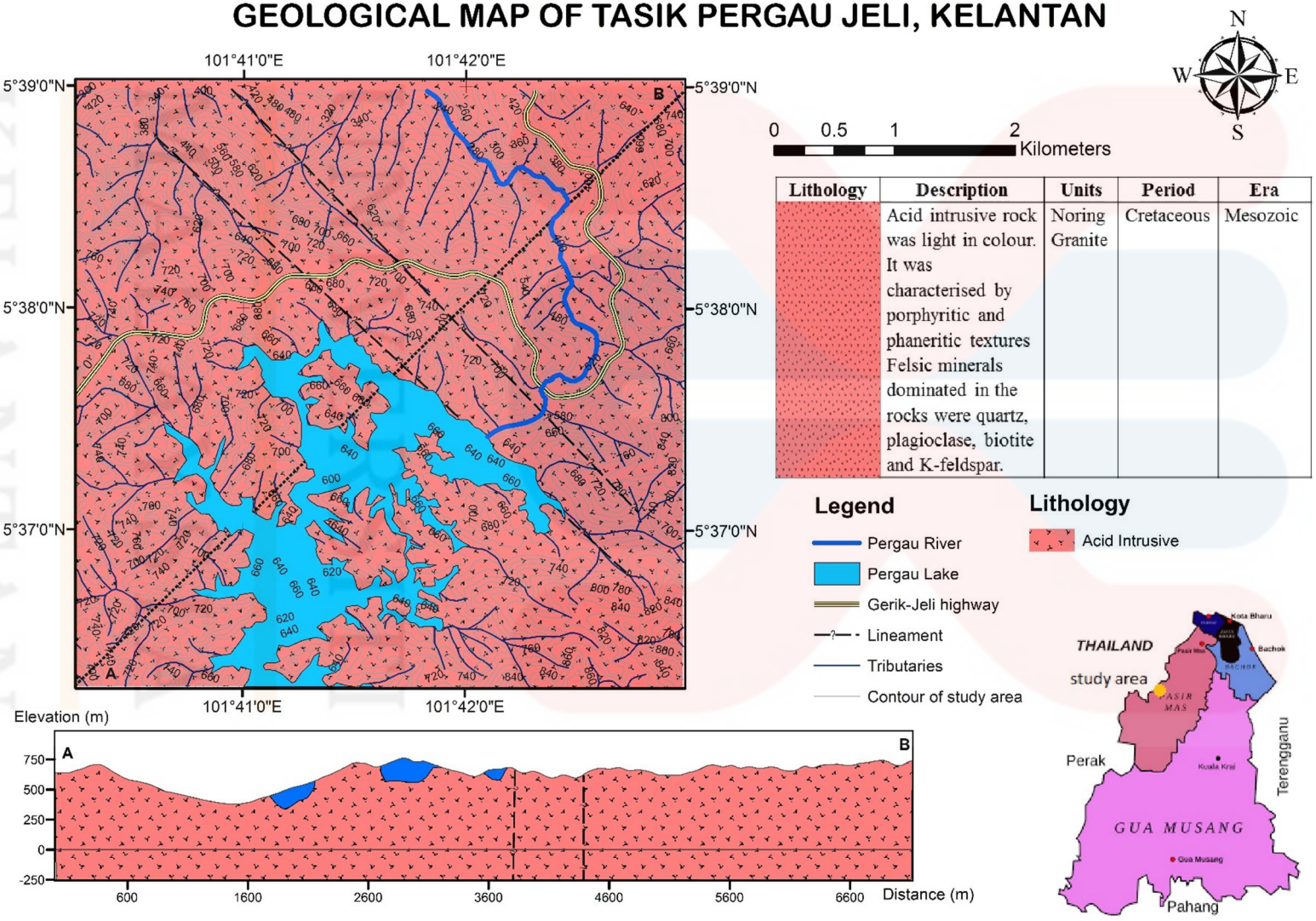

Figure 4.5.1: Geological map of Tasik Pergau Jeli, Kelantan

CHAPTER 5

RESULT AND DISCUSSION

5.1 Introduction

Rock masses comprise of rocks with the geological discontinuities such as bedding planes, fault, fissures, joints, fractures and other mechanical defects that possess the common characteristic of low shear strength (Priest & Hudson, 1976). Complex discontinuities can be widely distributed within the rock slope masses. The rock mass of less discontinuity with great spacing in favourable orientations is considered as a good rock mass. In contrast, poor rock mass possess close discontinuity spacing in unfavourable orientations.

Nevertheless, the Rock Mass Rating of the rock alone (Bieniawski, 1989) is not enough in evaluating the stability of the rock slope. Therefore, Slope Mass Rating introduced by Romana (1985) is used to rate the stability of the rock slope. Slope Mass Rating is taking accounts of Rock Mass Rating and kinematic analysis to determine the stability of the rock slope. Kinematic analysis must be conducted to analyse and interpret the possibility and the direction of rock slope to fail. Slope Mass Rating is calculated only for the slope that has potential to fail from kinematic analysis.

The discontinuities data and uniaxial compressive strength data of rock collected from the field were incorporated into the Rock Mass Rating system. The discontinuities data collected from the discontinuity survey were also input into the Stereonet Window software for kinematic analysis. The result of Rock Mass Rating

and kinematic analysis of the rock slope are incorporated each other to determine the Slope Mass Rating of the rock slope that had potential to fail.

Total five rock slopes evaluated along the Gerik-Jeli highways included Slope 1, Slope 2, Slope 3A, Slope 3B and Slope 4. These five rock slopes were located in different location as shown in Figure 5.1.1,

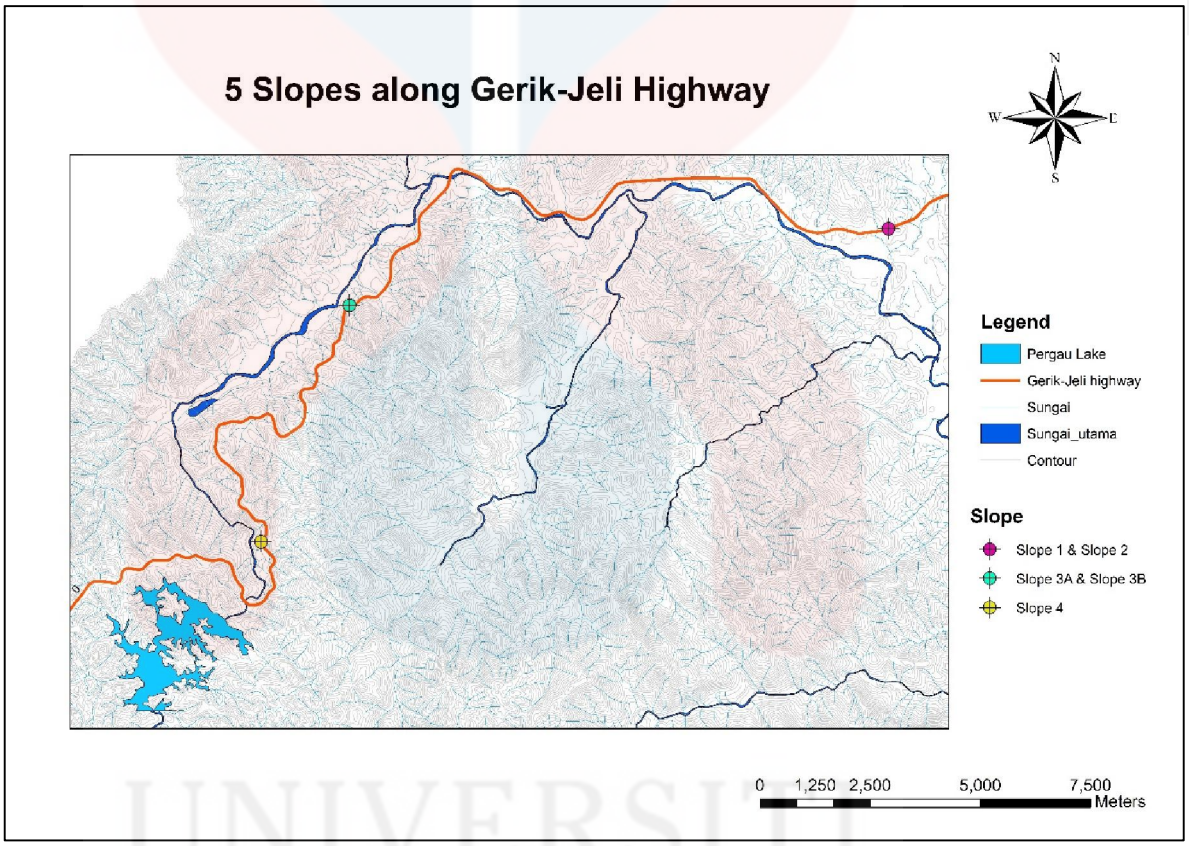

Figure 5.1.1: Map that shows the slopes long Gerik-Jeli highway

5.1.1 Geology of Slope 1

Slope 1 was a rock slope located the roadside of Gerik-Jeli highways (5°42'14.93"N, 101°50'14.53"E). It was a natural cut slope that was excavated during the construction of Gerik-Jeli Highway. The height of the slope was estimated about 7.2 m. The slope face of the slope had an orientation with dip direction of 160° and dip angle of 79°. The types of lithology that can be found in this slope are biotite granites. Biotite granitic rocks in the slope are highly fractured to produce fissures and joints. The bedding plane is absent in the slope because the rocks are igneous rock. The slope is covered partly by vegetation and moderately weathered as shown in Figure 5.1.2.

Figure 5.1.2: Photo taken at Slope 1

5.1.2 Geology of Slope 2

Slope 2 was located opposite near to the Slope 1. It was a rock cut slope with coordinates of (5°42'15.01"N, 101°50'14.19"E). The slope was about 6.16m in height with the slope face orientation of 005°/82°. The rocks in the Slope 2 were biotite granite that were same as those in Slope 1. The biotite granitic rocks were moderately weathered with discolouration at the outer surface of the rock. Discontinuities were widely distributed at the rock mass of Slope 2.

Figure 5.1.3: Photo taken at Slope 2

5.1.3 Geology of Slope 3A

Slope 3A was type of rock slope that was cut at the roadside of Gerik-Jeli Highway with coordinates (5°41'17.49"N, 101°43'37.10"E). The height of the Slope 3A was about 5.1 m. The slope face of the slope was dipping in the orientation of 008° with the dip angle of 81°. From the field observation, the lithology of the Slope 3 was made up of mica schist. The schists with a schistose texture had a cleavage along the plane of their weakness. Discontinuities such as bedding plane in the rocks were dipping in the direction of slope face. The rocks in Slope 3A were moderately subjected to chemical and mechanical weathering. Red brownish colour of iron oxide can be observed within the rocks in Slope 3A.

Figure 5.1.4: Photo taken at Slope 3A

5.1.4 Geology of Slope 3B

Slope 3B was also cut rock slope along the Gerik-Jeli Highway (5°41'17.49"N, 101°43'37.10"E). It was located near to the Slope 3. Slope 3A and Slope 3B were similar slope that formed a curve slope at the highway. However, the orientation of slope face and discontinuities between two slopes were different. The estimated height of the slope was around 6.61m. Dipping direction of the slope face was 320° whereas the dipping angle of the slope was 78°. The types of rock found in this slope were same as the rock in Slope 3A, which were mica schists. Bedding plane of the rocks were the most discontinuities that can be found in Slope 3B. The slope was also subjected to around Grade 3 of weathering.

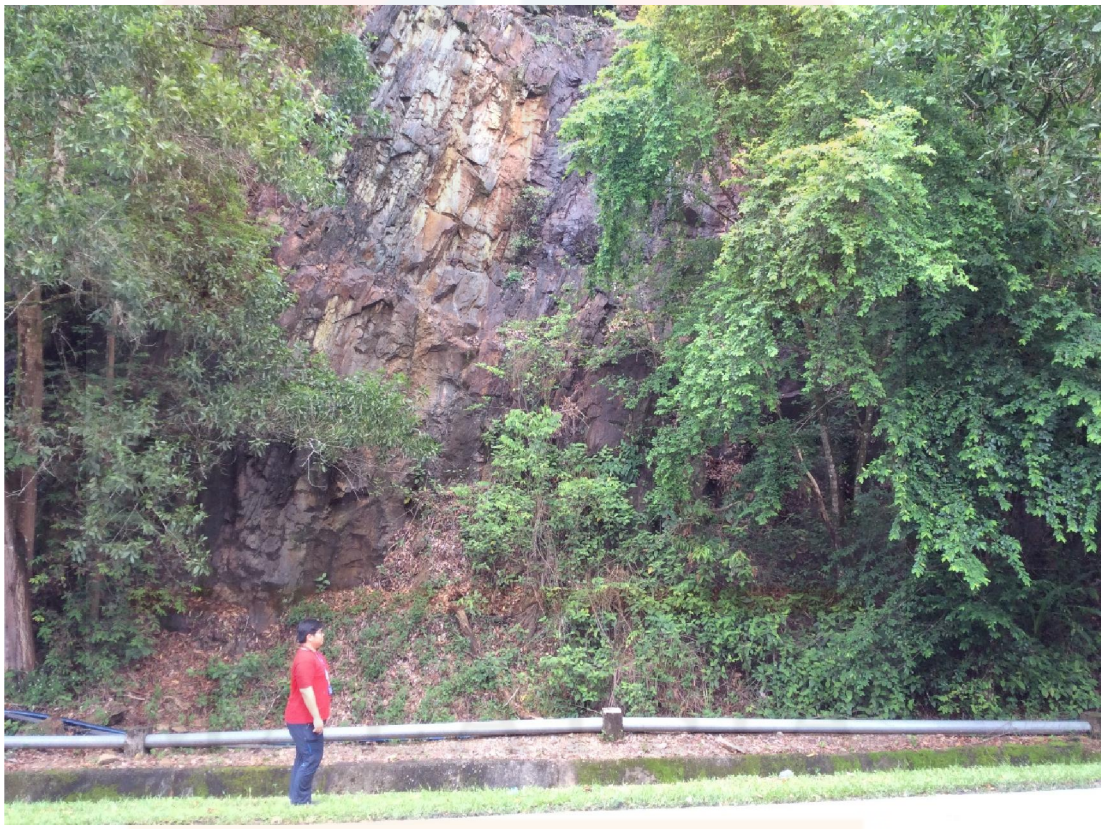

Figure 5.1.5: Photo taken at Slope 3B

5.1.5 Geology of Slope 4

Slope 4 was a rock slope located the roadside of Gerik-Jeli highways (5°38'22.92"N, 101°42'32.35"E). It was a cut slope that was excavated during the construction of Gerik-Jeli Highway. The height of the slope was estimated about 3.3m. The slope face of the slope had an orientation with dip direction of 290° and dip angle of 88°. The types of lithology that can be found in this slope were Feldspatic granites. Feldspatic granite in the slope were fractured to produce fissures and joints. The bedding plane was absent in the slope because the rocks were igneous rock. The slope was covered partly by vegetation and moderately weathered as shown in Figure 5.1.6.

Figure 5.1.6: Photo taken at Slope 4

5.2 Discontinuity Survey and Analysis

Discontinuity survey was conducted in each respective five slopes that had been designated as Slope 1, Slope 2, Slope 3A, Slope 3B and Slope 4. The survey was conducted to obtain the data required by kinematic analysis and Rock Mass Rating System. The data that were collected from the discontinuity survey are orientation of discontinuities, persistence, aperture, infilling material, roughness, water condition and spacing of discontinuities.

5.2.1 Discontinuity Survey of Slope 1

Slope 1 had orientation of $160^{o}/79^{o}$. The orientation, persistence, aperture, infilling material, roughness, water condition and spacing of discontinuities that intersect the scanline set up on the face of Slope 1 were recorded in the data sheet of discontinuity survey. Type of discontinuities that were present in Slope 1 were joints. The orientation of joints collected from Slope 1 were incorporated into the software DIPS 5.0 to identify the joint sets in Slope 1. From the contour plot diagram and rosette plot diagram produced by software DIPS 5.0 as shown in Figure 5.2.1 and Figure 5.2.2 respectively, three joints sets are identified and designated as J1, J2 and J3. The dip direction and dip angle of each joint sets are tabulated in Table 5.1.

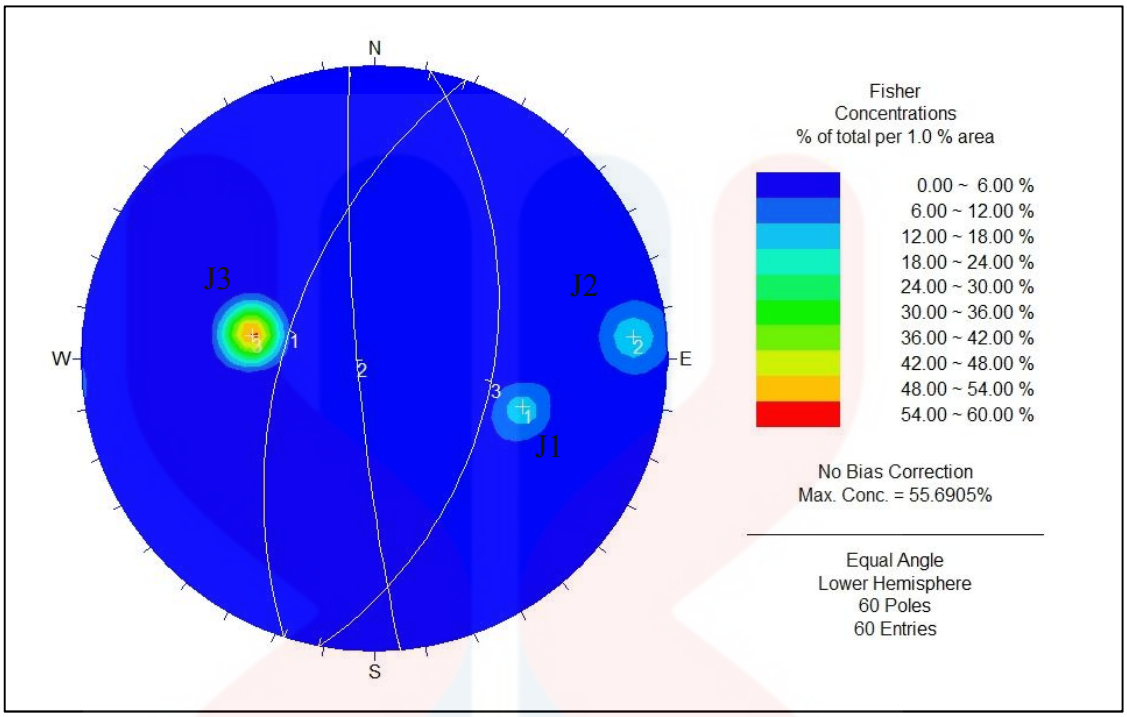

Figure 5.2.1: Contour plot of orientation of joints on Slope 1

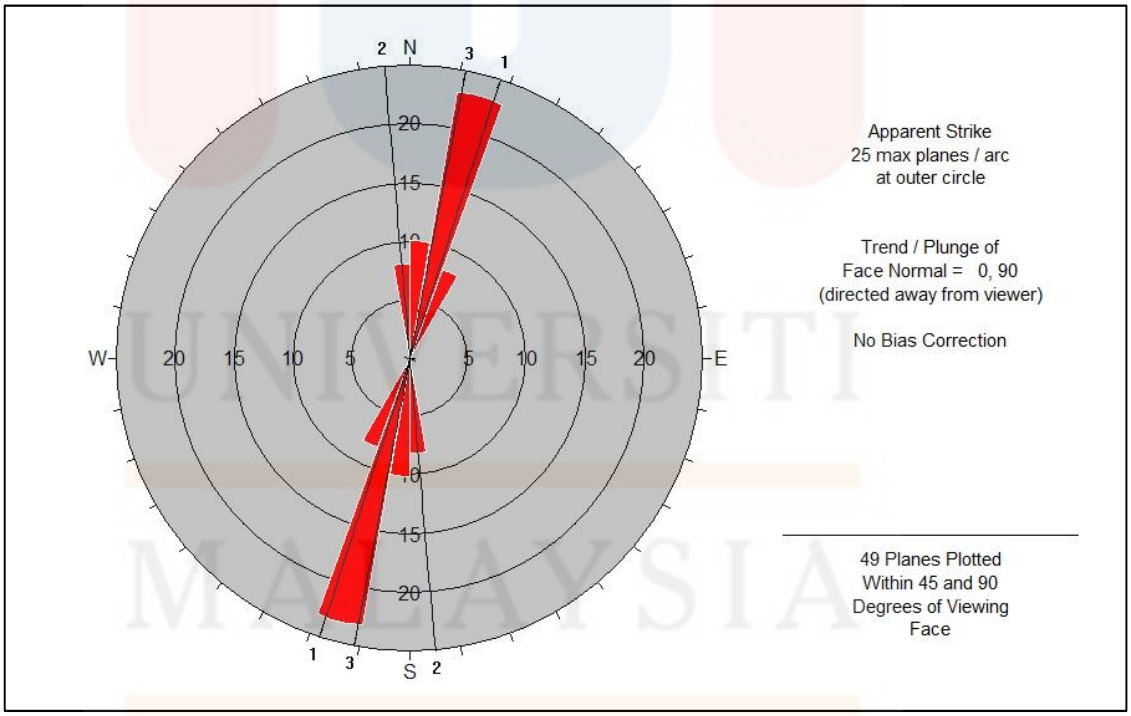

Figure 5.2.2: Rosette plot of orientation of joints on Slope 1

Table 5.1: Orientation of joint sets on Slope 1

Slope 1		
Joint Set	Dip Direction (°)	Dip Angle (°)
J1	288	56
J2	265	83
J3	101	46

In Figure 5.2.1, J1 had reached about 48% to 54% of Fisher concentration of total 1% of area in stereonet. J2 and J3 had the Fisher concentration of about 12% to 18% per 1% of the area. The identified joint sets with their respective joint spacing were categorised and tabulated in the Table 5.2 to determine the mean spacing of each joint sets. From the Table 5.2, the means spacing of J1, J2 and J3 are 0.45m, 0.34m and 0.31m respectively. Three means spacing of the joint sets were used to calculate the Rock Quality Designation (RQD) of rock by using the equation 3.2 in Chapter 3. The calculated RQD of Slope 1 was 87.12%. Furthermore, the aperture of discontinuities were gapped features which open about 1 to 3mm. the trace length of discontinuities in the slope were about 1 to 3m long. There were lack of infilling material in the discontinuities and water was absent in the slope.

Table 5.2: Spacing of discontinuities at Slope 1

	J3 (m)	J2 (m)	J1 (m)
	0.08	0.3	0.45
	0.08	0.32	0.41
	0.07	0.33	0.38
	0.08	0.29	0.42
	0.06	0.28	0.43
	0.17	0.34	0.44
	0.12	0.41	0.45
	0.13	0.42	0.46
	0.08		0.47
	0.14		0.43

Slope 1	0.14		0.45
	0.15		0.46
	0.16		
	0.09		
	0.08		
	0.1		
	0.1		
	0.1		
	0.18		
	0.17		
	0.52		
	0.51		
	0.49		
	0.51		
	0.53		
	0.48		
	0.49		
	0.55		
	0.56		
	0.54		
	0.53		
	0.52		
	0.51		
	0.5		
	0.55		
	0.53		
	0.54		
	0.47		
	0.46		
	0.47		
Means, $\bar{X}$	0.3135	0.33625	0.4375
$1/\bar{X}$	3.189793	2.973978	2.285714
Median	0.32	0.325	0.445
Mode	0.08	#N/A	0.45
Std Dev	0.204796	0.052627	0.025271

5.2.2 Discontinuity Survey of Slope 2

The orientation of face of Slope 2 was 005º/82º. The parameters of discontinuities within the scanline set up on the face of Slope 2 were collected and recorded. Joints were the most type of discontinuities formed on Slope 2. The orientation of the joints were input into the DIPS 5.0 software to determine the joint sets in Slope 2. From the contour plot diagram and rosette plot diagram as shown in Figure 5.2.3 and Figure 5.2.4 respectively, total three joint sets are identified in the diagram and designated as J1, J2 and J3. Then, the orientation of each joint sets are recorded in the Table 5.3.

In Figure 5.2.3, the Fisher concentration of J1 was about 14% to 16% of total 1 % of the area of stereonet. The Fisher concentration of set J2 and J3 were same with J1, which was 14% to 16%. Three joints sets with their respective spacing were categorised and grouped together in Table 5.4. The means spacing of each joints set were determined and used to calculate the RQD of the rock. The calculated RQD value of Slope 2 was 68.44%.

Besides that, the opening or aperture of the discontinuities in Slope 2 were moderately wide which were about 3 to 10mm width. The average persistence of the discontinuities were about 1 to 3m long that can be considered as low persistence according to ISRM (1978). There were no infilling material within the discontinuities and the condition of the water in the slope was dry.

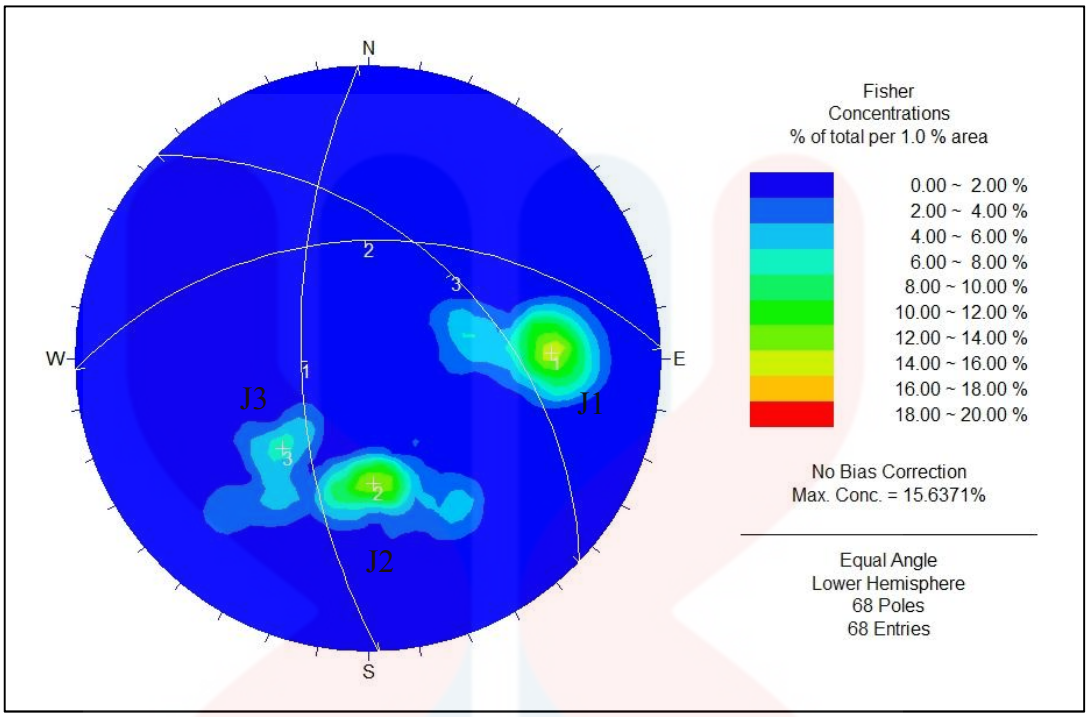

Figure 5.2.3: Contour plot of orientation of joints on Slope 2

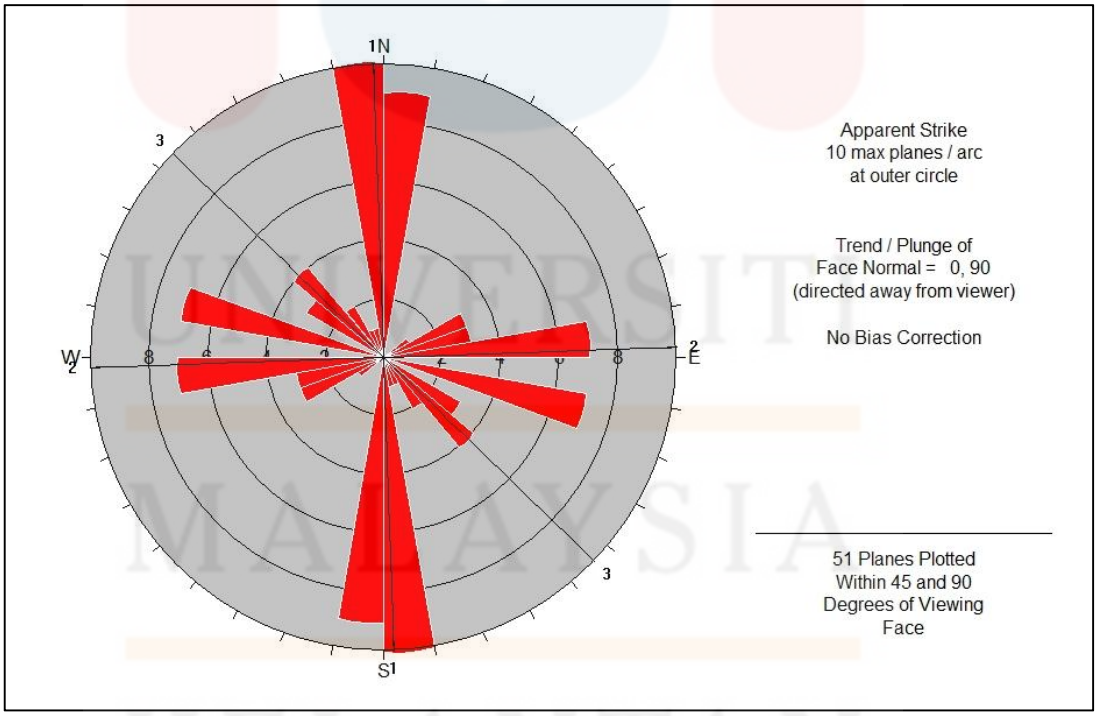

Figure: 5.2.4: Rosette plot of orientation of joints on Slope 2

Table 5.3: Orientation of joint set on Slope 2

Slope 2		
Joint Set	Dip Direction (^{o})	Dip Angle (^{o})
J1	268	64
J2	358	46
J3	044	46

Table 5.4: Spacing of discontinuities at Slope 2

	J1 (m)	J2 (m)	J3 (m)
Slope 2	0.3	0.16	0.3
	0.09	0.17	0.42
	0.08	0.17	0.34
	0.12	0.19	0.35
	0.15	0.23	0.35
	0.16	0.15	0.42
	0.15	0.15	0.42
	0.17	0.16	0.21
	0.18	0.17	0.32
	0.16	0.24	0.36
	0.15	0.25	0.36
	0.19	0.15	0.37
	0.2	0.16	0.4
	0.21	0.27	0.39
	0.18	0.11	
	0.17	0.12	
	0.18	0.2	
	0.16	0.21	
	0.17	0.22	
	0.18	0.23	
	0.09	0.19	
	0.08	0.2	
	0.11	0.21	
	0.13	0.24	
	0.16	0.24	
	0.17		
	0.19		
	0.22		

	0.23		
	0.19		
Means, $\bar{X}$	0.164	0.1916	0.357857
$1/\bar{X}$	6.097561	5.219207	2.794411
Median	0.17	0.19	0.36
Mode	0.16	0.16	0.42
Std Dev	0.047095	0.042099	0.056593

5.2.3 Discontinuity Survey of Slope 3A

Slope 3A had the face dipping in the direction of 008^{o} and inclining at an angle of 81^{o}. The same procedures were taken to collected the parameters of discontinuities in Slope 3A and identify the joint set in the contour plot diagram. Majority type of discontinuities in this slope were fractures. Based on the contour plot diagram and rosette plot diagram in Figure 5.2.5 and Figure 5.2.6 respectively, three joint sets are identified and designated as J1, J2 and J3. J3 has the highest Fisher concentration when compared with J2 and J1 that is 24% to 27%. J2 and J1 sets have the same concentration around 21% to 24%.

The orientation of the joint sets were then tabulated in Table 5.5. The spacing of the discontinuities collected from the discontinuity survey are categorized and grouped together according to the identified joints sets. The means spacing of discontinuities in each joint sets were determined as shown in Table 5.6 and used to calculate the RQD of Slope 3A. The RQD value calculated from the spacing of discontinuities is 61.84%.

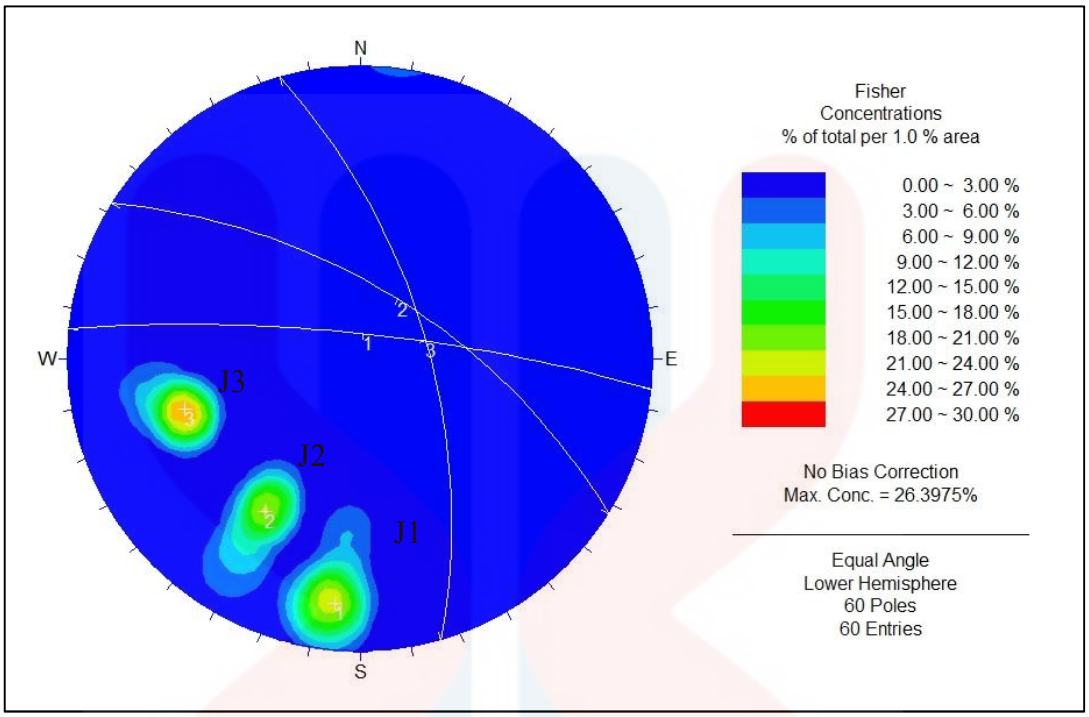

Figure 5.2.5: Contour plot of orientation of joints on Slope 3A

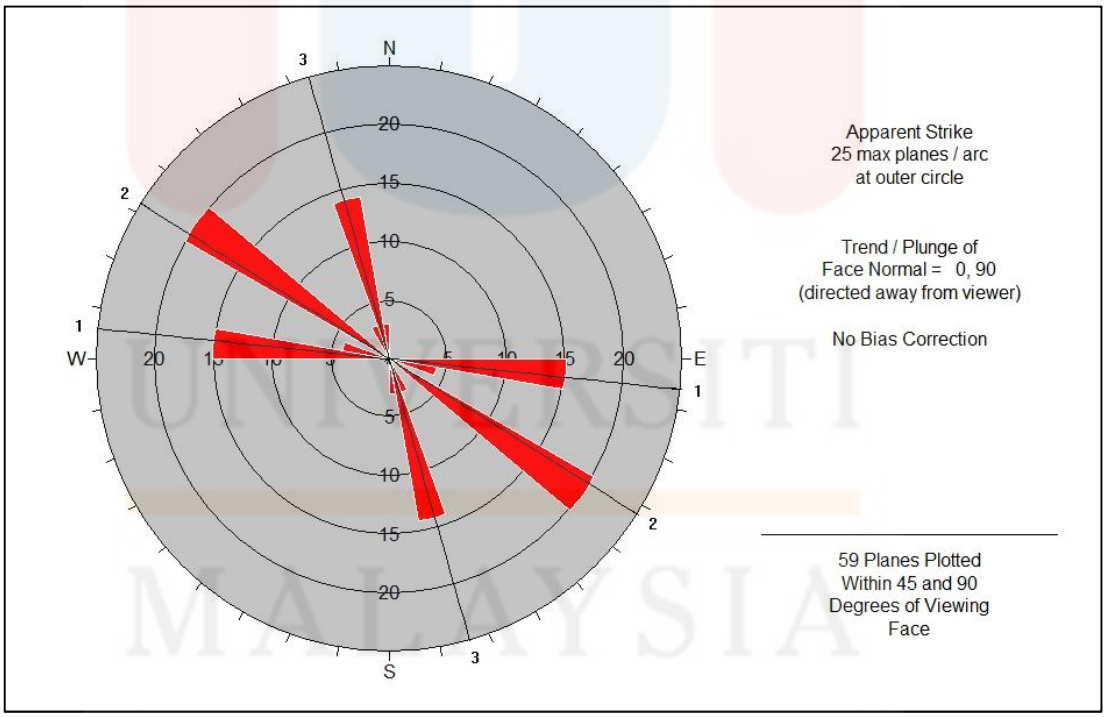

Figure 5.2.6: Rosette plot of orientation of joint on Slope 3A

The perpendicular distance that separated the discontinuity was wide which was more than 30 mm and the persistence of the discontinuity is about 3 to 10 m long. There were no infilling material between the discontinuities. However, the water, which was dripping in Slope 3A, can be observed. Therefore, it will reduce the shear strength between the discontinuities.

Table 5.5: Orientation of joint set on Slope 3A

Slope 3A		
Joint Set	Dip Direction (°)	Dip Angle (°)
J1	006	80
J2	032	63
J3	074	64

Table 5.6: Spacing of discontinuities at Slope 3A

	J1 (m)	J2 (m)	J3 (m)
Slope 3A	0.1	0.32	0.19
	0.09	0.47	0.18
	0.11	0.48	0.16
	0.11	0.36	0.19
	0.13	0.35	0.17
	0.16	0.34	0.18
	0.12	0.33	0.16
	0.11	0.45	0.24
	0.12	0.29	0.23
	0.13	0.38	0.22
	0.14	0.38	0.23
	0.15	0.27	0.2
	0.16	0.37	0.21
	0.17	0.39	0.17
	0.14	0.28	0.18
	0.11	0.4	0.21
	0.12	0.37	0.18
	0.1	0.36	0.2
	0.09	0.3	0.21
	0.08		0.17
Means, $\bar{X}$	0.122	0.362632	0.194
$1/\bar{X}$	8.196721	2.75762	5.154639
Median	0.12	0.36	0.19
Mode	0.11	0.36	0.18
Std Dev	0.025257	0.059614	0.024149

5.2.4 Discontinuity Survey of Slope 3B

Face of Slope 3B had a dip direction of 320^{o} and dip angle of 78^{o}. The discontinuities found in this slope were bedding plane. Based on the contour plot diagram and rosette plot diagram produced by DIPS 5.0 software as shown in Figure 5.2.7 and Figure 5.2.8 respectively, only one joint set was identified and designated as J1. J1 set has approximately 85% to 95% of Fisher concentration per 1% of area of stereonet. From the contour plot diagram, the orientation that was dip direction and dip angle of the J1 set are tabulated in Table 5.7.

Table 5.8 below showed the spacing of discontinuities collected from the survey. From the table, the mean spacing of J1 set was 0.27m. The value of RQD, which was 100%, was calculated from the mean spacing of discontinuities by using the equation 2.2. Next, the average aperture of the discontinuities found in Slope 3B was about 1 to 3 mm in width whereas the average persistence of the discontinuities was about 3 to 10m long. The water condition of the slope was dry and no infilling material present in the discontinuities.

Table 5.7: Orientation of joint set on Slope 3B

Slope 3B		
Joint Set	Dip Direction (^{o})	Dip Angle (^{o})
J1	042	71

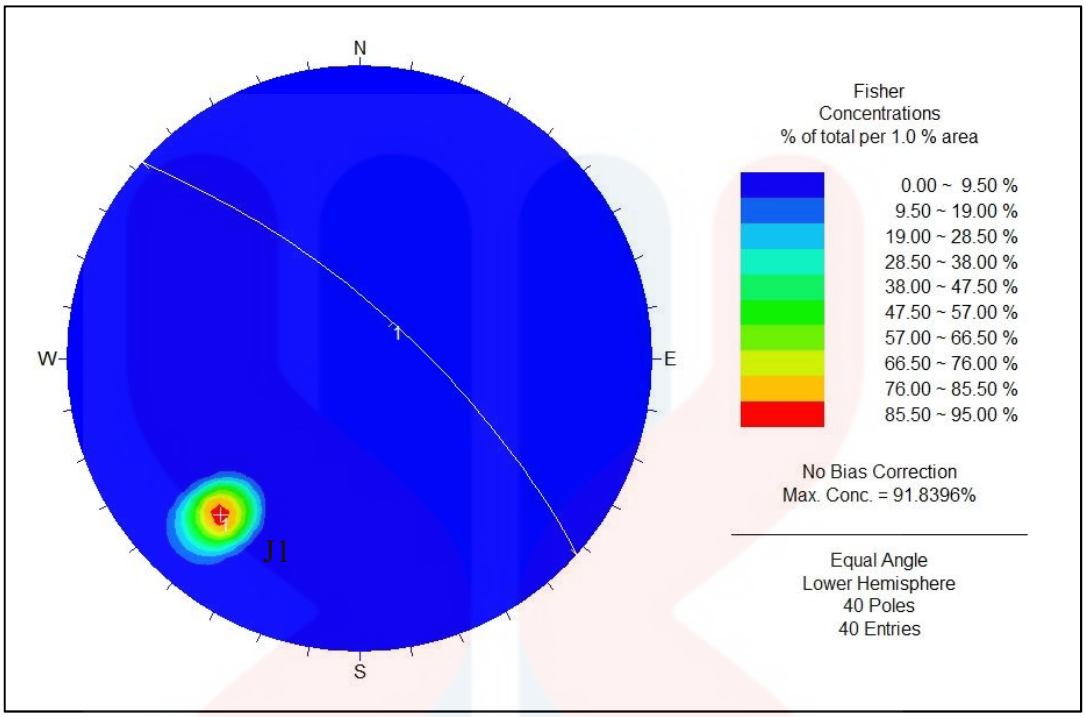

Figure 5.2.7: Contour plot of orientation of joints on Slope 3B

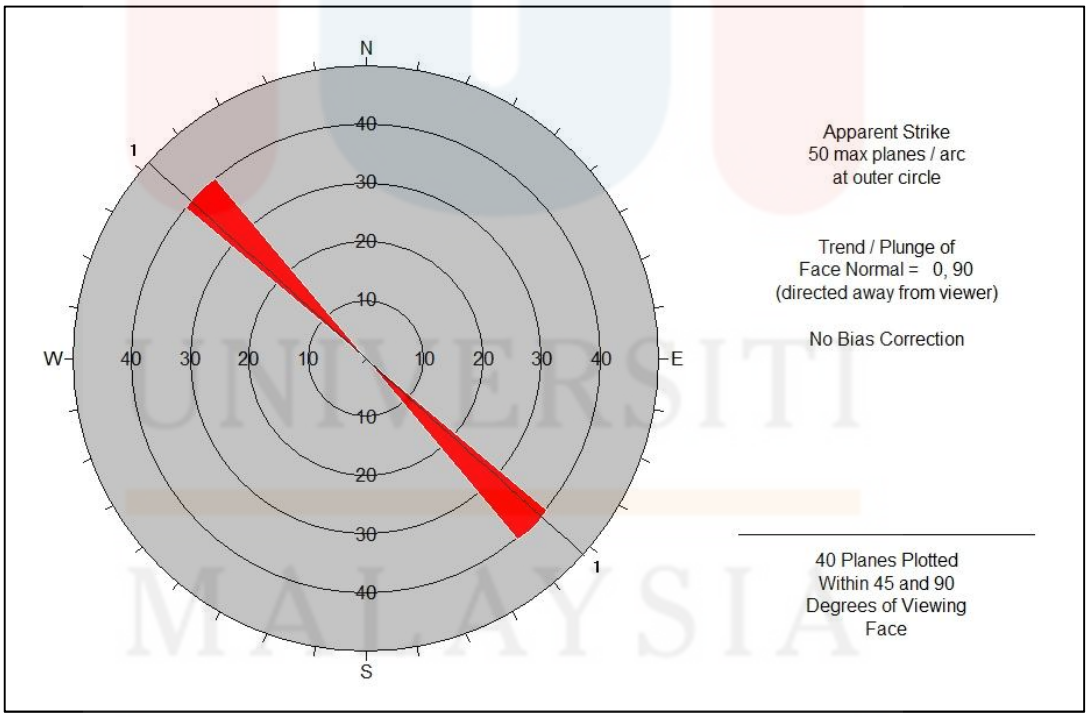

Figure 5.2.8: Rosette plot of orientation of joints on Slope 3B

Table 5.8: Spacing of joint sets at Slope 3B

	J1 (m)
Slope 3B	0.25
	0.21
	0.14
	0.28
	0.17
	0.22
	0.23
	0.28
	0.27
	0.21
	0.18
	0.17
	0.36
	0.34
	0.28
	0.38
	0.29
	0.28
	0.32
	0.31
	0.31
	0.25
	0.26
	0.17
	0.31
	0.28
	0.27
	0.3
	0.29
	0.28
	0.3
	0.29
	0.3
	0.28
	0.31
	0.32
	0.33
	0.32
	0.32
	0.33
Means, $\bar{X}$	0.27475
$1/\bar{X}$	3.639672
Median	0.28
Mode	0.28
Std Dev	0.055377

5.2.5 Discontinuity Survey of Slope 4

The slope face of Slope 4 was found to dip in the direction of 290° with dip angle of 88°. Most of the discontinuities observed in Slope 4 were joints. By using the discontinuities data obtained from the survey, the contour plot diagram and rosette plot diagram were produced using DIPS 5.0 software to identify the joint set. Based on the Figure 5.2.9, two joint sets were identified from the contour plot diagram and were designated as J1 and J2. The Fisher concentration of J1 set was higher than Fisher concentration of J2 set. This indicated that the frequency of joints found in J1 was higher than in J2. The orientation of each joint sets were recorded in the Table 5.9.

The spacing of the discontinuities were categorized based on the joint sets in Table 5.10. From Table 5.10, the means spacing of each joint sets were determined. The means spacing of J1 was 0.72 m, which was larger than spacing of J2, set which was 0.39 m. From the value of means spacing of each joint sets, calculated RQD value was 100%. Besides that, the average apertures of the discontinuities were wide which were more than 30 mm. The average persistence of the discontinuities in this slope was about 1 to 3 m long and the discontinuities did not have infilling material. The water condition in the slope was dry.

Table 5.9: Orientation of joint set on Slope 4

Slope 3A		
Joint Set	Dip Direction (°)	Dip Angle (°)
J1	104	5
J2	192	76

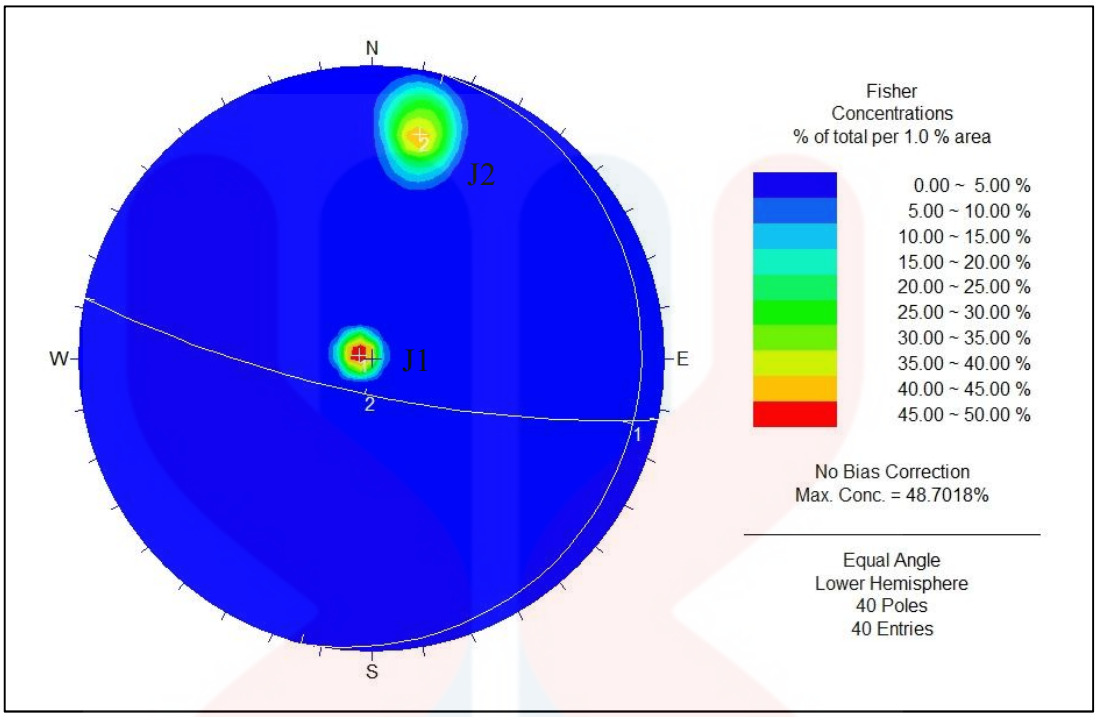

Figure 5.2.9: Contour plot of orientation of joints on Slope 4

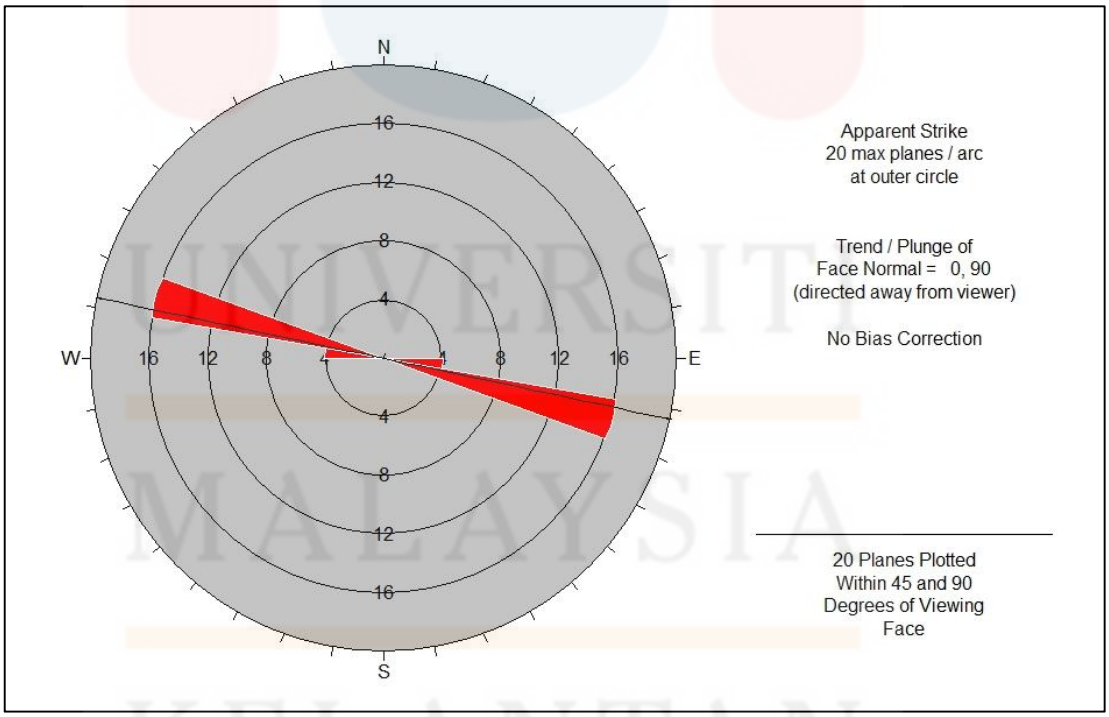

Figure 5.2.10: Rosette plot of orientations of joints on Slope 4

Table 5.10: Spacing of joint sets at Slope 4

	J1 (m)	J2 (m)
Slope 4	0.83	0.39
	0.8	0.45
	0.75	0.44
	0.76	0.38
	0.77	0.32
	0.8	0.33
	0.81	0.31
	0.75	0.35
	0.65	0.35
	0.66	0.36
	0.63	0.37
	0.67	0.38
	0.55	0.39
	0.69	0.37
	0.75	0.38
	0.73	0.45
	0.74	0.44
	0.75	0.43
	0.69	0.41
	0.67	0.45
Means, $\bar{X}$	0.7225	0.3875
$1/\bar{X}$	1.384083	2.580645
Median	0.745	0.38
Mode	0.75	0.45
Std Dev	0.070103	0.044589

5.3 Schmidt Hammer Rebound Test Analysis

Schmidt hammer rebound test was conducted at each slopes to determine uniaxial compressive strength of rock. Type-N Schmidt hammer with the impact energy of 2.207 Nm was used to determine the rebound number of rock, as it was more ideally suited for field-testing and less sensitive to surface irregularities when compared with Type-L Schmidt hammer.

Rebound number obtained from Type-N Schmidt hammer. R_N was converted to rebound number of Type-L Schmidt hammer by using the equation 3.1. Rebound number, R_L obtained was correlated with the chart introduced by ISRM (1978) as shown in Figure 2.9 to get the UCS value.

5.3.1 Rebound number of each rock slope

The following Figure 5.3.1, Figure 5.3.2, Figure 5.3.3 and Figure 5.3.4 are the charts that represent the rebound number of Type-N Schmidt hammer obtained from Slope 1, Slope 2, Slope 3A-3B and Slope 4 respectively. Total eight rebounds were tested on the flat surface of Slope 1 and the average rebound number, R_N was 71.0. The calculated value of rebound number, R_L was 48.7. For Slope 2, total eight rebound number readings were taken and the means value of rebound number, R_N was 70.0. R_L value of Slope 2, therefore, was 48. The lithology at Slope 3A and Slope 3B were same, therefore the average rebound number, R_N was 50.5 and R_L was 34.8. At Slope 4, total eight readings of rebound number were taken and the average rebound number, R_N was 59.5. Therefore, the rebound number, R_L of Slope 4 was 40.9.

Impact counter	Name	Date & Time	Mean value	Averaging mode	Upper outliers	Lower outliers	Valid/Total	Std dev.
Σ 234	Slope 1	10-10-2018 14:12	71.0 R	Mean	0	0	8/8	5.5 R

R-Values diagram [measurement order]

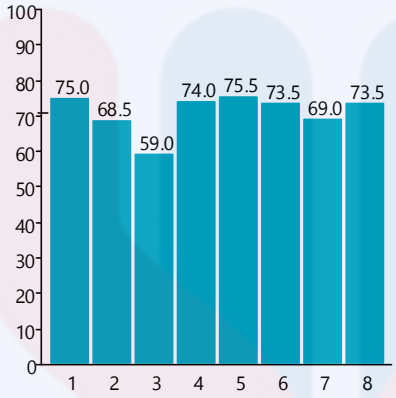

R-Values

75.0
68.5
59.0
74.0
75.5
73.5
69.0
73.5

Statistics

Measurements	N = 8
Invalid measurements	Ni = 0 (0%)
Mean value	f = 71.0 R
Range	R = 16.5 R
Standard deviation	s = 5.5 R

Settings

Averaging mode	Mean
Conversion curve	---
Correction factor	1.00
Unit	R
Serial number	SH01-007-0853
Spring type	RockSchmidt N

Comment

RL = 0.605 + 0.677RN (Look, 2007)

RL is the rebound number for Type-L Schmidt hammer
RN is the rebound number for Type-N Schmidt hammer

RN = 71.0
RL = 48.7

Figure 5.3.1: Chart of Type-N Schmidt hammer rebound number at Slope 1

Impact counter	Name	Date & Time	Mean value	Averaging mode	Upper outliers	Lower outliers	Valid/Total	Std dev.
Σ 226	Slope 2	10-10-2018 14:03	70.0 R	Mean	0	0	8/8	6.6 R

R-Values diagram [measurement order]

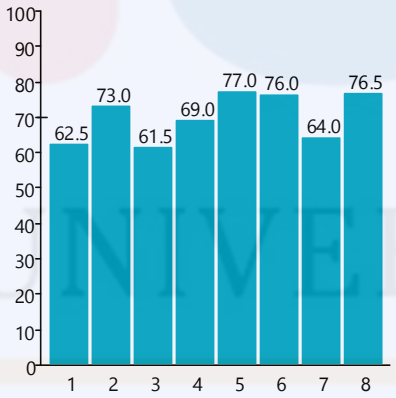

R-Values

62.5
73.0
61.5
69.0
77.0
76.0
64.0
76.5

Statistics

Measurements	N = 8
Invalid measurements	Ni = 0 (0%)
Mean value	f = 70.0 R
Range	R = 15.5 R
Standard deviation	s = 6.6 R

Settings

Averaging mode	Mean
Conversion curve	---
Correction factor	1.00
Unit	R
Serial number	SH01-007-0853
Spring type	RockSchmidt N

Comment

RL = 0.605 + 0.677RN (Look, 2007)

RL is the rebound number of Type-L Schmidt hammer
RN is the rebound number of Type-N Schmidt hammer

RN = 70.0
RL = 48.0

Figure 5.3.2: Chart of Type-N Schmidt hammer rebound number at Slope 2

Impact counter	Name	Date & Time	Mean value	Averaging mode	Upper outliers	Lower outliers	Valid/Total	Std dev.
Σ 204	Slope 3	10-10-2018 12:58	50.5 R	Mean	0	0	6/6	9.9 R

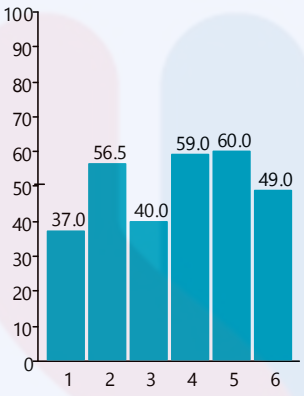

R-Values
37.0
56.5
40.0
59.0
60.0
49.0

Statistics

Measurements	N = 6
Invalid measurements	Ni = 0 (0%)
Mean value	f = 50.5 R
Range	R = 23.0 R
Standard deviation	s = 9.9 R

Settings

Averaging mode	Mean
Conversion curve	---
Correction factor	1.00
Unit	R
Serial number	SH01-007-0853
Spring type	RockSchmidt N

Comment

RL = 0.605 + 0.677RN (Look, 2007)

RL is the rebound number of Type-L Schmidt hammer
RN is the rebound number of Type-N Schmidt hammer

RN = 50.5
RL = 34.8

Figure 5.3.3: Chart of Type-N Schmidt hammer rebound number at Slope 3A and Slope 3B

Impact counter	Name	Date & Time	Mean value	Averaging mode	Upper outliers	Lower outliers	Valid/Total	Std dev.
Σ 210	Slope 4	10-10-2018 13:23	59.5 R	Mean	0	0	8/8	12.8 R

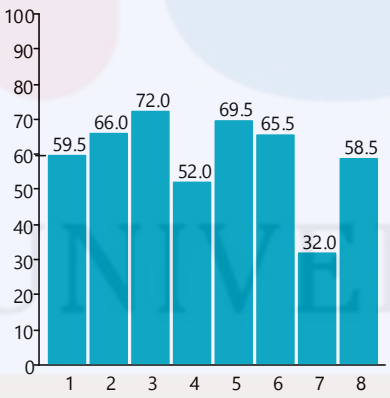

R-Values
59.5
66.0
72.0
52.0
69.5
65.5
32.0
58.5

Statistics

Measurements	N = 8
Invalid measurements	Ni = 0 (0%)
Mean value	f = 59.5 R
Range	R = 40.0 R
Standard deviation	s = 12.8 R

Settings

Averaging mode	Mean
Conversion curve	---
Correction factor	1.00
Unit	R
Serial number	SH01-007-0853
Spring type	RockSchmidt N

Comment

RL = 0.605 + 0.677RN (Look, 2007)

RL is the rebound number of Type-L Schmidt hammer
RN is the rebound number of Type-N Schmidt hammer

RN = 59.5
RL = 40.9

Figure 5.3.4: Chart of Type-N Schmidt hammer rebound number at Slope 4

5.3.2 Uniaxial Compressive Strength (UCS)

When all the rebound number, R_L of rock in each slopes were calculated, they were used to determine uniaxial compressive strength of the rock by correlating the rebound value with the chart suggested by ISRM (1978) as shown in Figure 5.3.5. Slope 1 had the highest value of uniaxial compressive strength which was 145MPa because Slope 1 was made up of granitic rock which was very hard and compact. Slope 2 had the second highest uniaxial compressive strength, which was 142.5MPa followed by Slope 4 which was 100MPa. Rock of Slope 4 had the lowest uniaxial compressive strength that was 73.33MPa. Table 5.11 below showed the rebound number, R_L, density of rock and UCS value of the rock.

Table 5.11: Rebound number, R_L, density of rock and UCS value of the rock.

Slope	Type of rock	Density (kNm^{-3})	Rebound Number (R_L)	UCS Value
Slope 1	Biotite granite	27	48.7	145
Slope 2	Biotite granite	27	48	142.5
Slope 3A	Mica schist	28	34.8	73.33
Slope 3B	Mica schist	28	34.8	73.33
Slope 4	Alkali feldspathic granite	27.5	40.9	100

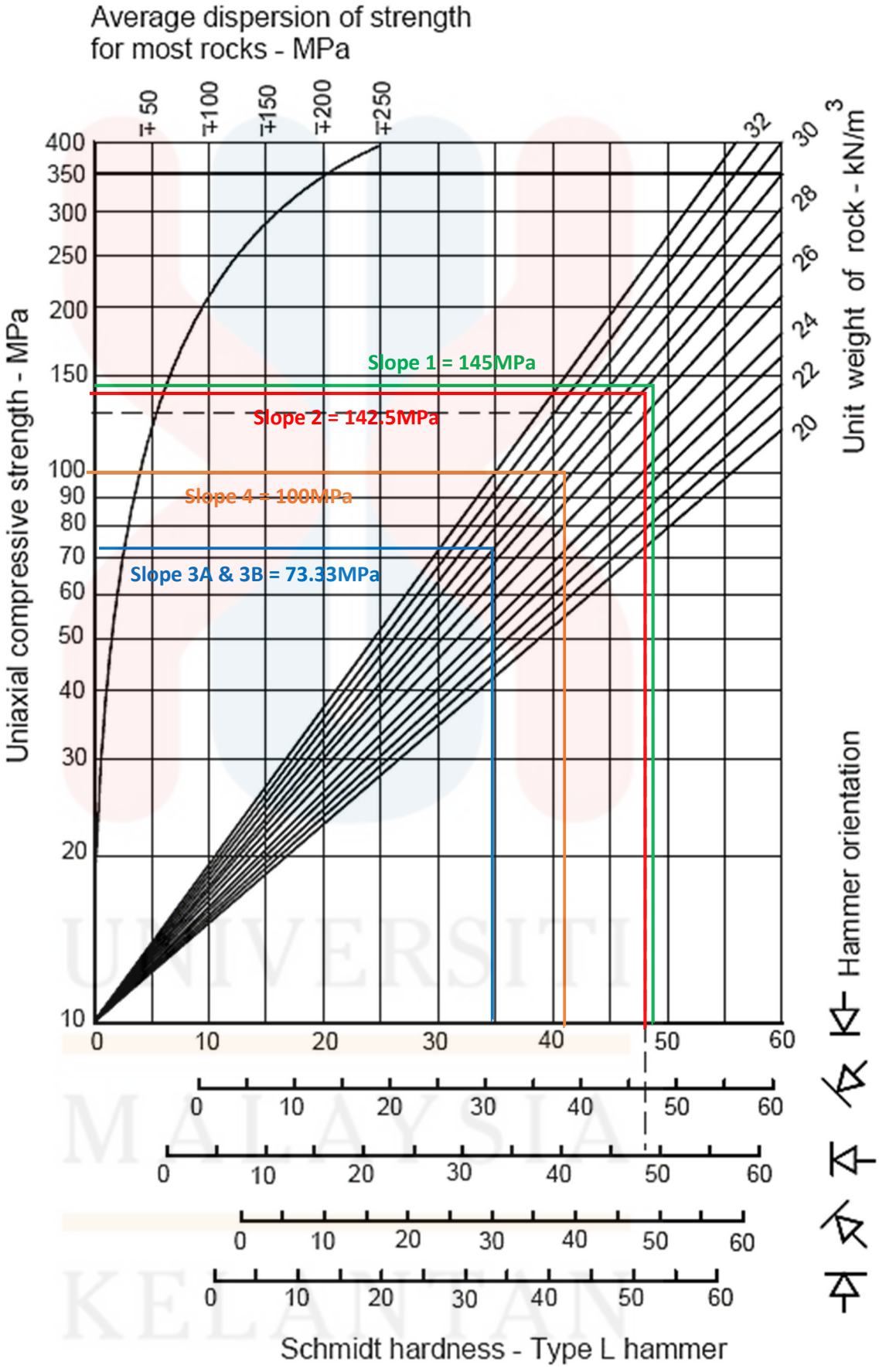

Figure 5.3.5: Correlation of rebound number, R_L with UCS value

5.4 Discussion of Rock Mass Rating

As mentioned before, few parameters that were required to characterize the rock masses included condition of discontinuities, uniaxial compressive strength (UCS), Rock Quality Designation (RQD), spacing of discontinuities, condition of groundwater and orientation of discontinuities. These parameters will give the value of rock masses to show the quality of rock from good to poor rock.

The condition of discontinuities such as aperture, persistence, roughness, weathering and infilling material were used to rate the rock masses. For Slope 1, the discontinuities were moderately weathered and had low persistence. The discontinuities were rough undulating without infilling material. The wall rock surface separation was gapped. The rating of condition of discontinuities given to Slope 1 was 19. The rating value of condition of discontinuities of Slope 2 and Slope 3A were 16 and 18 respectively. The persistence of discontinuities in Slope 2 was low whereas persistence of discontinuities in Slope 3A was medium. The roughness of discontinuities in both Slope 2 and Slope 3A were different in which discontinuities in Slope 2 were smooth undulating whereas those in Slope 3A were rough undulating. Discontinuities of both Slope 2 and Slope 3A were moderately weathered. For Slope 3B and Slope 4, the rating value for condition of discontinuities were 15 and 16 respectively. Both slopes did not have infilling material in the discontinuities but the roughness of discontinuities were different. The discontinuities at Slope 3B were smooth and stepped whereas those in Slope 4 were smooth undulating. The persistence of discontinuities in Slope 3B was longer compared to persistence of discontinuities in Slope 4.

For the intact rock uniaxial compressive strength, the results obtained from the Type-N Schmidt hammer rebound tests were 145MPa, 142.5MPa, 73.3MPa, and

100MPa for Slope 1, Slope 2, Slope 3A-3B and Slope 4 respectively. According to ISRM (1978), the rocks in Slope 1, Slope 2 and Slope 4 were considered as very high strength whereas the rock in Slope 3A-3B was considered as high strength. For the parameter of UCS, the rating value of Slope 1, Slope 2 and Slope 4 were same which was 12 whereas rating value for Slope 3A and Slope 3B was 7.

Rock Quality Designation (RQD) for Slope 1 had accounted for 87.12% , whereas Slope 2 and Slope 3A had accounted for 68.44% and 61.84% respectively. For Slope 3B and Slope 4, the RQD value was same that is 100%. The RQD values ranged from 90% to 100% accounts to the excellent quality of rock as proposed by Deere (1988). Nevertheless, rocks masses at the slopes were ranged from slightly weathered to highly weathered. All these RQD values accounted for very high percentage in which they were contradictory to the RQD values description proposed by Deere (1988). This could be due to the value of Jv obtained was not suitable to be correlated with RQD. The rating value of RQD for Slope 1, Slope 2, Slope 3A, Slope 3B and Slope 4 were 17, 13, 13, 20 and 20 respectively.

The average mean spacing of Slope 1, Slope 2, Slope 3A, Slope 3B and Slope 4 were 0.36m, 0.24m, 0.23m, 0.27m and 0.56m respectively. The spacing of discontinuities were not much different between five slopes. Hence, rating value of 10 was given to all five slopes.

The rating value of the water condition parameter was maximum for all the slopes except Slope 3A since there had dripping water in the slope. Therefore, rating value for Slope 3A was 4 while the rest was 15.

The RMR value of Slope 1, Slope 2 Slope 3B and Slope 4 were 73, 66, 67 and 73 respectively, which caused them to fall into class 2 rock mass (good rock). On the

other hand, RMR value of Slope 3A was 52 that was accounted as Class III rock mass (fair rock).

Table 5.12: Rock Mass Rating for Slope 1

Parameter	Range of Value	
	Value	Rating
Uniaxial Compressive Strength (MPa)	145	12
Rock Quality Designation (%)	87.12	17
Spacing of discontinuities (m)	0.36	10
Condition of discontinuities	Persistence 1-3m Aperture 1-3mm Rough, Undulating No infilling material Moderately weathered	19
Groundwater condition	Dry	15
TOTAL RATING		73
ROCK MASS CLASSES	Class II (good rock)	

Table 5.13: Rock Mass Rating for Slope 2

Parameter	Range of Value	
	Value	Rating
Uniaxial Compressive Strength (MPa)	142.5	12
Rock Quality Designation (%)	68.44	13
Spacing of discontinuities (m)	0.24	10
Condition of discontinuities	Persistence 1-3m Aperture 3-10mm Smooth, Undulating No infilling material Moderately weathered	16
Groundwater condition	Dry	15
TOTAL RATING		66
ROCK MASS CLASSES	Class II (Good rock)	

Table 5.14: Rock Mass Rating for Slope 3A

Parameter	Range of Value	
	Value	Rating
Uniaxial Compressive Strength (MPa)	73.33	7
Rock Quality Designation (%)	61.84	13
Spacing of discontinuities (m)	0.23	10
Condition of discontinuities	Persistence 1-3m Aperture > 30mm Rough, Undulating No infilling material Moderately weathered	18
Groundwater condition	Dripping	4
TOTAL RATING		52
ROCK MASS CLASSES	Class III (Fair rock)	

Table 5.15: Rock Mass Rating for Slope 3B

Parameter	Range of Value	
	Value	Rating
Uniaxial Compressive Strength (MPa)	73.33	7
Rock Quality Designation (%)	100	20
Spacing of discontinuities (m)	0.27	10
Condition of discontinuities	Persistence 3-10m Aperture 1-3mm Smooth, Stepped No infilling material Moderately weathered	15
Groundwater condition	Dry	15
TOTAL RATING		67
ROCK MASS CLASSES	Class II (good rock)	

Table 5.16: Rock Mass Rating for Slope 4

Parameter	Range of Value	
	Value	Rating
Uniaxial Compressive Strength (MPa)	100	12
Rock Quality Designation (%)	100	20
Spacing of discontinuities (m)	0.56	10
Condition of discontinuities	Persistence 1-3m Aperture >30mm Smooth, Undulating No infilling material Moderately weathered	16
Groundwater condition	Dry	15
TOTAL RATING		73
ROCK MASS CLASSES	Class II (good rock)	

5.5 Discussion of Kinematic Analysis

Kinematic analysis was employed to identify the type of slope failure that will occur and examine the direction in which the block will slide. It was carried out under stereographic projection. The discontinuities data obtained from discontinuities survey, slope face orientations and friction angle of rocks of five respective slopes were projected into the stereonet by using STEREONET computer software. The software will carry out kinematic analysis on the input data to identify the mode of slope failure and the direction of sliding of the block.

The result of kinematic analysis for Slope 1, Slope 2, Slope 3A, Slope 3B and Slope 4 were shown in Figure 5.5.1, Figure 5.5.2, Figure 5.5.3, Figure 5.5.4, and Figure 5.5.5 respectively. Red colour lines in the Figures represented the slope faces and their daylight envelopes whereas green circle lines represented the friction angle cone. The purple colour lines represented 20^{o} of lateral limit plane. Black dotted lines represented the joint set planes. The blue shaded line represented the critical zone of failure Since Slope 1, Slope 2 and Slope 4 made up of intrusive igneous rock, the friction angle of the slopes were predicted to be 50^{o} according to their geologic origin (Look, 2007). For Slope 3A and Slope 3B, the friction angle of the slopes were predicted to be 30^{o} since the slopes were made up of metamorphic rocks. The symbol J represented the joint set planes whereas the symbol N represented poles of planes.

5.5.1 Kinematic Analysis for Plane Failure

According to Wyllie & Mah (2004), plane failure will occur when the discontinuities planes dip gentler than dip of slope face and greater than friction angle

of slope. Besides that, the difference between dip orientation of slope face and dip orientation of discontinuities must not exceeds 20^{o}

Slope 1 comprised of three joint sets, which were J1, J2 and J3. The poles of J2 and J1 sets did not daylight on the envelope of the slope face. J2 and J1 sets dipped into the opposite direction of slope face. Hence, plane failure was not possible in J2 and J1 sets. The pole for J3 were daylighting in the envelope of the slope face as shown in Figure 5.5.1. This means that most of the planes in J3 dipped gentler than slope face. However, the dipping orientation between J3 set and slope face was greater than 20^{o}. Therefore, all the joint sets in Slope 1 did not have plane failure since all the poles of joint sets did not fall in the critical zone.

Slope 2 comprised of J1, J2 and J3 sets. The pole of J3 plane daylighted on the envelope of the slope face. However, its pole lie outside the lateral limit of the slope. This means that the difference between dipping orientations of J3 set and dipping orientation of slope was greater than 20^{o}. As a result, J3 set was considered stable in Slope 2. The pole of J2 set in Slope 2 was daylighting within the envelope of slope face and lying within the lateral limit of slope. Nevertheless, the pole of J2 was locating inside the friction angle cone. In other words, dipping angle of J2 plane was gentler than friction angle of slope. Hence, the plane of J2 set was stable. J1 set did not have plane failure since the plane was dipping in the opposite direction of slope face. Since all the poles did not lie within the critical zone, Slope 2 did not have potential of plane failure.

For Slope 3A, the poles of J1, J2 and J3 sets were daylighting on the daylight envelope of slope face. The poles of J1 and J2 sets were locating within the lateral limit of slope and outside the friction angle cone that meant within critical zone. In

other words, dipping plane of J1 and J2 sets were greater than friction angle of slope and the dipping orientation was near to the slope face. Therefore, J1 and J2 sets in Slope 3A were unstable and had potential of plane failure in the direction of north. Even though J3 set daylighting on the envelope of slope face, the pole of J3 set was locating outside the lateral limit of slope. Hence, J3 set was considered partially unstable in Slope 3A.

Only J1 set was present in Slope 3B. Even though dipping angle of J1 set was greater than friction angle of slope, the pole of J1 set did not daylight within the envelope of slope face. As a result, J1 set was stable in Slope 3B since the pole of J1 set located outside the critical zone.

In Slope 4, both J1 and J2 sets are stable since their poles were locating outside the critical zone.

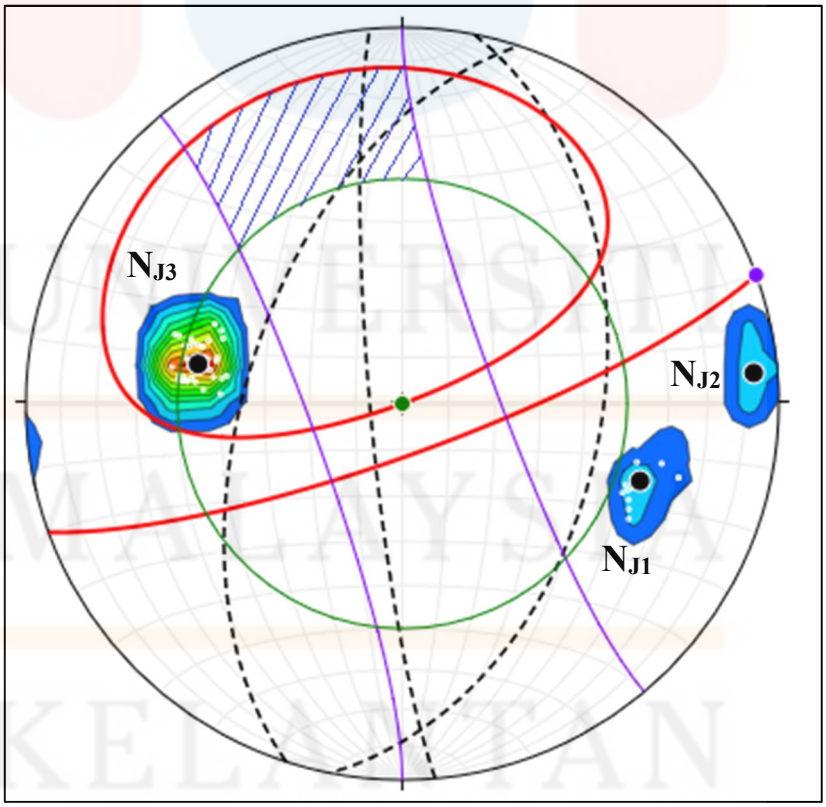

Figure 5.5.1: Kinematic Analysis of Slope 1

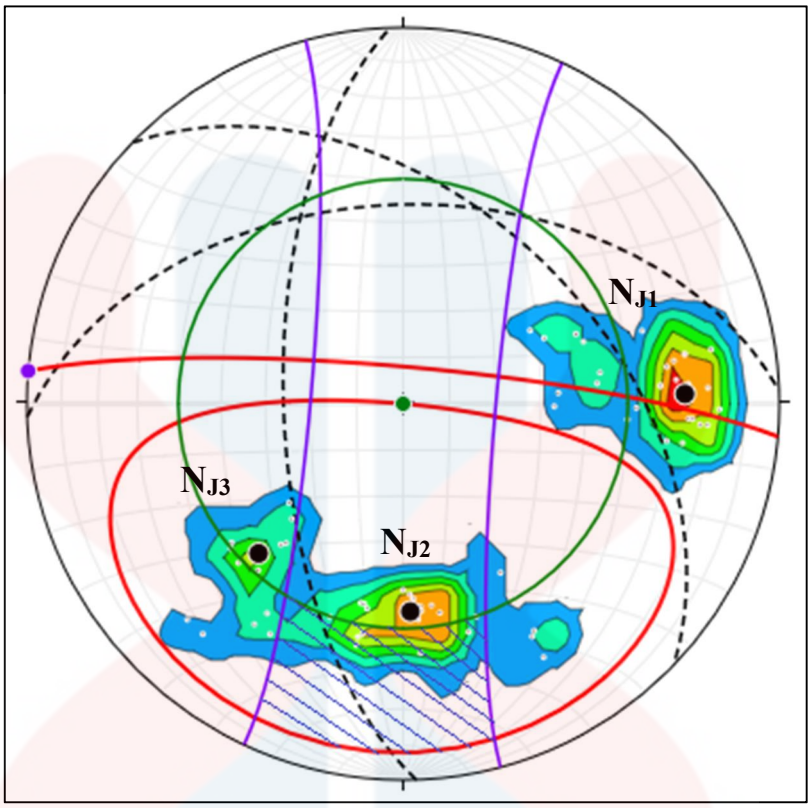

Figure 5.5.2: Kinematic Analysis of Slope 2

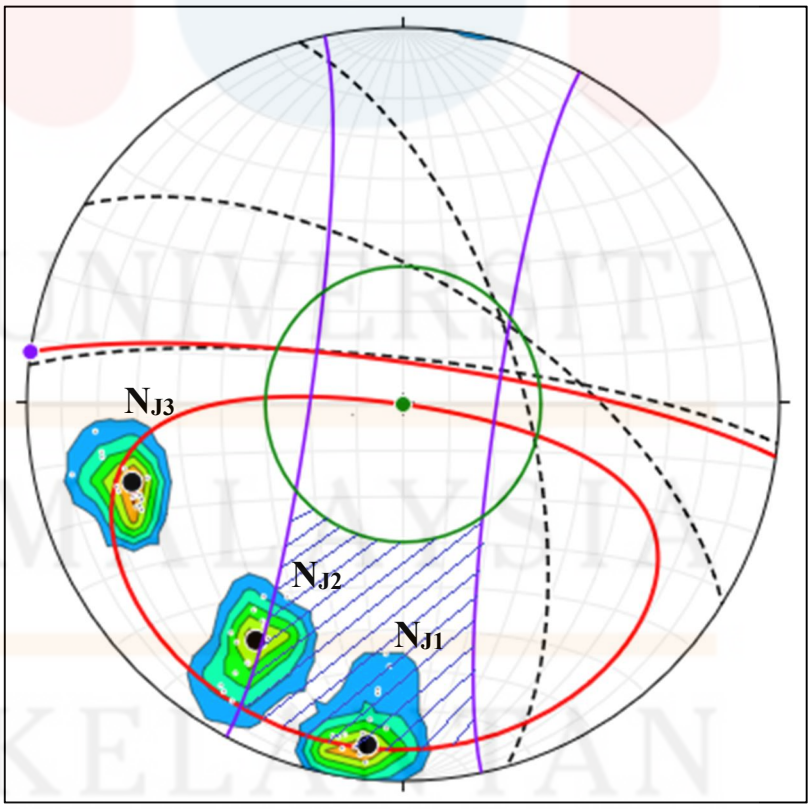

Figure 5.5.3: Kinematic Analysis of Slope 3A

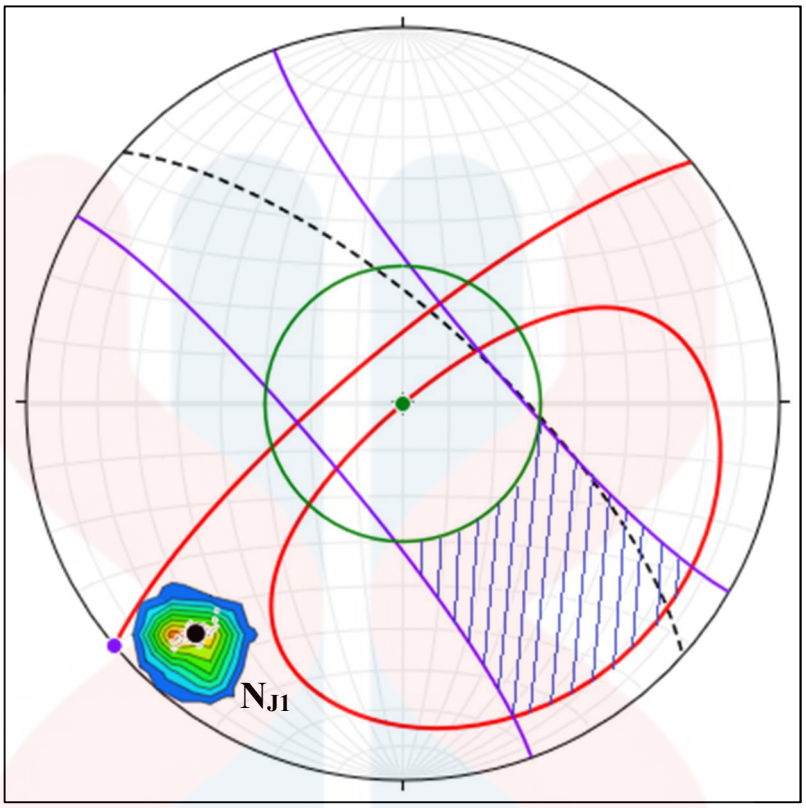

Figure 5.5.4: Kinematic Analysis of Slope 3B

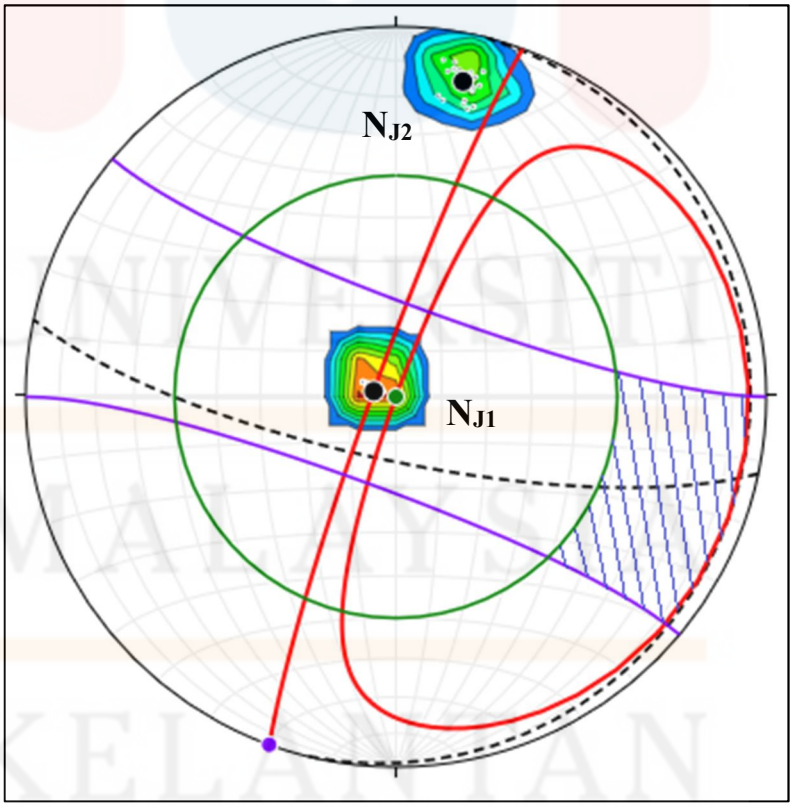

Figure 5.5.5: Kinematic Analysis of Slope 4

5.5.2 Kinematic Analysis of Wedge Failure

Wedge failure occurs when the dip angle of the slope face exceed the dip angle of the line of intersection of plane between the joint sets. In other words, the poles of the intersection of the planes will daylight on the envelope of the slope face. Another criteria for the occurrence of wedge failure is the angle of line of intersection from horizontal must be greater than friction angle of slope. Figure 5.5.6, Figure 5.5.7, Figure 5.5.8, and Figure 5.5.9 represented the kinematic analysis of wedge failure for Slope 1, Slope 2, Slope 3A and Slope 4 respectively. The line of intersection of joint set planes were designated as J1J2, J1J3 or J2J3. The poles of the line of the intersections were plotted on the stereonet in the Figures for the analysis.

There were three lines of intersections in Slope 1 included J1J2, J1J3 and J2J3. The intersection line of J1J2 and J1J3 did not have translational sliding in Slope 1 because their poles were plotted outside the daylight envelope of slope face. The pole of J2J3 intersection line was daylighting in the envelope of slope face but inside the friction cone angle. The sliding was impossible to occur in J2J3 intersection line. Hence, Slope 1 did not have potential of wedge failure since all the poles of intersection fell outside the critical zone of failure.

In Slope 2, all the poles of the intersection lines J1J2, J1J3 and J2J3 were daylighting on the envelope of the slope face. However, all the poles were plotted within the friction angle cone. This means that the angle of intersection lines J1J2, J1J3 and J2J3 from horizontal were smaller than the friction angle of slope. Hence, wedge failure cannot occur at Slope 2.

The poles of intersection line J1J2, J1J3 and J2J3 in Slope 3A were lying within critical zone of failure. They were daylighting on the envelope of slope face

and lying outside the friction angle cone. As a result, the slope was unstable and was predicted to have wedge failure sliding in the direction of 050.6º, 064º and 061.9º.

Slope 3B did not have wedge failure since the slope did not have discontinuities that intersect each other to cause sliding of wedge failure. In Slope 4, the wedge failure also impossible to occur since the pole of the line of intersection between two planes was not daylighting on the envelope of the slope face and lying outside the critical zone of failure.

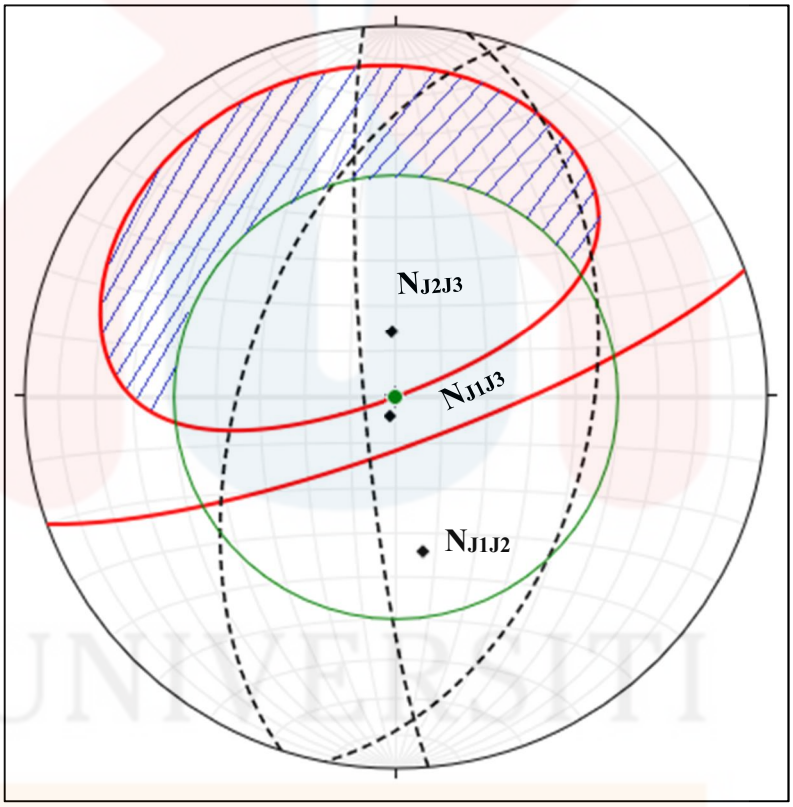

Figure 5.5.6: Kinematic analysis of wedge failure for Slope 1

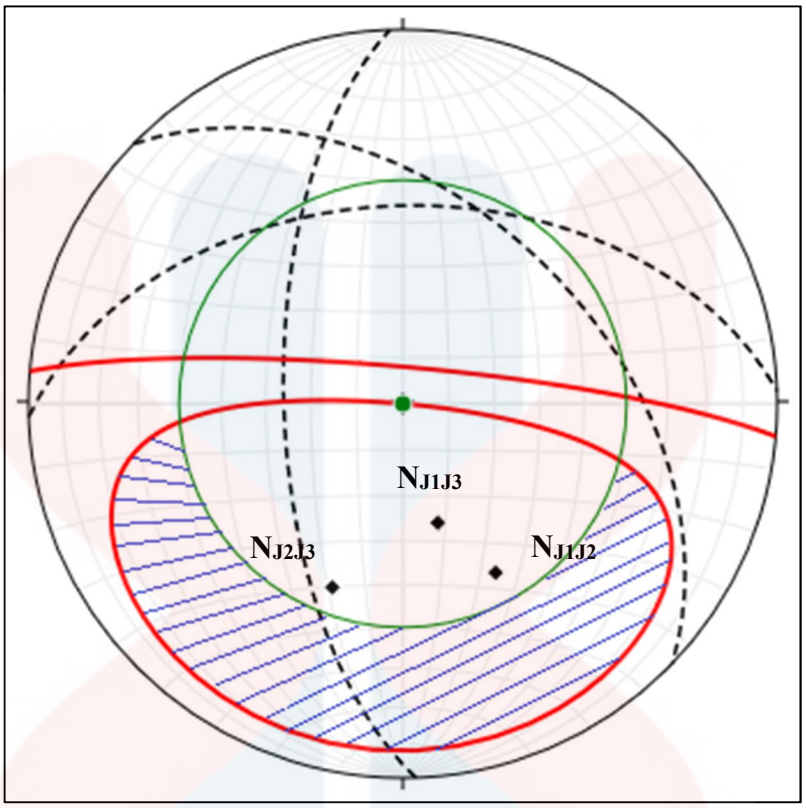

Figure 5.5.7: Kinematic analysis of wedge failure for Slope 2

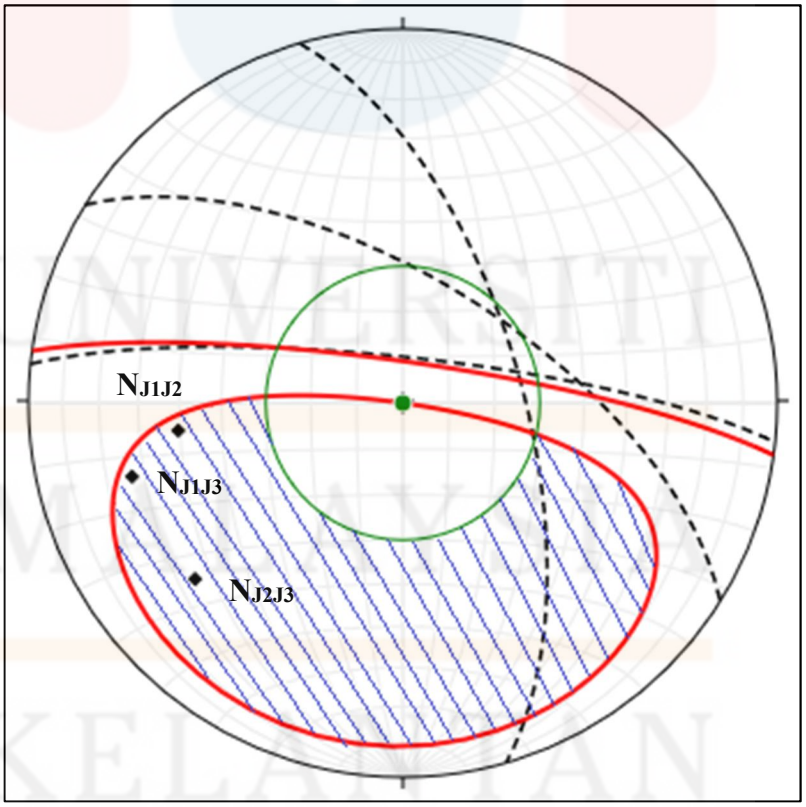

Figure 5.5.8: Kinematic analysis of wedge failure for Slope 3A

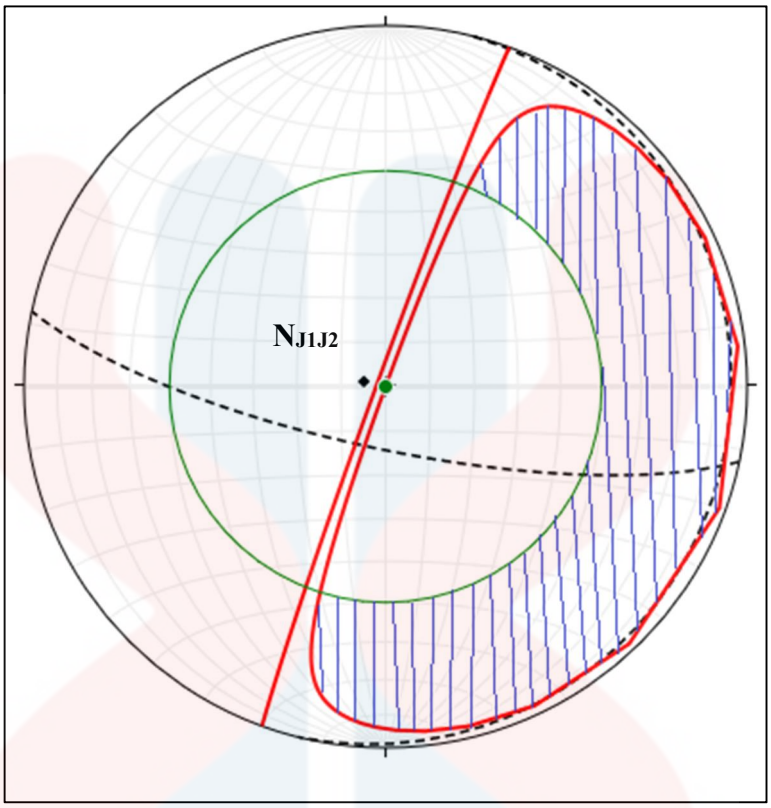

Figure 5.5.9: Kinematic analysis of wedge failure for Slope 4

5.5.3 Kinematic Analysis of Toppling Failure

Toppling failure occurs when the dip direction of the discontinuities dipping into the face within about 10° of the dip direction of the face so that a series of slabs are formed parallel to the face. Besides that, the dip of discontinuities must be steep enough for interlayer slip to occur. The slip of toppling will only occur if the direction of applied compressive stress is at angle greater than friction angle of the face, φ_j. The direction of the major principal stress in the cut is parallel to the dip angle of face, ψ_f, so interlayer slip and toppling failure will occur on plane with dip ψ_p when the following condition are met, $(90^o-\psi_f)+\varphi_j < \psi$ (Goodman & Bray, 1976).

From the kinematic analysis as shown in Figure 5.5.5, the J1 set in Slope 4 was dipping into the face of slope about 5° from horizontal. But the poles of J1 set were

plotted within the friction angle cone which means that the dipping angle of J1 set was smaller than friction angle. Hence, toppling failure cannot occur. The joint sets in the rest of the slopes did not dip into the face of the slopes. As a result, there were no toppling failure in all five slopes.

5.6 Discussion of Slope Mass Rating

Based on the result produced by kinematic analysis and Rock Mass Rating for each slopes, Slope Mass Rating of the slopes can be calculated by using the equation 2.3 in Chapter 2. Slope Mass Rating was only accounted for plane failure and toppling failure (Romana, 1985). For toppling failure, Slope Mass Rating of joints sets were not discussed because no slopes had potential of toppling failure. Kinematic analysis had shown that only joint sets in Slope 3A were susceptible to fail. Therefore, Slope Mass Rating value for each joint sets in Slope 3A were calculated.

J1, J2 and J3 in Slope 3A had Slope Mass Rating value of 17, 43 and 58 respectively. J1 set had the lowest value of SMR because it was striking nearly parallel to the slope face. Therefore, it was falling into Class 5 in SMR classes. It was completely bad and unstable discontinuities set in Slope 3A. Kinematic analysis also showed that dipping angle of J1 set was greater than friction angle of slope. As a result, the J1 set will have the planar failure. J2 and J3 set were falling into Class 3 in SMR classes and considered as normal discontinuities. Kinematic analysis showed that poles of J2 and J3 set were plotted outside the friction angle cone and were daylighting on the envelope of slope face. Therefore, it was deduced that J2 and J3 set in Slope 3A were partially unstable.

Table 5.17: Slope Mass Rating at Slope 3A

Slope Mass Rating at Slope 3A								
J1			J2			J3		
	Value	Rating		Value	Rating		Value	Rating
F_1	2°	1.00	F_1	24°	0.40	F_1	66°	0.15
F_2	80°	1.00	F_2	63°	1.00	F_2	64°	1.00
F_3	-1°	-50	F_3	-18°	-60	F_3	-17°	-60
F_4	Natural Slope	15	F_4	Natural Slope	15	F_4	Natural Slope	15
RMR		52	RMR		52	RMR		52
Total Rating		17	**Total Rating**		43	**Total Rating**		58
Class IV (Completely Unstable)			Class III (Partially Unstable)			Class III (Partially Unstable)		

CHAPTER 6

CONCLUSION AND RECOMMEDATION

6.1 Conclusion

In conclusion, the research had successfully achieved the objectives that had been targeted. In Rock Mass Rating, Slope 1 and Slope 4 had the highest rating value that was 73 whereas Slope 3A had the lowest rating value that was 52. The rating value of Slope 2and Slope 3B was 66 and 67 respectively. From the value of rating, Slope 3A was classified as Class III rock because the rock mass of Slope 3A was fair. The rock of the rest of the slopes were classified as Class II rock, which were good rock masses. From overall kinematic analysis, only Slope 3A had a greater potential to had plane failure in the direction of north and wedge failure in the direction of northeast. Toppling failure in Slope 3A was impossible. The rest of the slopes did not have potential of plane, wedge and toppling failure.

By taking the consideration of Rock Mass Rating and kinematic analysis, Slope Mass Rating was accounted for each of the discontinuities set in the Slope 3A. Slope Mass Rating of J1, J2 and J3 sets of Slope 3A were 17, 43 and 58 respectively. Hence, the slope was unstable since J1 set was Class V completely unstable discontinuities where J2 and J3 were Class III partially unstable discontinuities. As a result, Slope 3A can have slope failure since most of the discontinuities had low value of SMR.

Another objective of the research was achieved where the geological mapping of the study area was completed. The lithology of the study area is made up entirely of one type of rock that is granite. The granitic rocks in the study area had the

porphyritic texture where the alkali feldspar phenocrysts grains grew within groundmass of other minerals. The geological age of the rock was Cretaceous. Field observation had shown that the geomorphology of the study area consist of mountainous ridges, hills, V-shaped and U-shaped type of valley. The analysis of rose diagram showed that the principal stresses, σ_1 exerting on the study area was from the direction of NE-SW. The stresses were intense because abundant of discontinuities such as fractures and joints were present in the outcrops of granites. The presence of aplite veins in the field and the mantled feldspar in petrographic analysis showed that there was two times of magmatic intrusion in the study area.

6.2 Recommendations

There are few limitations when carrying out the research. The most prominent of the limitation is the friction angle. The friction angle of the slopes that were used in plotting the friction angle cone in kinematic analysis were predicted according to the geological origin of the slopes that is proposed by Look (2007). The friction angles might be inappropriate to be used since the condition of the slopes might alter the friction angle from the predicted friction angle. Therefore, the direct shear test is recommended to determine the friction angle of the slope (Hencher & Richards, 1989).

Furthermore, the rebound number of Type-L Schmidt hammer, R_L might be unsuitable to determine the uniaxial compressive strength of the rock. Type-L Schmidt hammer used to collect rebound number, R_L was not available; therefore, Type-N Schmidt hammer was used in the in-situ testing of rebound number, R_N. In order to correlate with the correlation chart of Type-L Schmidt hammer, the rebound number of Type-N Schmidt hammer, R_N was changed to rebound number of Type-L Schmidt

hammer, R_L by using equation 3.1 introduced by Look (2007). The calculated rebound number, R_L might be inaccurate and had the percentage error. Besides that, direct use of Type-L Schmidt hammer in the in-situ testing may has its own limitations because the hammer is sensitive to the rough surface rock and it is not so suitable to be used in hard rocks such as igneous rock. Thus, uniaxial compressive test is highly recommended to determine the uniaxial compressive strength of the rock.

Besides that, the calculation of RQD from J_V is not so appropriate because Palmstrom (1982) mentioned that the correlation between RQD and J_V was poor. The best method recommended to obtain the RQD value is from drill core logs but UMK has no coring machine and the cost of coring is high.

Apart from that, the accuracy of discontinuities data in the field can be supported by the photogrammetric technique and remote sensing which can improve the collection of discontinuities data in broader area. A better method of analysing the slope stability through factor of safety of slope is recommended. The factor of safety of slope is determined by calculating the ratio of the shear strength of the rock over the shear stress. The slope is considered stable if the factor of safety is more than 1 whereas it is unstable when the value is less than 1.

REFERENCE

Aydin, A. (2008). ISRM Suggested Method ISRM Suggested method for determination of the Schmidt hammer rebound hardness : Revised version $. *International Journal of Rock Mechanic & Mining Science*, 1–8. https://doi.org/10.1016/j.ijrmms.2008.01.020

Aydin, A. (2015). The ISRM Suggested Methods for Rock Characterization, Testing and Monitoring: 2007-2014. https://doi.org/10.1007/978-3-319-07713-0

Azman, A. (2000). Mantled feldspar from the Noring granite, Peninsular Malaysia: petrography, chemistry and petrogenesis. *Geological Society of Malaysian Bulletin 44*, (July), 109–115. Retrieved from https://gsmpubl.files.wordpress.com/2014/09/bgsm2000014.pdf

Bieniawski, Z. T. (1989). Engineering rock mass classifications : a complete manual for engineers and geologists in mining, civil, and petroleum engineering. *Engineering Rock Mass Classifications : A Complete Manual for Engineers and Geologists in Mining, Civil, and Petroleum Engineering*.

Deere, D.U. & Deere, D. W. (1988). The RQD Index in Practice. In *Proc. Symp. Rock Classif. Eng. Purp* (pp. 91–101). ASTM Special Technical Publication 984.

Deere, D.U. & Miller, R. P. (1966). Engineering classification and index properties for intact rock. In *Air Force Weapons Lab Tech Report* (pp. 65–116).

Ghani, A. (2006). Geochemistry of the Stong Igneous Complex. *Geologic Correlation Programme*, (May).

Gobbett, D.J. & Tjia, H. D. (1973). *Geology of Malay Peninsula*. Wiley-Interscience, New York.

Goodman, R. & Bray, J. (1976). Toppling of rock slope. In *SCE, Proc. Specialty Conf. on Rock* (pp. 201–234).

Hencher, S. R., & Richards, L. R. (1989). Laboratory direct shear testing of rock discontinuities. *Ground Engineering*, *22*(2), 24–31. https://doi.org/10.1061/(ASCE)1090-0241(2005)131:10(1295)

Hoek, E. & Bray, J. (1981). *Rock Slope Engineering* (Third Edit). Institute of Mining and Metallurgy.

Howarth, R. J. (1996). History of stereographic projection and its early use in geology. *Blackwell Science Ltd*, 499–513.

Huggett, R. J. (2007). *FUNDAMENTALS OF GEOMORPHOLOGY*. Routledge Taylor & Francis Group. Retrieved from https://www.cec.uchile.cl/~fegallar/Fundamentals_of_Geomorphology.pdf

Hutchison, C.S. & Tan, D.K. (Department of Geology, U. of M. (Ed.). (2009). *GEOLOGY OF PENINSULAR MALAYSIA*. Geological Society of Malaysia and Department of Geology University of Malaya.

Hutchison, C. S. (1977). Granite emplacement and tectonic subdivision of Peninsular Malaysia. *Geological Society Bulletin*, 187–207.

ISRM. (1978). Suggested methods for the quantitative description of discontinuities in rock masses. *Int. J. Rock Mech. Min. Sci. Geomech. Abstr.,*. https://doi.org/10.1016/0148-9062(79)91476-1

Khoo, H. P. (1983). Mesozoic Stratigraphy in Peninsula Malaysia. In *Proceeding of the workshop on stratigraphic correlation of Thailand and Malaysia* (pp. 370–383). Geological Society of Thailand & Geological Society of Malaysia.

Look, B. (2007). *Handbook of Geotechnical Investigation and Design Tables*. Taylor & Francis Group, London, UK.

MacDonald, S. (1955). Brief notes on the geology of the valleys of the Pergau and Lebir, Kelantan. *Geological Survey, Federation of Malaya*.

MacDonald, S. (1967). The geology and mineral resources of North Kelantan and North Terrenganu. *Geol. Surv. Malaysia. District Memoir*, *10*, 202.

Markland, J. T. (1972). A useful technique for estimating the stability of rock slopes when the rigid wedge sliding type of failure is expected. *Imperial College Rock Mechanics Research Report*..

Palmstrom, A. (1982). The Volumetric Joint Count-a Useful and Simple Measure of the Degree of Rock Jointing. In *Proc. 4th Int. Congr., Int. Assoc. Eng. Geol., Dehli* (pp. 221–228).

Priest, S. D., & Hudson, J. A. (1976). Discontinuity spacings in rock. *International Journal of Rock Mechanics and Mining Sciences And*, *13*(5), 135–148. https://doi.org/10.1016/0148-9062(76)90818-4

Rafek, G. & Komoo, I. (1989). Kegagalan cerun di Lebuh Raya Timur Barat : survei dari Jeli ke Sri Banding. *Warta Geologi*, 167–179.

Romana, M. (Universidad Politecnica Valencia, S. (1985). A Geomechanical Classification for Slopes : Slope Mass Rating. *ROCK TESTING AND SITE CHARACTERIZATION: COMPREHENSIVE ROCK ENGINEERING: Principles, Practice & Projects*, *575–600*, 575–600. https://doi.org/10.1016/B978-0-08-042066-0.50029-X

Santokh Singh, D. (1984). The Stong Complex. *Geological Society Bulletin 17*, 61–77.

Shakoor, A. & Admassu, Y. (2010). *Rock Slope Design Criteria*.

Shuib, M. K., Hj Taib, S., & Abdullah, M. (2006). Discontinuity Controlled Cut-Slope Failures on Weathered Low Grade Metamorphic Rocks along the East-West Highway, Grik to Jeli. *Geological Society of Malaysian Bulletin*, *52*, 43–53.

Wells, A. K., & Bishop, A. C. (1954). The Origin of Aplites. *Proceedings of the Geologists Association*, *65*(2), 95–114. https://doi.org/10.1016/S0016-7878(54)80001-0

Wyllie, D.C and Mah, C. . (2004). *Rock Slope Engineering*. *The Institute of Mining and Metallurgy* (Vol. 13). https://doi.org/10.2113/gseegeosci.13.4.369

Wyllie, D. C. (1980). Toppling rock slope failures examples of analysis and stabilization. *Rock Mechanics Felsmechanik Mécanique Des Roches*, *13*(2), 89–98. https://doi.org/10.1007/BF01238952

Zhang, L., & Guilbert, E. (2012). A STUDY OF VARIABLES CHARACTERIZING DRAINAGE PATTERNS IN RIVER NETWORKS, *XXXIX*(September), 29–34. Retrieved from https://www.int-arch-photogramm-remote-sens-spatial-inf-sci.net/XXXIX-B2/29/2012/isprsarchives-XXXIX-B2-29-2012.pdf

APPENDIX

(Raw Data of Discontinuity Survey)

APPENDIX

UNIVERSITY MALAYSIA KELANTAN

FACULTY OF EARTH SCIENCE

DATA SHEET FOR DISCONTINUITY SURVEY IN **SLOPE 1**

LOCATION : 5º 42' 14.93" N / 101º 50' 14.53" E	SURVEYOR : Low	DIP DIRECTION OF SLOPE : 160º
DATE : 6 October 2018	NO OF DATA SHEET : 1	DIP AMOUNT OF SLOPE : 79º

NO	TYPE	DIP DIRECTION (º)/DIP (º)	PERSISTANCE	APERTURE	FILLING	ROUGHNESS	WATER	REMARK		
								Joint Set 1	Joint Set 2	Joint Set 3
1	3	096/46	P2	A2	1	IV	W1			J3
2	3	096/48	P2	A2	1	IV	W1			J3
3	3	096/50	P2	A2	1	IV	W1			J3
4	3	098/42	P2	A2	1	IV	W1			J3
5	3	096/48	P2	A2	1	IV	W1			J3
6	3	096/46	P2	A2	1	IV	W1			J3
7	3	097/47	P2	A2	1	IV	W1			J3
8	3	097/50	P2	A2	1	IV	W1			J3
9	3	098/40	P2	A2	1	IV	W1			J3
10	3	099/39	P2	A2	1	IV	W1			J3
11	3	093/40	P2	A2	1	IV	W1			J3
12	3	094/44	P2	A2	1	IV	W1			J3
13	3	096/49	P2	A2	1	IV	W1			J3
14	3	097/49	P2	A2	1	IV	W1			J3
15	3	099/52	P2	A2	1	IV	W1			J3
16	3	100/48	P2	A2	1	IV	W1			J3
17	3	101/48	P2	A2	1	IV	W1			J3

18	3	112/43	P2	A2	1	IV	W1			J3
19	3	113/45	P2	A2	1	IV	W1			J3
20	3	110/42	P2	A2	1	IV	W1			J3
21	3	101/48	P2	A2	1	IV	W1			J3
22	3	103/42	P2	A2	1	IV	W1			J3
23	3	104/42	P2	A2	1	IV	W1			J3
24	3	100/43	P2	A2	1	IV	W1			J3
25	3	101/45	P2	A2	1	IV	W1			J3
26	3	102/49	P2	A2	1	IV	W1			J3
27	3	107/52	P2	A2	1	IV	W1			J3
28	3	107/53	P2	A2	1	IV	W1			J3
29	3	106/48	P2	A2	1	IV	W1			J3
30	3	107/49	P2	A2	1	IV	W1			J3
31	3	103/44	P2	A2	1	IV	W1			J3
32	3	103/45	P2	A2	1	IV	W1			J3
33	3	103/45	P2	A2	1	IV	W1			J3
34	3	102/45	P2	A2	1	IV	W1			J3
35	3	105/50	P2	A2	1	IV	W1			J3
36	3	105/49	P2	A2	1	IV	W1			J3
37	3	106/47	P2	A2	1	IV	W1			J3
38	3	106/46	P2	A2	1	IV	W1			J3
39	3	106/46	P2	A2	1	IV	W1			J3
40	3	108/45	P2	A2	1	IV	W1			J3
41	3	265/83	P2	A2	1	IV	W1		J2	
42	3	265/83	P2	A2	1	IV	W1		J2	
43	3	265/83	P2	A2	1	IV	W1		J2	
44	3	265/83	P2	A2	1	IV	W1		J2	
45	3	265/83	P2	A2	1	IV	W1		J2	
46	3	265/82	P2	A2	1	IV	W1		J2	
47	3	265/82	P2	A2	1	IV	W1		J2	
48	3	266/83	P2	A2	1	IV	W1		J2	
49	3	293/55	P2	A2	1	IV	W1	J1		
50	3	295/56	P2	A2	1	IV	W1	J1		
51	3	297/57	P2	A2	1	IV	W1	J1		

52	3	290/53	P2	A2	1	IV	W1	J1		
53	3	292/53	P2	A2	1	IV	W1	J1		
54	3	290/55	P2	A2	1	IV	W1	J1		
55	3	291/54	P2	A2	1	IV	W1	J1		
56	3	280/53	P2	A2	1	IV	W1	J1		
57	3	285/65	P2	A2	1	IV	W1	J1		
58	3	285/65	P2	A2	1	IV	W1	J1		
59	3	283/60	P2	A2	1	IV	W1	J1		
60	3	284/54	P2	A2	1	IV	W1	J1		

TYPE	PERSISTANCE	APERTURE	ROUGHNESS	FILLING	WATER
1. Fault zone 2. Fault 3. Joint 4. Bedding 5. Foliation 6. Fracture 7. Cleavage 8. Schistosity 9. Fissure 10. Shear	P1. < 1m P2. 1-3m P3. 3-10m P4. 10-20m P5. > 20m	A1. < 1mm A2. 1-3mm A3. 3-10mm A4. 10-30mm A5. > 30mm	I. Rough, stepped II. Smooth, stepped III. Slickensided, stepped IV. Rough, undulating V. Smooth, undulating VI. Slickensided, undulating VII. Rough, planar VIII. Smooth, planar IX. Slickensided, planar	1. Clean 2. Colour 3. Non-cohesive 4. Non-active clay 5. Active clay 6. Cemented 7. Chlorite, talc & gypsum 8. Others	W1. Dry W2. Damp W3. Wet W4. Dripping W5. Flowing

UNIVERSITY MALAYSIA KELANTAN

FACULTY OF EARTH SCIENCE

DATA SHEET FOR DISCONTINUITY SURVEY IN **SLOPE 2**

LOCATION : 5º 42' 15.01" N / 101º 50' 14.19" E	SURVEYOR : Low	DIP DIRECTION OF SLOPE : 005º
DATE : 6 October 2018	NO OF DATA SHEET : 2	DIP AMOUNT OF SLOPE : 82º

NO	TYPE	DIP DIRECTION (º)/DIP (º)	PERSISTANCE	APERTURE	FILLING	ROUGHNESS	WATER	REMARK		
								Joint Set 1	Joint Set 2	Joint Set 3
1	3	350/46	P2	A3	1	V	W1		J2	
2	3	350/47	P2	A3	1	V	W1		J2	
3	3	352/45	P2	A3	1	V	W1		J2	
4	3	360/41	P2	A3	1	V	W1		J2	
5	3	358/42	P2	A3	1	V	W1		J2	
6	3	030/60	P2	A3	1	V	W1			J3
7	3	041/70	P2	A3	1	V	W1			J3
8	3	010/52	P2	A3	1	V	W1		J2	
9	3	011/53	P2	A3	1	V	W1		J2	
10	3	011/55	P2	A3	1	V	W1		J2	
11	3	019/50	P2	A3	1	V	W1		J2	
12	3	355/46	P2	A3	1	V	W1		J2	
13	3	356/48	P2	A3	1	V	W1		J2	
14	3	034/60	P2	A3	1	V	W1			J3
15	3	033/56	P2	A3	1	V	W1			J3
16	3	012/45	P2	A3	1	V	W1		J2	
17	3	011/45	P2	A3	1	V	W1		J2	
18	3	355/45	P2	A3	1	V	W1		J2	
19	3	331/60	P2	A3	1	V	W1		J2	
20	3	010/46	P2	A3	1	V	W1		J2	

21	3	040/40	P2	A3	1	V	W1			J3
22	3	050/50	P2	A3	1	V	W1			J3
23	3	045/70	P2	A3	1	V	W1			J3
24	3	066/55	P2	A3	1	V	W1			J3
25	3	049/33	P2	A3	1	V	W1			J3
26	3	041/41	P2	A3	1	V	W1			J3
27	3	044/35	P2	A3	1	V	W1			J3
28	3	051/49	P2	A3	1	V	W1			J3
29	3	041/49	P2	A3	1	V	W1			J3
30	3	330/59	P2	A3	1	V	W1		J2	
31	3	320/57	P2	A3	1	V	W1		J2	
32	3	331/66	P2	A3	1	V	W1		J2	
33	3	330/43	P2	A3	1	V	W1		J2	
34	3	344/53	P2	A3	1	V	W1		J2	
35	3	356/56	P2	A3	1	V	W1		J2	
36	3	357/43	P2	A3	1	V	W1		J2	
37	3	347/65	P2	A3	1	V	W1		J2	
38	3	331/30	P2	A3	1	V	W1		J2	
39	3	341/50	P2	A3	1	V	W1		J2	
40	3	046/51	P2	A3	1	V	W1			J3
41	3	265/62	P2	A3	1	V	W1	J1		
42	3	260/72	P2	A3	1	V	W1	J1		
43	3	266/65	P2	A3	1	V	W1	J1		
44	3	264/43	P2	A3	1	V	W1	J1		
45	3	274/50	P2	A3	1	V	W1	J1		
46	3	273/65	P2	A3	1	V	W1	J1		
47	3	266/34	P2	A3	1	V	W1	J1		
48	3	278/64	P2	A3	1	V	W1	J1		
49	3	273/66	P2	A3	1	V	W1	J1		
50	3	260/65	P2	A3	1	V	W1	J1		
51	3	262/60	P2	A3	1	V	W1	J1		
52	3	271/72	P2	A3	1	V	W1	J1		
53	3	274/70	P2	A3	1	V	W1	J1		
54	3	278/60	P2	A3	1	V	W1	J1		

55	3	240/32	P2	A3	1	V	W1	J1		
56	3	245/34	P2	A3	1	V	W1	J1		
57	3	248/41	P2	A3	1	V	W1	J1		
58	3	251/42	P2	A3	1	V	W1	J1		
59	3	261/44	P2	A3	1	V	W1	J1		
60	3	271/32	P2	A3	1	V	W1	J1		
61	3	261/62	P2	A3	1	V	W1	J1		
62	3	271/52	P2	A3	1	V	W1	J1		
63	3	274/68	P2	A3	1	V	W1	J1		
64	3	266/58	P2	A3	1	V	W1	J1		
65	3	267/70	P2	A3	1	V	W1	J1		
66	3	260/65	P2	A3	1	V	W1	J1		
67	3	266/58	P2	A3	1	V	W1	J1		
68	3	253/56	P2	A3	1	V	W1	J1		

TYPE	PERSISTANCE	APERTURE	ROUGHNESS	FILLING	WATER
1. Fault zone	P1. < 1m	A1. < 1mm	X. Rough, stepped	1. Clean	W1. Dry
2. Fault	P2. 1-3m	A2. 1-3mm	XI. Smooth, stepped	2. Colour	W2. Damp
3. Joint	P3. 3-10m	A3. 3-10mm	XII. Slickensided, stepped	3. Non-cohesive	W3. Wet
4. Bedding	P4. 10-20m	A4. 10-30mm	XIII. Rough, undulating	4. Non-active clay	W4. Dripping
5. Foliation	P5. > 20m	A5. > 30mm	XIV. Smooth, undulating	5. Active clay	W5. Flowing
6. Fracture			XV. Slickensided, undulating	6. Cemented	
7. Cleavage			XVI. Rough, planar	7. Chlorite, talc & gypsum	
8. Schistosity			XVII. Smooth, planar	8. Others	
9. Fissure			XVIII. Slickensided, planar		
10. Shear					

UNIVERSITY MALAYSIA KELANTAN

FACULTY OF EARTH SCIENCE

DATA SHEET FOR DISCONTINUITY SURVEY IN **SLOPE 3A**

LOCATION : : 5º 41' 17.49" N / 101º 43' 37.10" E	SURVEYOR : Low	DIP DIRECTION OF SLOPE : 008º
DATE : 5 October 2018	NO OF DATA SHEET : 3	DIP AMOUNT OF SLOPE : 81º

NO	TYPE	DIP DIRECTION (º)/DIP (º)	PERSISTANCE	APERTURE	FILLING	ROUGHNESS	WATER	REMARK		
								Joint Set 1	Joint Set 2	Joint Set 3
1	6	030/61	P2	A5	1	IV	W4		J2	
2	6	030/80	P2	A5	1	IV	W4		J2	
3	6	031/62	P2	A5	1	IV	W4		J2	
4	6	030/63	P2	A5	1	IV	W4		J2	
5	6	031/63	P2	A5	1	IV	W4		J2	
6	6	032/59	P2	A5	1	IV	W4		J2	
7	6	033/58	P2	A5	1	IV	W4		J2	
8	6	035/66	P2	A5	1	IV	W4		J2	
9	6	031/63	P2	A5	1	IV	W4		J2	
10	6	030/61	P2	A5	1	IV	W4		J2	
11	6	031/69	P2	A5	1	IV	W4		J2	
12	6	032/79	P2	A5	1	IV	W4		J2	
13	6	037/65	P2	A5	1	IV	W4		J2	
14	6	036/57	P2	A5	1	IV	W4		J2	
15	6	031/50	P2	A5	1	IV	W4		J2	
16	6	032/58	P2	A5	1	IV	W4		J2	
17	6	036/53	P2	A5	1	IV	W4		J2	
18	6	031/69	P2	A5	1	IV	W4		J2	
19	6	032/73	P2	A5	1	IV	W4		J2	
20	6	033/78	P2	A5	1	IV	W4		J2	

21	6	006/80	P2	A5	1	IV	W4	J1		
22	6	006/85	P2	A5	1	IV	W4	J1		
23	6	007/83	P2	A5	1	IV	W4	J1		
24	6	003/75	P2	A5	1	IV	W4	J1		
25	6	005/79	P2	A5	1	IV	W4	J1		
26	6	005/78	P2	A5	1	IV	W4	J1		
27	6	006/81	P2	A5	1	IV	W4	J1		
28	6	007/83	P2	A5	1	IV	W4	J1		
29	6	010/78	P2	A5	1	IV	W4	J1		
30	6	011/78	P2	A5	1	IV	W4	J1		
31	6	006/73	P2	A5	1	IV	W4	J1		
32	6	005/60	P2	A5	1	IV	W4	J1		
33	6	004/56	P2	A5	1	IV	W4	J1		
34	6	003/59	P2	A5	1	IV	W4	J1		
35	6	005/65	P2	A5	1	IV	W4	J1		
36	6	007/77	P2	A5	1	IV	W4	J1		
37	6	008/81	P2	A5	1	IV	W4	J1		
38	6	010/82	P2	A5	1	IV	W4	J1		
39	6	011/79	P2	A5	1	IV	W4	J1		
40	6	012/79	P2	A5	1	IV	W4	J1		
41	6	075/64	P2	A5	1	IV	W4			J3
42	6	075/63	P2	A5	1	IV	W4			J3
43	6	074/60	P2	A5	1	IV	W4			J3
44	6	077/65	P2	A5	1	IV	W4			J3
45	6	074/60	P2	A5	1	IV	W4			J3
46	6	080/70	P2	A5	1	IV	W4			J3
47	6	081/70	P2	A5	1	IV	W4			J3
48	6	085/71	P2	A5	1	IV	W4			J3
49	6	071/64	P2	A5	1	IV	W4			J3
50	6	073/63	P2	A5	1	IV	W4			J3
51	6	070/63	P2	A5	1	IV	W4			J3
52	6	069/64	P2	A5	1	IV	W4			J3
53	6	068/64	P2	A5	1	IV	W4			J3
54	6	071/65	P2	A5	1	IV	W4			J3

55	6	069/55	P2	A5	1	IV	W4			J3
56	6	071/63	P2	A5	1	IV	W4			J3
57	6	074/62	P2	A5	1	IV	W4			J3
58	6	073/68	P2	A5	1	IV	W4			J3
59	6	074/68	P2	A5	1	IV	W4			J3
60	6	078/79	P2	A5	1	IV	W4			J3

TYPE	PERSISTANCE	APERTURE	ROUGHNESS	FILLING	WATER
1. Fault zone 2. Fault 3. Joint 4. Bedding 5. Foliation 6. Fracture 7. Cleavage 8. Schistosity 9. Fissure 10. Shear	P1. < 1m P2. 1-3m P3. 3-10m P4. 10-20m P5. > 20m	A1. < 1mm A2. 1-3mm A3. 3-10mm A4. 10-30mm A5. > 30mm	9. Rough, stepped 10. Smooth, stepped 11. Slickensided, stepped 12. Rough, undulating 13. Smooth, undulating 14. Slickensided, undulating 15. Rough, planar 16. Smooth, planar 17. Slickensided, planar	1. Clean 2. Colour 3. Non-cohesive 4. Non-active clay 5. Active clay 6. Cemented 7. Chlorite, talc & gypsum 8. Others	W1. Dry W2. Damp W3. Wet W4. Dripping W5. Flowing

UNIVERSITY MALAYSIA KELANTAN

FACULTY OF EARTH SCIENCE

DATA SHEET FOR DISCONTINUITY SURVEY IN **SLOPE 3B**

LOCATION : 5º 41' 17.49" N / 101º 43' 37.10" E	SURVEYOR : Low	DIP DIRECTION OF SLOPE : 320º
DATE : 5 October 2018	NO OF DATA SHEET : 4	DIP AMOUNT OF SLOPE :78º

NO	TYPE	DIP DIRECTION (º)/DIP (º)	PERSISTANCE	APERTURE	FILLING	ROUGHNESS	WATER	REMARK		
								Joint Set 1	Joint Set 2	Joint Set 3
1	3	041/69	P3	A2	1	II	W1	J1		
2	3	041/69	P3	A2	1	II	W1	J1		
3	3	041/69	P3	A2	1	II	W1	J1		
4	3	040/68	P3	A2	1	II	W1	J1		
5	3	040/72	P3	A2	1	II	W1	J1		
6	3	040/73	P3	A2	1	II	W1	J1		
7	3	042/73	P3	A2	1	II	W1	J1		
8	3	042/74	P3	A2	1	II	W1	J1		
9	3	041/70	P3	A2	1	II	W1	J1		
10	3	041/71	P3	A2	1	II	W1	J1		
11	3	043/75	P3	A2	1	II	W1	J1		
12	3	044/77	P3	A2	1	II	W1	J1		
13	3	044/77	P3	A2	1	II	W1	J1		
14	3	041/65	P3	A2	1	II	W1	J1		
15	3	042/63	P3	A2	1	II	W1	J1		
16	3	042/69	P3	A2	1	II	W1	J1		
17	3	044/70	P3	A2	1	II	W1	J1		
18	3	043/74	P3	A2	1	II	W1	J1		
19	3	040/69	P3	A2	1	II	W1	J1		
20	3	041/65	P3	A2	1	II	W1	J1		

21	3	041/69	P3	A2	1	II	W1	J1		
22	3	041/68	P3	A2	1	II	W1	J1		
23	3	041/68	P3	A2	1	II	W1	J1		
24	3	040/67	P3	A2	1	II	W1	J1		
25	3	040/66	P3	A2	1	II	W1	J1		
26	3	042/71	P3	A2	1	II	W1	J1		
27	3	042/72	P3	A2	1	II	W1	J1		
28	3	040/69	P3	A2	1	II	W1	J1		
29	3	040/68	P3	A2	1	II	W1	J1		
30	3	043/78	P3	A2	1	II	W1	J1		
31	3	043/78	P3	A2	1	II	W1	J1		
32	3	043/76	P3	A2	1	II	W1	J1		
33	3	042/70	P3	A2	1	II	W1	J1		
34	3	042/68	P3	A2	1	II	W1	J1		
35	3	044/70	P3	A2	1	II	W1	J1		
36	3	044/71	P3	A2	1	II	W1	J1		
37	3	044/75	P3	A2	1	II	W1	J1		
38	3	043/75	P3	A2	1	II	W1	J1		
39	3	044/73	P3	A2	1	II	W1	J1		
40	3	043/71	P3	A2	1	II	W1	J1		

TYPE	PERSISTANCE	APERTURE	ROUGHNESS	FILLING	WATER
1. Fault zone 2. Fault 3. Joint 4. Bedding 5. Foliation 6. Fracture 7. Cleavage 8. Schistosity 9. Fissure 10. Shear	P1. < 1m P2. 1-3m P3. 3-10m P4. 10-20m P5. > 20m	A1. < 1mm A2. 1-3mm A3. 3-10mm A4. 10-30mm A5. > 30mm	9. Rough, stepped 10. Smooth, stepped 11. Slickensided, stepped 12. Rough, undulating 13. Smooth, undulating 14. Slickensided, undulating 15. Rough, planar 16. Smooth, planar 17. Slickensided, planar	1. Clean 2. Colour 3. Non-cohesive 4. Non-active clay 5. Active clay 6. Cemented 7. Chlorite, talc & gypsum 8. Others	W1. Dry W2. Damp W3. Wet W4. Dripping W5. Flowing

UNIVERSITY MALAYSIA KELANTAN

FACULTY OF EARTH SCIENCE

DATA SHEET FOR DISCONTINUITY SURVEY IN **SLOPE 4**

LOCATION : 5º 38' 22.92" N / 101º 42' 32.35" E	SURVEYOR : Low	DIP DIRECTION OF SLOPE : 290º
DATE : 5 October 2018	NO OF DATA SHEET : 5	DIP AMOUNT OF SLOPE : 85º

NO	TYPE	DIP DIRECTION (º)/DIP (º)	PERSISTANCE	APERTURE	FILLING	ROUGHNESS	WATER	REMARK		
								Joint Set 1	Joint Set 2	Joint Set 3
1	3	110/5	P2	A5	1	V	W1	J1		
2	3	110/5	P2	A5	1	V	W1	J1		
3	3	110/5	P2	A5	1	V	W1	J1		
4	3	111/4	P2	A5	1	V	W1	J1		
5	3	111/3	P2	A5	1	V	W1	J1		
6	3	112/6	P2	A5	1	V	W1	J1		
7	3	110/6	P2	A5	1	V	W1	J1		
8	3	113/5	P2	A5	1	V	W1	J1		
9	3	115/7	P2	A5	1	V	W1	J1		
10	3	115/8	P2	A5	1	V	W1	J1		
11	3	113/8	P2	A5	1	V	W1	J1		
12	3	112/4	P2	A5	1	V	W1	J1		
13	3	110/4	P2	A5	1	V	W1	J1		
14	3	109/5	P2	A5	1	V	W1	J1		
15	3	114/6	P2	A5	1	V	W1	J1		
16	3	114/7	P2	A5	1	V	W1	J1		
17	3	115/7	P2	A5	1	V	W1	J1		
18	3	114/3	P2	A5	1	V	W1	J1		
19	3	115/4	P2	A5	1	V	W1	J1		
20	3	114/5	P2	A5	1	V	W1	J1		

21	3	193/79	P2	A5	1	V	W1		J2	
22	3	191/79	P2	A5	1	V	W1		J2	
23	3	190/81	P2	A5	1	V	W1		J2	
24	3	190/79	P2	A5	1	V	W1		J2	
25	3	189/70	P2	A5	1	V	W1		J2	
26	3	188/71	P2	A5	1	V	W1		J2	
27	3	193/70	P2	A5	1	V	W1		J2	
28	3	188/81	P2	A5	1	V	W1		J2	
29	3	195/76	P2	A5	1	V	W1		J2	
30	3	194/75	P2	A5	1	V	W1		J2	
31	3	194/74	P2	A5	1	V	W1		J2	
32	3	190/79	P2	A5	1	V	W1		J2	
33	3	189/78	P2	A5	1	V	W1		J2	
34	3	194/69	P2	A5	1	V	W1		J2	
35	3	195/70	P2	A5	1	V	W1		J2	
36	3	195/80	P2	A5	1	V	W1		J2	
37	3	198/78	P2	A5	1	V	W1		J2	
38	3	194/78	P2	A5	1	V	W1		J2	
39	3	190/79	P2	A5	1	V	W1		J2	
40	3	193/71	P2	A5	1	V	W1		J2	

TYPE	PERSISTANCE	APERTURE	ROUGHNESS	FILLING	WATER
1. Fault zone 2. Fault 3. Joint 4. Bedding 5. Foliation 6. Fracture 7. Cleavage 8. Schistosity 9. Fissure 10. Shear	P1. < 1m P2. 1-3m P3. 3-10m P4. 10-20m P5. > 20m	A1. < 1mm A2. 1-3mm A3. 3-10mm A4. 10-30mm A5. > 30mm	9. Rough, stepped 10. Smooth, stepped 11. Slickensided, stepped 12. Rough, undulating 13. Smooth, undulating 14. Slickensided, undulating 15. Rough, planar 16. Smooth, planar 17. Slickensided, planar	1. Clean 2. Colour 3. Non-cohesive 4. Non-active clay 5. Active clay 6. Cemented 7. Chlorite, talc & gypsum 8. Others	W1. Dry W2. Damp W3. Wet W4. Dripping W5. Flowing